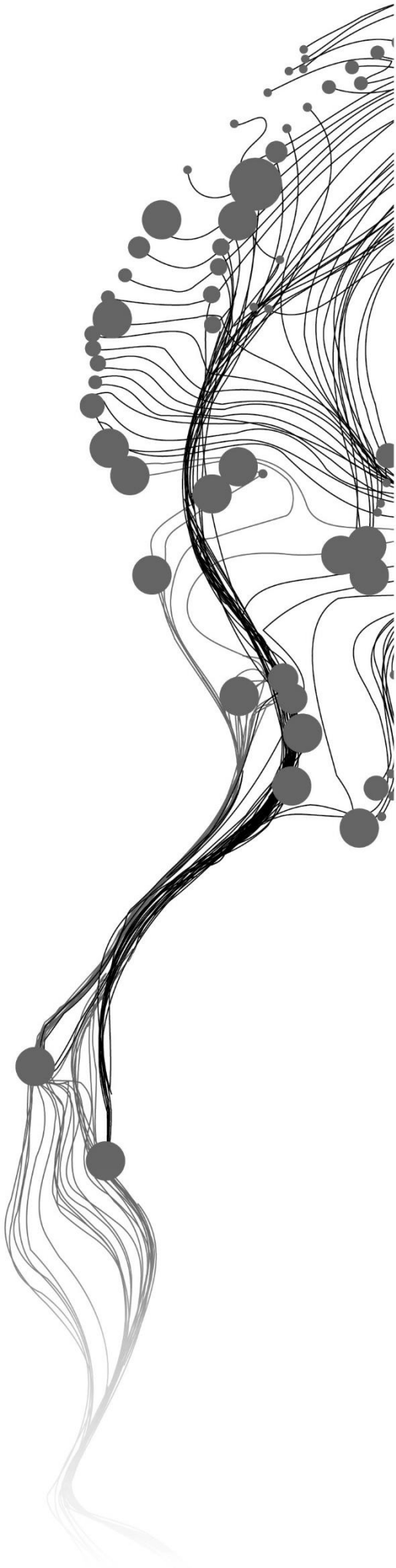


Characterizing clouds over Arsia Mons using OMEGA and CRISM

ASHWATHY NAIR
July 2023

SUPERVISORS:
Dr. Frank van Ruitenbeek
Wim Bakker MSc



Characterizing clouds over Arsia Mons using OMEGA and CRISM

ASHWATHY NAIR

Enschede, The Netherlands, July 2023

Thesis submitted to the Faculty of Geo-Information Science and Earth Observation of the University of Twente in partial fulfilment of the requirements for the degree of Master of Science in Geo-information Science and Earth Observation.

Specialization: Geoinformatics

SUPERVISORS:

Dr. Frank van Ruitenbeek
Wim Bakker MSc

THESIS ASSESSMENT BOARD:

Dr. H.M.A van der Werff (Chair)
Dr. Ottaviano Ruesch (External examiner, University of Münster)

DISCLAIMER

This document describes work undertaken as part of a programme of study at the Faculty of Geo-Information Science and Earth Observation of the University of Twente. All views and opinions expressed therein remain the sole responsibility of the author, and do not necessarily represent those of the Faculty.

ABSTRACT

Mars, our neighboring planet, has been a source of fascination for scientists and planetary enthusiasts for its unique atmospheric phenomena. Clouds are an intriguing feature observed on Mars, which play a crucial role in influencing the planet's weather patterns and climate system. Arsia Mons is a Martian volcanic mountain that experiences distinct types of cloud occurrences, including the recently discovered mysterious elongated cloud called the AMEC (Arsia Mons Elongated Cloud). This research focuses on investigating the clouds observed over the Martian volcanic mountain, Arsia Mons using spectral datasets to gain insights into the cloud occurrences in this area with respect to its morphology and composition. Data obtained over a period of 18 years from OMEGA and CRISM spectrometers was utilized to search for new cloud images, characterize clouds based on their morphologies and investigate cloud constituents using spectral analysis techniques.

The study compiled a total of 102 cloud images from both OMEGA and CRISM. A novel observation of an elongated cloud was discovered at the volcanic mountain Pavonis Mons, situated adjacent to the Arsia Mons volcano. Additionally, a distinct cloud morphology was identified in the Pavonis Mons region, referred to as the 'puffy' cloud in this research. The study also adds an observation of a rarely observed spiral cloud in the Arsia Mons region along with other cloud morphologies such as streaky clouds, orographic clouds and small cloud regions. Spectral analysis of the clouds to investigate cloud constituents and confirm the presence of dust, H₂O ice, and CO₂ ice showed no contribution of dust and CO₂ ice in the clouds. H₂O ice was detected in the examined clouds characterized by the 3.2 μm absorption feature. New cloud observations, their observed morphologies and inferred cloud constituents in this study will be useful to add to our current knowledge and understanding of clouds in the Arsia Mons region.

ACKNOWLEDGMENTS

I would like to express my deepest gratitude to my supervisors Dr. Frank van Ruitenbeek and Mr. Wim Bakker, for their guidance, continuous support and valuable advice throughout this research journey. Their insightful feedback and constant encouragement have been instrumental in enhancing the quality of this research. A special thanks to my internship supervisor, Dr. Daniela Tirsch, for providing me with the opportunity to gain a better understanding of the Martian clouds through my internship journey which has been very helpful in my research endeavor. I would also like to thank Mr. Jorge Hernandez Bernal for answering my queries and helping me provide resources for understanding the time-keeping concept on Mars.

I am deeply grateful to the Faculty of ITC for providing me with this opportunity to work on the topic of my interest and for making my dream of working on a planetary topic come true.

I would like to thank my teacher, Ms. Jaya Pallav who has been my source of inspiration and reason to love the world of space science. Finally, a big thanks to my mom and dad for being the biggest support in good and tough times and believing in me and my dream.

TABLE OF CONTENTS

1.	INTRODUCTION.....	7
1.1.	Types of clouds on Mars.....	8
1.2.	Arsia Mons Elongated Cloud phenomenon.....	9
1.3.	Seasons on Mars.....	10
1.4.	Research objectives and Questions.....	11
1.4.1.	Research objectives.....	11
1.4.2.	Research questions.....	11
2.	STUDY AREA AND DATASET.....	12
2.1.	Study Area.....	12
2.2.	Datasets.....	13
3.	METHODOLOGY.....	15
3.1.	Data search for cloud images.....	15
3.1.1.	Identifying spatial location and extent.....	15
3.1.2.	Identifying and converting temporal range.....	16
3.2.	Visual inspection and identifying morphology.....	17
3.3.	Investigating cloud spectral properties.....	18
3.3.1.	Defining cloud and non-cloud areas.....	19
3.3.2.	Image classification and creating zonal files.....	20
3.3.3.	Spectral analysis.....	21
4.	RESULTS.....	23
4.1.	New cloud observations.....	23
4.2.	Cloud Morphologies.....	29
4.2.1.	Cloud streaks or cirrus clouds.....	29
4.2.2.	'Puffy' cloud.....	29
4.2.3.	Spiral cloud.....	29
4.2.4.	Small cloudy regions.....	30
4.2.5.	Orographic clouds.....	30
4.3.	Spectral Analysis.....	32
4.3.1.	Identifying dust aerosols in clouds.....	32
4.3.2.	Identifying H ₂ O ice and CO ₂ ice clouds.....	34
5.	DISCUSSION.....	36
5.1.	Data collection.....	36
5.2.	Visual inspection and identifying morphologies.....	38
5.3.	Spectral Analysis.....	41
5.3.1.	Technique used for spectral investigation.....	41
5.3.2.	Selection of ROIs.....	42
5.3.3.	Interpretation of spectral results.....	44
6.	Conclusions and Recommendations.....	45
6.1.	Recommendations.....	46

LIST OF ABBREVIATIONS

1. **Ls**: Areocentric Longitude of the Sun
2. **AMEC**: Arsia Mons Elongated Cloud
3. **OMEGA**: Observatoire pour la Minéralogie, l'Eau, les Glaces et l'Activité
4. **CRISM**: Compact Reconnaissance Imaging Spectrometer for Mars
5. **LTST**: Local True Solar Time
6. **MY**: Martian Year
7. **VMCT**: Valles Marineris Cloud Trails
8. **ACB**: Aphelion Cloud Belt
9. **ODE**: Orbital Data Explorer

LIST OF FIGURES

Figure 1 The AMEC as observed from MEX HRSC.....	9
Figure 2 Ls values corresponding to the positions of Mars in its orbit around the Sun.....	10
Figure 3 Map of Tharsis Montes region with its four major shield volcanoes	12
Figure 4 Spatial extent chosen for cloud search in Arsia Mons	16
Figure 5 Median stretch applied to image strips.....	17
Figure 6 Interaction of the electromagnetic radiation between surface and cloud	19
Figure 7 ROIs selected for CRISM image strip.....	20
Figure 8 Reference spectra for H ₂ O ice clouds and CO ₂ ice clouds	22
Figure 9 Reference spectrum of Mars dust	22
Figure 10 Examples of cloud images obtained from CRISM sensor.....	27
Figure 11 Examples of cloud images obtained from OMEGA sensor	28
Figure 12 Examples of cloud morphologies obtained from CRISM and OMEGA.....	31
Figure 13 Reflectance ratio and difference obtained for CRISM strip (Visible range).....	32
Figure 14 Reflectance ratio and difference obtained for OMEGA strip(Visible range)	33
Figure 15 Comparison of resultant spectra with dust spectrum	33
Figure 16 Reflectance ratio and difference obtained for CRISM strip (NIR range)	34
Figure 17 Reflectance ratio and difference obtained for OMEGA strip (NIR range)	35
Figure 18 Distribution of cloud observations obtained from OMEGA and CRISM sensors	37
Figure 19 Cloud observation distribution in the Ls ranges.....	37
Figure 20 Morphologies observed in the collected cloud observations.....	38
Figure 21 Total number of cloud observations for each morphology.....	39
Figure 22 Cloud occurrences in the AMEC vs non-AMEC seasons.....	40
Figure 23 Reflectance ratio and difference obtained at same surface elevation	43
Figure 24 Reflectance ratio and difference obtained at different surface elevation	43
Figure 25 Spectral library of observed and compared cloud constituents.....	44

LIST OF TABLES

Table 1 Different types of cloud morphologies observed on Mars	8
Table 2 Correlation between the Ls values and the Martian season	11
Table 3 Specifications of the CRISM targeted multispectral and hyperspectral subsets	15
Table 4 OMEGA images with cloud observations and demarcated AMEC seasons	23
Table 5 CRISM images with cloud observations in VNIR + IR wavelengths	24
Table 6 CRISM observations with cloud observations in VNIR wavelengths	26

1. INTRODUCTION

Outer space has always been a source of fascination for humanity. The urge to discover new worlds through scientific knowledge has led us to encounter intriguing phenomena on other planets. During our exploration of the universe, several missions have been involved in studying our solar system, with a significant emphasis placed on Mars, our neighbouring planet. Over the past decades, research and exploration of the dynamic climate systems of Mars have gained increasing attention. In addition to its proximity, the red planet exhibits similarities in geological and atmospheric characteristics, making it an interesting research target. Previous studies suggest that life could have once existed on Mars (Mckay, 2010). However, the evolution of the planet experienced a major transformation and saw a significant shift in its climate systems (Jakosky et al., 2015). Understanding this dramatic alteration in its global climate would be beneficial to determine what factors can affect the climate system on planets including the Earth. Moreover, due to the considerable effort and resources invested in planetary missions, it is even more imperative to do an in-depth analysis of the data available today.

A planet's climate system is influenced by the atmosphere and its diverse phenomena. While dust storms are a well-known atmospheric phenomenon on Mars, the spatially and temporally varying Martian cloud structures have also attracted scientists' attention. Early observations of Martian clouds date back to the telescopic era, appearing as 'blue clearings' that were clearly distinguishable from the yellow clouds associated with dust storms (Dollfus Audouin, 1957; Slipher & C., 1962). The Viking missions played a major role in expanding our understanding of the dynamics and physical characteristics of clouds with the aid of colour imaging (French et al., 1981; James, 1982). In addition to this, it provided data for analysing seasonal and spatial variability of clouds from limb observations (Jaquin et al., 1986). With the advancement of research technology, there have been many new observations and discoveries related to Martian clouds with varying shapes, extent, and composition over the years (Clancy et al., 2017a).

A more definitive estimation of the cloud properties was made possible only later until the 1970s with the aid of infrared spectroscopy (Hanel et al., 1972). This was followed by simulations and modelling techniques to get a better understanding of atmospheric temperatures, water vapor content, aerosol particle sizes and other climate drivers (Clancy et al., 2017b; Daerden et al., 2010; Hernández Bernal et al., 2019; Hinson & Wilson, 2004; Michaels et al., 2006; Michelangeli et al., 1993; Neary & Daerden, 2017; Spiga et al., 2012; Yiğit et al., 2015). The major components observed in Martian clouds are usually found to be water ice, carbon dioxide ice and dust (Clancy et al., 2017a).

This thesis will attempt to discuss the characteristics of clouds observed over the Martian volcanic mountain, Arsia Mons which is known for its distinctive cloud formations using spectral datasets. The analysis of these clouds may also be able to give an insight into the recently observed mysterious cloud phenomenon called AMEC (Arsia Mons Elongated Cloud) in the Tharsis region.

1.1. Types of clouds on Mars

Cloud morphology in the Tharsis volcanic plateau including the Arsia Mons region is primarily characterized by cirrus and cumulus clouds (Clancy et al., 2017c). Apart from these common observations, Arsia Mons is known for exhibiting distinct types of cloud morphologies as opposed to its neighboring volcanic mountains. Topography, wind regimes and various atmospheric conditions influence the morphology of Martian clouds. Lee waves and orographic clouds are often generated in association with certain topographic features like crater rims and mountain slopes (French et al., 1981; Hernández-Bernal et al., 2021). Dust plays an important role in forming some cloud types such as aster, plumes, and spiral clouds (Rafkin et al., 2002; Wang & Ingersoll, 2002a). Meanwhile, other cloud types such as wave clouds, cloud streets and streaky clouds are more generic showcasing varying spatial and temporal patterns (Kahn, 1984). Table 1 summarizes the cloud types that have been documented in the Tharsis region from previous observations.

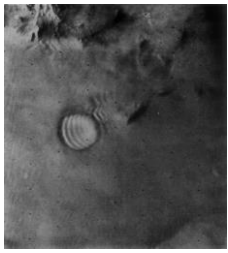
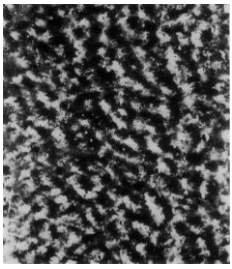
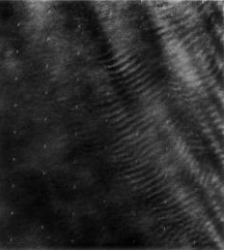


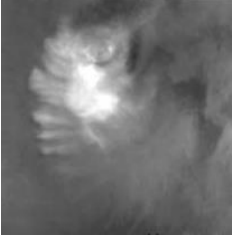


Cloud type	Image	Description	Cloud type	Image	Description
Lee waves		Clouds appearing in the lee side of terrain such as craters, mountains, valleys, etc. in periodic ridges	Cloud streets		Linear rows of clouds that are bubble shaped
Wave clouds		Linear clouds arranged in rows	Orographic cloud		Elongated clouds forming on the lee side of mountains
Streaky clouds		Appear as linear streaks with no particular periodicity	Aster clouds		Clouds with rays around a central disc (forms over Arsia Mons)
Plumes		Elongated clouds which spread in a single direction	Spiral cloud		Clouds characterized by a spiral shape (forms over Arsia Mons)

Table 1 Different types of cloud morphologies observed on Mars from various Mars missions (Clancy et al., 2017b; French et al., 1981; Hernández Bernal et al., 2019)

1.2. Arsia Mons Elongated Cloud phenomenon

In 2020, a previously unnoticed cloud phenomenon was discovered on Mars, referred to as the AMEC (Arsia Mons Elongated Cloud). A detailed analysis of the AMEC from various past and current missions revealed that it is rather a daily event occurring over the Arsia Mons volcano during the Southern Spring. Unlike any other cloud, the AMEC is proposed to be an orographic cloud that has a remarkable length and elevation estimated to be around 1800 km and 45 km respectively (Hernández-Bernal et al., 2021). A high-resolution satellite image of the AMEC as acquired in Martian Year (MY) 34 by the Mars Express is shown in Figure 1. A specific concurrence of atmospheric conditions such as temperature, water vapor abundances and winds is believed to be responsible for the formation of this mysterious cloud phenomenon (Hernández-Bernal et al., 2021).



Figure 1 The AMEC as observed from MEX HRSC high resolution camera (MY 34)

It is interesting to study this phenomenon for a variety of reasons. Firstly, the entire Tharsis region is found to have almost no cloud activity during the season in which AMEC and other clouds are observed over Arsia Mons (Benson et al., 2003, 2006; Wang & Ingersoll, 2002b). During this time, dust storms are also frequent, making it crucial to investigate whether dust has an impact on cloud composition. Furthermore, the cloud's spatial and temporal variability indicates its formation follows a pattern. According to (Hernández-Bernal et al., 2021), the cloud forms early in the morning and lasts for around 2.5 hours. After this period, the cloud gradually fades away, and new clouds emerge persisting until later in the local afternoon. Elongated clouds called VMCT (Valles Marineris Cloud Trails) were also observed in the Valles Marineris with a length of around 1000 km and a width of 75 km in MY 28 (Clancy et al., 2009, 2014). It is proposed that the VMCT resembles some of the physical characteristics and temporal variability of the AMEC (Hernández-Bernal et al., 2021). The presence of CO₂ ice in clouds within the Valles Marineris and equatorial region as indicated in previous studies (Inada et al., 2008), makes it interesting to investigate whether the clouds over Arsia Mons are solely composed of water ice or if they contain carbon dioxide ice as well. Using spectral datasets to study cloud properties will contribute to a better understanding of the cloud composition over Arsia Mons including clouds like the AMEC and other regional clouds. This approach will help infer the factors that cause cloud formations in a particular season and spatial extent. It can also be compared with cloud

phenomena in other parts of Mars to determine if they are influenced by geography or some other climate drivers like dust and aerosols for further studies.

1.3. Seasons on Mars

The axes of rotation of Mars and Earth are tilted to around the same angle relative to their orbital plane (23.5° for Earth and 25.1894° for Mars) (Kieffer et al., 1992; Yoder & Standish, 1997). Due to this, Mars experiences the same seasons as Earth. However, due to its greater distance from the Sun and higher eccentric orbit, Mars experiences a longer year (~ 687 Earth days) and undergoes seasons that are approximately twice as long as the seasons on Earth. Ls or Areocentric longitude is used to mark the position of Mars in its orbit with respect to the Sun and thus helps in marking time on Mars (Allison, 1997a). It is calculated as 0° at the position of Martian northern spring equinox and each season begins at 90° from the previous one. This method of timekeeping on Mars allows for convenient tracking of geological and atmospheric events for research purposes. Figure 2 shows the Ls values corresponding to various positions of Mars within its orbit around the Sun. Numbers 1 to 12 represent the positions of Mars relative to the Sun, while the values 0° to 330° denote the corresponding Ls values for those positions. Aphelion and perihelion are the positions of Mars when it is farthest and closest from the Sun respectively.

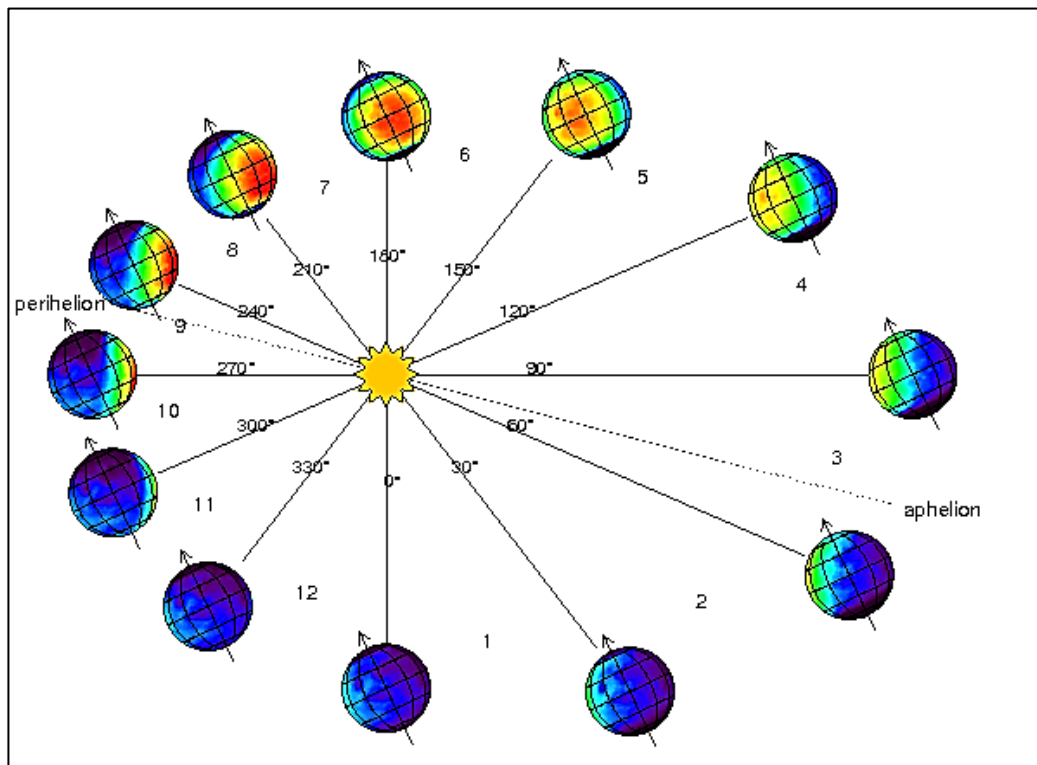


Figure 2 Ls values corresponding to the positions of Mars in its orbit around the Sun (Bhattacharyya et al., 2015)

The AMEC phenomenon is observed in the Ls range of 220° - 320° in the Southern solstice when the planet is closer to the Sun (Hernández-Bernal et al., 2021). This indicates that AMEC usually occurs in the Southern spring and summer. The table below with details shows a correlation between Ls values and seasons in the two hemispheres indicating the Martian seasons in which AMEC would occur (marked in red) according to the observations till date. The observations obtained from different seasons in which AMEC occurs will also be studied and compared in this work.

Ls (Solar longitude)	Martian season	
	Southern Hemisphere	Northern Hemisphere
0° - 90°	Autumn	Spring
90° - 180°	Winter	Summer
180° - 270°	Spring	Autumn
270° - 360°	Summer	Winter

Table 2 Correlation between the Ls values and the Martian season in both Northern and Southern hemispheres

1.4. Research objectives and Questions

This study aims to observe and investigate clouds over the Martian volcanic mountain, Arsia Mons where the recently mysterious cloud phenomenon, AMEC was discovered. This includes a long-term and detailed analysis of clouds observed in the morning and afternoon period with an extensive search for new cloud observations using multispectral and hyperspectral datasets from OMEGA and CRISM. It will progress with the identification of morphologies, conducting spectral investigation to examine cloud composition and performing spatio-temporal analysis with a focus on identifying any variations that can contribute to a better understanding of the AMEC.

1.4.1. Research objectives

- To search for cloud images in the study area
- To identify and study cloud morphologies in the specific study area and temporal range
- To identify the cloud constituents over Arsia Mons volcano using spectral methods
- To check for seasonal differences in clouds in the AMEC and non-AMEC season
- To use multispectral and hyperspectral datasets for investigating Martian clouds

1.4.2. Research questions

- What different kinds of cloud morphologies can be identified?
- What constituents can be found in the clouds over Arsia Mons for the period considered?
- How effective are the selected datasets in estimating the cloud constituents?
- What differences can be observed in the clouds in the AMEC occurring season as opposed to other seasons?

The research objectives and questions stated in the proposal underwent changes during the course of this study and a thorough discussion of these modifications is stated in Chapter 5.

2. STUDY AREA AND DATASET

2.1. Study Area

The Tharsis region is a large volcanic plateau in the western hemisphere. It is famous for its four massive shield volcanoes, considered to be some of the largest in the Solar System, including Olympus Mons, the tallest known volcano. Olympus Mons extends to a height of about 21km and has a diameter of approximately 600 km. The other three volcanoes include Arsia Mons (height ~ 19km; diameter ~ 450 km), Pavonis Mons (height ~ 14km; diameter ~ 370km) and Ascraeus Mons (height ~ 18km; diameter ~ 430 km) (Maltagliati et al., 2008). Figure 3 is a map of the Tharsis region and its four major volcanoes. The legend shows the surface elevation values and the black arrow shows the location of Arsia Mons in the Tharsis region.

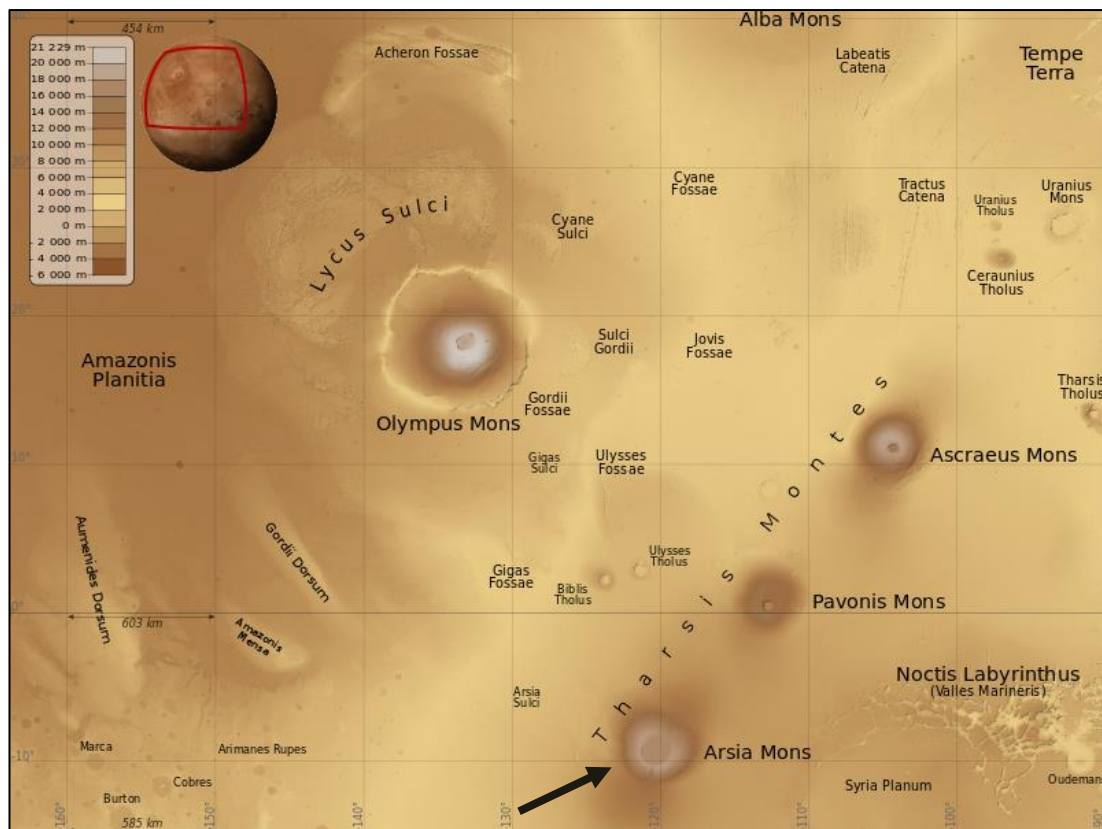


Figure 3 Map of Tharsis Montes region with its four major shield volcanoes. The black arrow indicates the Arsia Mons volcano modified from (*Mars: The Red Planet*, 2012)

Early observations of clouds in the Tharsis were obtained from the Mariner 6 and 7 flybys as detached limb hazes (cloudy features observed at the edge of the atmosphere) (Leovy CB et al., 1971). Some of the earliest missions including the Mariner and Viking provide information about the presence of water-ice clouds in this region (Curran et al., 1973). Additionally, the presence of clouds in the Tharsis region was observed, some of which were later referred to as Orographic clouds given their characteristics (Hunt et al., 1980). As the easterly winds move westwards and blow along the flanks of the volcanoes, the high-altitude terrain and local atmospheric conditions

lead to the formation of orographic clouds (Will Robertson, 2021). Water ice clouds observed in the region are commonly spotted as a part of the ACB (Aphelion Cloud Belt) in the Ls $\sim 40^\circ - 140^\circ$ within a latitudinal extent of 10°N to 30°S (Clancy et al., 2017b). These clouds have been studied previously using spectral datasets and modelling techniques (Clancy et al., 1996; James et al., 1996). Though the occurrence of clouds is quite common in Tharsis for certain times of the year, a lack of cloud activity is observed in the regional dust storm season ranging from around 200° to 360° Ls (Benson et al., 2003, 2006). Contrary to this observation in the entire Tharsis region, clouds can still be observed near Arsia Mons during the dust season (Benson et al., 2003, 2006; Wang & Ingersoll, 2002c). Additionally, water ice clouds were observed over Arsia Mons in all seasons (Noe Dobrea & Bell, 2005; Wang & Ingersoll, 2002c). Apart from water ice clouds, few observations of CO_2 ice clouds have also been noted in the Tharsis (Määttänen, 2010; Montmessin et al., 2007; Vincendon et al., 2011). The reason for such an unusual phenomenon to occur in the dusty season with its specialty to the Arsia Mons geographical area, inspired planetary researchers to study it elaborately. The need for a better comprehension of cloud occurrences further encourages us to investigate the components of these clouds and look for seasonal variations.

2.2. Datasets

Spectrometers on board space missions have played a crucial role in observing and providing valuable information about the composition of Martian clouds in the past. OMEGA and CRISM are two such important spectrometers onboard the MEX (Mars Express) and MRO (Mars Reconnaissance Orbiter) missions respectively which have contributed significantly to our present-day knowledge of clouds on Mars. OMEGA (Observatoire pour la Minéralogie, l'Eau, les Glaces et l'Activité) is an imaging spectrometer launched in 2003, onboard Mars Express which provides visible and near-infrared mapping of the Martian surface and atmosphere (Bibring et al., 2004). OMEGA acquires images in 352 spectral bands with a spatial resolution as high as $300\text{m}/\text{pixel}$ to a medium resolution of around 2-5 kms and has been previously used to identify clouds and investigate their properties in different regions on Mars (Määttänen, 2010; Määttänen et al., 2009; Madeleine et al., 2012; Maltagliati et al., 2008). In addition to this, there have been studies utilizing OMEGA datasets that particularly focused on mapping clouds in the Tharsis region to retrieve ice particle sizes and information on opacity of the clouds (Madeleine et al., 2012). The three spectral channels: VNIR (Visible Near infrared), SWIR (Shortwave infrared) 'C' and 'L' are appropriate for detecting absorption features of cloud constituents such as dust, water ice and carbon dioxide ice unambiguously (Määttänen, 2010; Montmessin et al., 2007). The VNIR channel operates in the wavelength range of 0.38 to $1.05 \mu\text{m}$ wavelength while the SWIR covers a wavelength range of $0.93 - 2.73 \mu\text{m}$ (SWIR-C) and $2.55-5.1 \mu\text{m}$ (SWIR-L). OMEGA datasets contain scientific and geometric data and have been analyzed using the OAT version 1.0.2 (OMEGA Analysis Tool) (*PDS Geosciences Node*, 2019) package. OAT is a set of ENVI and IDL procedures which can be used for displaying and processing OMEGA datasets.

CRISM (Compact Reconnaissance Imaging Spectrometer for Mars) is another visible infrared imaging spectrometer which has been used for cloud observations in the past with varying modes and spatial resolution. It covers a wavelength range of ~ 0.4 to $4.0 \mu\text{m}$ (Murchie et al., 2007). It operates in the VNIR ($0.36 - 1.05 \mu\text{m}$) and IR ($1.02 - 3.92 \mu\text{m}$) wavelength range and was launched as a part of the MRO mission in March 2006. CRISM datasets have been utilized in different modes such as limb (observations scanned across the limb) (Clancy et al., 2014, 2019) and Targeted observation (provides nadir and multiangular pointing high resolution data) (Khayat

et al., 2022; Vincendon et al., 2011) for studying Martian clouds. CRISM's high spatial resolution ranging from 20 to 200m/pixel depending on its altitude is highly valuable for detecting clouds. Thus, it is an appropriate source of data in addition to the OMEGA datasets. CRISM files are analyzed using the CAT version 7.4 (CRISM Analysis Tool) (*PDS Geosciences Node*, 2019), a similar package to the OAT plugin.

3. METHODOLOGY

This section provides an overview of the steps carried out to study the properties of the clouds over Arsia Mons using spectral datasets. It progresses with data collection, identification and analysis of cloud observations. The research involved the use of general and geospatial softwares such as Mars24 (*NASA GISS: Mars24 Sunclock*, 2022), ENVI+IDL, and HypPy (*Hyperspectral Python*, 2017) at various stages.

A series of subsections follow, which elaborate on the methods applied, including:

- a) Data search for cloud images
- b) Visual inspection and identifying morphology
- c) Investigating cloud spectral properties

3.1. Data search for cloud images

The Mars ODE (Orbital Data Explorer) (*Mars Orbital Data Explorer*, 2019) supported by the Geosciences node of NASA PDS (Planetary Data System) provides access to data and tools for datasets from various Mars missions. This interface allows for data search based on the geographical location and time filters to obtain data based on the project's requirement.

3.1.1. Identifying spatial location and extent

ODE's Map Tool was used to specify the datasets and their observation modes. The CRISM modes selected for this study utilized the Targeted observation subsets which include the multispectral and hyperspectral survey data, covering thin strips of area extending in the N-S direction as shown in figure 4(a). The multispectral and hyperspectral targeted survey modes operate in nadir pointing with medium spatial resolution. Observations vary in lengths depending on the altitude of the sensor. Table 3 lists the varying footprint sizes covered by the datasets. OMEGA observations were selected from the Experiment Data Record (EDR) which contains all the scientific and geometric data produced by the sensor. The footprint area for OMEGA observations varies from moderate resolution mode (5-8 kms wide and extending to hundreds of kilometres in length) as well as global mode (300-500 kms wide and extending to thousands of kilometres in length). Figure 4(b) depicts an example of an OMEGA image footprint for the year 2005.

TRDR subsets	Spatial resolution (m/pixel)	Footprint size (kms)
MSP (Multispectral Survey)	200	~10x45/10x180/10x540
MSV (Multispectral VNIR)	100	~5x45/5x180/5x540
HSP (Hyperspectral Survey)	200	~10x45/10x180/10x540
HSV (Hyperspectral VNIR)	200	~10x45/10x180/10x540

Table 3 Specifications of the CRISM targeted multispectral and hyperspectral subsets

Specification of the datasets was followed by defining the spatial coverage to be considered for searching cloud images. The spatial coverage chosen for this study extends from -4.65°N to -11.76°N latitude and -116.23°E to -130.18°E longitude. This spatial extent covers cloud images westwards and over Arsia Mons which is useful to give valuable insights into the formation of clouds on the leeward side of the Arsia Mons volcano, such as the AMEC. Considering the large volume of data and time limitations for the study, an area of approximately 50 kms west of the volcano was deemed to be an appropriate distance considering the AMEC extends westwards from the volcano. Figure 4 (red box) shows the spatial extent considered for this research

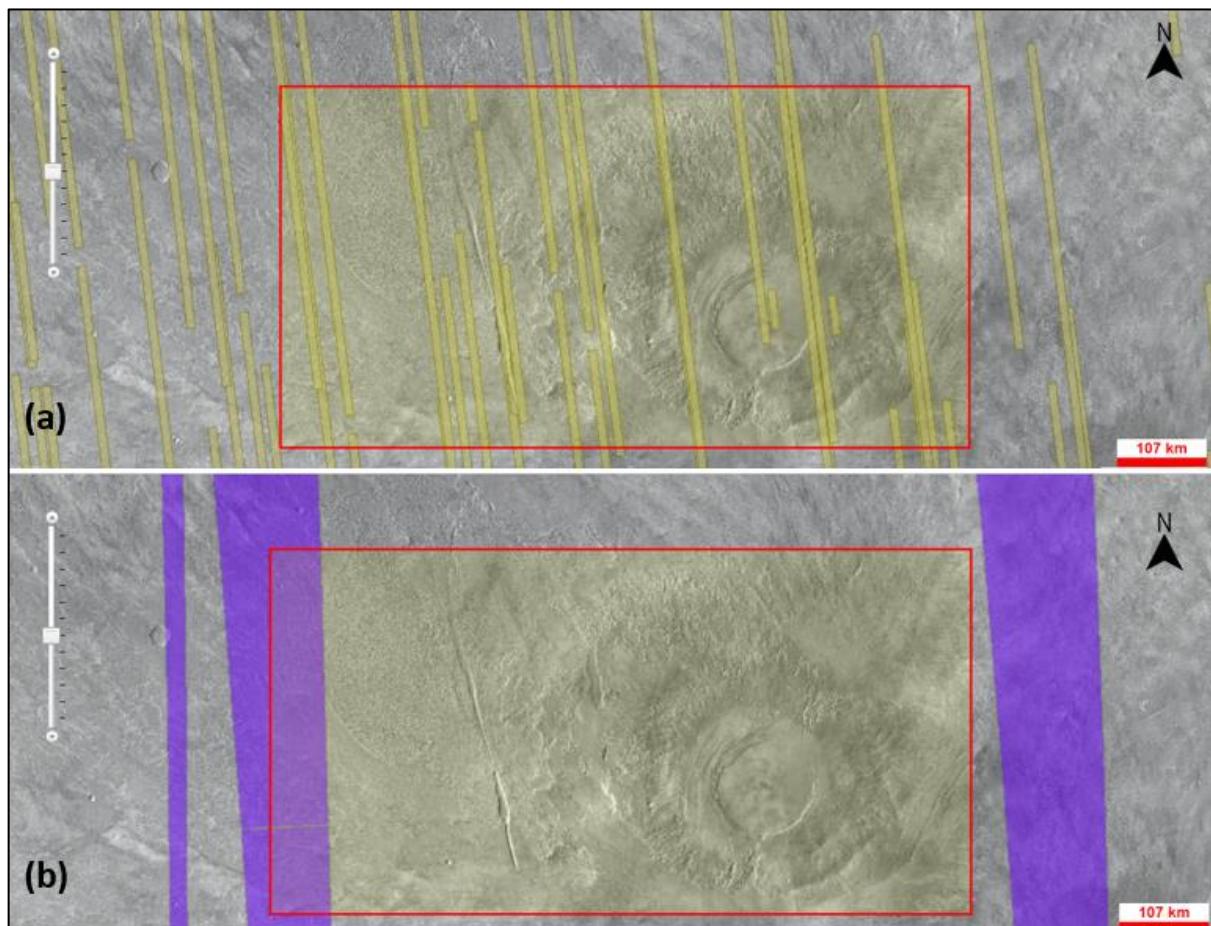


Figure 4 Spatial extent chosen for cloud search in Arsia Mons marked by red box (a) Footprint of CRISM strips (yellow) in the year 2010 includes HSP, MSP and HSV modes; (b) Footprint of OMEGA (purple) in the year 2010. The scale corresponds to the entire image.

3.1.2. Identifying and converting temporal range

To specify the time range for obtaining the cloud observations, Date/time range filters were used from the Mars ODE interface. AMEC observations were reported in the months (corresponding to the sensor observations): August, September, October, November, December, and January. Data from OMEGA and CRISM in the Arsia Mons region for the considered extent was downloaded for these six terrestrial months. Since the duration of seasons and days is different on Mars from the observation time as recorded by the sensor, there is a need for conversion to LTST (Local True Solar Time) to determine the local time and Ls of cloud occurrence on Mars.

LTST on Mars refers to the measurement of time with reference to the position of the Sun (Allison, 1997b). The Mars24 Sunclock website/app provided by NASA was used for this purpose. This platform offers tools to convert Earth time to corresponding local Martian time (LTST) and season (Ls value) for a specified region. UTC observation time for each of the images were converted to Martian local time (LTST) for further analysis.

3.2. Visual inspection and identifying morphology

Observations acquired from the selected spatial and temporal range were further examined to check for images with clouds and identify their morphology. The downloaded data was imported into ENVI using OAT and CAT plugins for visual inspection. Basic processing steps were involved for importing CRISM and OMEGA files. CRISM files were downloaded from PDS as I/F format which represents the ratio of reflected to incident sunlight and provides reflectance values. These files did not require any additional processing. OAT plugin provides 'Raw OMEGA to IoF conversion' tool to convert the downloaded OMEGA datasets into I/F format. Since the study proceeds with working on reflectance values, images were required to be converted into I/F format. HypPy provides image stretch options for better interpretation of images by improving the contrast and brightness of images and adjusting intensity values. Median stretch function ($\pm 3 \times \text{MAD}$) is one such feature which involves stretching pixels of an image based on the value of median and is specifically useful when working with a wide range of pixel values. It enables improved visualization and makes it easier to distinguish subtle variations in the image data. Figure 5 shows the clouds as they appear before and after applying median stretch viewed with RGB combination (5,2,1). This is an important step in interpreting the morphology of the clouds. The two images show that without applying the stretch, the clouds resemble blurred areas whereas they actually show striated morphology. Thereafter, observations with clear indications of clouds were added to the inventory to be used for further analysis. Spatial cloud patterns in the images were compared to previous literature for identifying their cloud morphology.

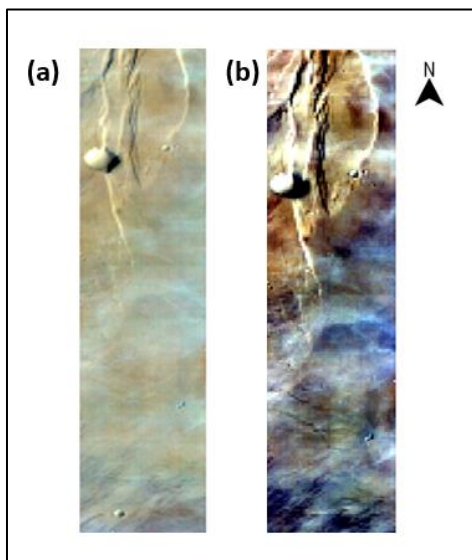


Figure 5 Part of CRISM image strip (MSP00015155_01)
Image acquired on 30th December 2009; Ls: 30.94°
(a) before applying median stretch (b) after applying median stretch

3.3. Investigating cloud spectral properties

The spectral properties obtained from cloud observations can be indicative of the cloud composition based on the absorption features they exhibit in the electromagnetic spectrum. This study focusses on identifying evidence of cloud components over Arsia Mons by studying absorption features of clouds in the near infrared wavelengths of the electromagnetic spectrum. Since the cloud is above the surface, the image observation is expected to contain the combined spectral signature of both cloud and surface components. Consequently, it is essential to extract the spectral signature solely associated with the cloud from the image observation to estimate the components present within the cloud. Comparing the spectral properties above a cloud and above the nearby surface without the cloud (with the same surface composition as below the cloud) can give an approximate spectral feature for the cloud. This can be explained by the following equation as described by (Vincendon et al., 2011):

$$C_R = S_R * C_T + C_S \quad (\text{Equation 1})$$

Where,

- C_R is the measured reflectance above the cloud
- S_R is the measured reflectance above the surface without the cloud,
- C_T is the transmission factor of the cloud (corresponding to the light passing through the cloud from the ground) and,
- C_S is the reflectance of the cloud (light that is scattered upward by a cloud without interacting with its surface).

To the first order, C_T (reflectance ratio) of the cloud can be calculated from the ratio C_R / S_R when the value of S_R is sufficiently high. Similarly, $C_R - S_R$ (reflectance difference) is the estimated value of C_S when the value of C_T is close to 1. The assumptions of the equation will be further discussed in chapter 5. The reflectance values for the cloud region (C_R) and the surface region without the cloud (S_R) can be derived from the I/F values available in the image observations. The method for specifying the two regions is further explained in section 3.3.1. Since both reflectance of the cloud and the surface nearby is available in the observations, the ratio (C_R / S_R) and difference ($C_R - S_R$) can be plotted to look for evidence of cloud components. Thus, the components present in the clouds can be identified based on the absorption features observed in the reflectance ratio and difference. The interactive components involved in the electromagnetic radiation are as follows and have been numbered in Figure 6:

1. Irradiance from the Sun reaching the cloud and surface
2. Reflectance from the cloud without transmission and interaction with the surface
3. Reflectance from the cloud after transmission but no interaction with the surface
4. Reflectance from the cloud after transmission and no interaction with surface (2 + 3)
5. Reflectance from the surface

6. Reflectance from the surface undergoing scattering
7. Reflectance from the cloud after transmission and no interaction with surface
8. Reflectance above the cloud after scattering, transmission and interaction with surface

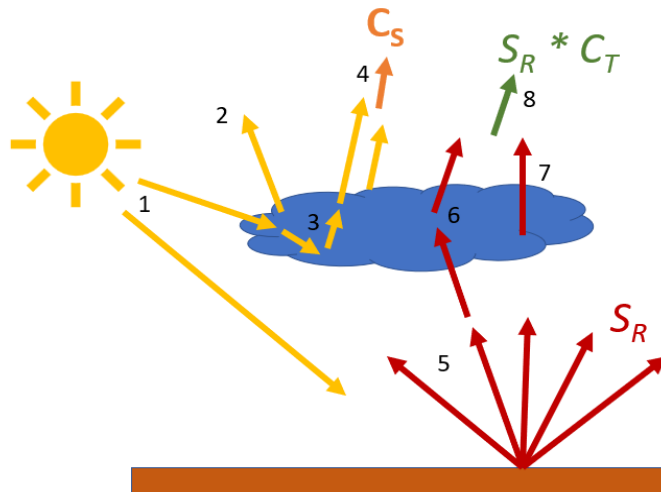


Figure 6 Interaction of the electromagnetic radiation between the surface and the cloud

Figure 6 is a diagrammatic representation of the equation considered. It can be inferred that C_S (Figure 6 denotation 4) is influenced by the irradiance from the Sun and cloud transmission. S_R is the reflectance solely from the surface (Figure 6 denotation 5). $S_R * C_T$ (Figure 6 denotation 8) provides the value for C_R (Figure 6 denotation 8). The figure and equation neglect the light scattered downward by the cloud and scattered by the surface upwards through the cloud (Figure 6 denotation 6). Further discussion on the impact of the assumptions on the conclusions will be presented in Chapter 5.

3.3.1. Defining cloud and non-cloud areas

Image strips obtained from OMEGA and CRISM that contain areas with and without cloud coverage were utilized for specifying the regions corresponding to C_R and S_R . ROI (Region of Interest) files were created for the cloud area and the nearby surface area (without clouds) using ENVI's 'Region of Interest' tool. These are defined as 'cloud' (region above the cloud) and 'noncloud' (region above the surface near the cloud) in this study. Approximately, the density of the atmosphere can be described as a double exponential decay with height (Petty, 2006). This means, at lower altitudes when the CO_2 column is denser, the absorption features of CO_2 dominate the spectra, especially in the near infrared range. As the altitude increases, the CO_2 column becomes thinner, resulting in lesser domination of the CO_2 column on the spectra. It is important to note that the surface elevation and relative illumination should be similar in both ROI classes to minimize the effect of air column and reflectance on the spectral results. To ensure comparable atmospheric conditions such as total air column, illumination and aerosol

content, ROIs for a single observation were collected from the same OMEGA/CRISM data strip and relatively similar surface elevation by comparing average depth of the CO₂ column in the spectrum. In some image strips, where the extent of cloud coverage was minimal it may only allow for creation of limited number of ROIs with sufficient pixel coverage. To maintain consistency across all image strips, it was considered appropriate to select five ROIs for each of the ‘cloud’ and ‘non-cloud’ regions with a pixel coverage of 100 to 200 pixels. Figure 7 shows an example of the ROIs considered for one of the CRISM images (MSP000031C9_05).

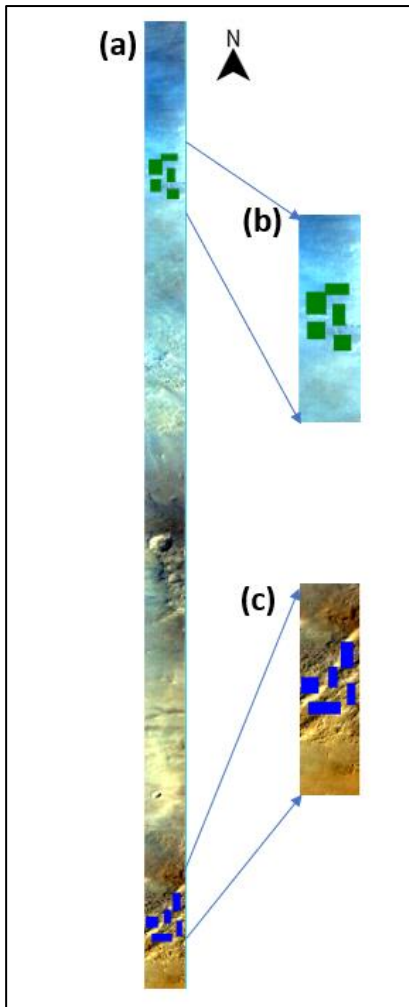


Figure 7 ROIs selected for image strip (MSP000031C9_05). Image acquired on 23rd November 2006; Ls: 139.56°
 (a) Entire strip showing locations of cloud region ROIs and non-cloud region ROIs
 (b) ROIs in cloud region
 (c) ROIs in non-cloud region

3.3.2. Image classification and creating zonal files

The ROIs created for the two regions of each image were further converted into a classification image using the ROI classification tool on ENVI. This creates three classes for each image strip, which includes: ‘ROI#cloud’ (classes from selected cloud region pixels), ‘ROI#noncloud’ (classes from selected non-cloud region pixels) and ‘Unclassified’ (region apart from the selected ROI regions). Post creating classification image, zonal statistics for the ‘cloud’ and ‘non-cloud’ regions was calculated. Zonal Statistics is a geospatial analytical operation that allows calculations of statistics (average, sum, minimum, maximum, etc.) of cell values from a raster based on the

specified zones which are vector datasets (Song et al., 2015). The Zonal statistics tool provided by HypPy was used for calculating the mean spectral values for the ROI regions. In this study, the Zonal files were selected as the classes obtained post classification process and the input raster included the image strip that was used for defining the ROIs. The options for sorting bands on wavelength should be checked to ensure the output spectra is created with wavelengths in proper order. Additionally, checking the option for using bad bands list is suggested to avoid the effect of bands that are corrupted due to sensor malfunction, calibration issues and atmospheric interferences which could be the case for both OMEGA and CRISM.

3.3.3. Spectral analysis

HypPy creates ASCII text files for the average spectral values of the ‘cloud’ and ‘non-cloud’ regions after the zonal statistics operation is applied. The Spectral Library Viewer is a tool that allows viewing ENVI spectral libraries. The mean spectra for the two regions were viewed and compared using this tool. Finally, the reflectance ratio and difference were calculated from the earlier discussed equation. This was performed using a python code utilizing the spectral class from HypPy which calculates the reflectance ratio and difference. The output spectrum was further used for interpretation and comparison with the ratio and difference spectra from the study of (Vincendon et al., 2011) pertaining to H₂O and CO₂ ice clouds. A characteristic feature of H₂O ice clouds is the 3.2 μm feature which is not observed in CO₂ ice clouds (Raponi et al., 2016). This was used as the principal method to discriminate between a H₂O ice cloud and a CO₂ ice cloud. Comparisons with surface frost were also analyzed using USGS spectral library to confirm the composition was obtained pertaining to the cloud and not the surface. Martian dust aerosols are easily differentiable from ice particles in the visible range of the spectrum. Martian dust shows strong ferric absorption with the reflectance ratio increasing from 0.4 μm to 1 μm whereas H₂O ice and CO₂ ice are characterized by no major absorption with their reflectance ratio in the visible wavelength range remaining close to 1 (Vincendon et al., 2009). The spectra obtained from the visible range of the wavelength was used for the spectral analysis of dust and comparison with dust features from the CRISM spectral library was conducted. Details of the spectra obtained, and absorption features noticed will be discussed in the next chapter. Figure 8(a) and (b) show examples of reference spectra after performing reflectance ratio and subtraction respectively, where spectra in blue color indicates H₂O ice and spectra in red indicates CO₂ ice. Figure 9 presents the reference spectrum for Martian dust obtained from the RELAB spectral library (*PDS Geosciences Node*, 2019) showing the gradual increase in slope from 0.4 μm to 1 μm.

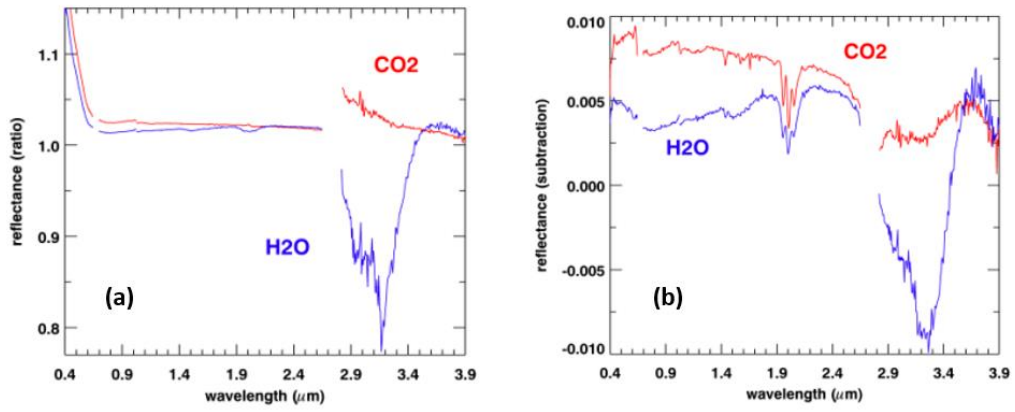


Figure 8 a) reflectance ratio and (b) reflectance difference obtained for H₂O ice clouds (blue) and CO₂ ice clouds (red) by (Vincendon et al., 2011)

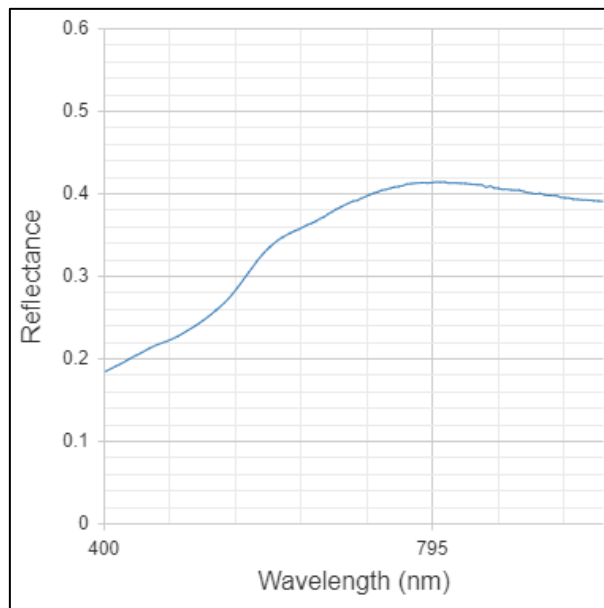


Figure 9 reference spectrum of Mars dust from RELAB spectral library

4. RESULTS

The previous chapter discussed the process for data collection, visual inspection of cloud observations, and spectral analysis of the cloud images. In continuation of the methodology, this chapter discusses the details of the results.

4.1. New cloud observations

All cloud observations obtained from CRISM and OMEGA were compiled for this study. Images of clouds were collected from the beginning of the mission to the present day for each sensor. Data considered most suitable for processing and analysis were added to the inventory after filtering out noisy and uninterpretable images from visual inspection and converting local time and season. The inventory summarizes the Observation IDs, type of sensor, date of acquisition, LTST and Ls corresponding to each image. As indicated previously, the LTST and Ls were calculated for each acquisition date. The highlighted rows include the range of Ls (220° - 320°) when the AMEC occurs.

A total of 102 cloud images were obtained from both OMEGA and CRISM which includes:

- a) **OMEGA: 8 images**
- b) **CRISM: 94 images**

The inventory comprises of three tables: list of OMEGA images, list of CRISM images with VNIR and IR channels and list of CRISM images with only VNIR channels. All images were used for identification of cloud morphologies.

The SWIR channels ('C' and 'L') of OMEGA, were found to be broken after 2009. Since SWIR channels are crucial for differentiation of H₂O ice and CO₂ ice clouds, only data until 2009 was utilized for identification of these clouds. Spectral analysis of all OMEGA images was conducted to determine the presence of dust. Table 4 lists the OMEGA images studied in this thesis where the rows highlighted in blue depict AMEC occurring seasons.

Observation	Sensor	Date	LTST	Ls
ORB1316_2	OMEGA	26/01/2005	12:15:52	150.13
ORB2274_3	OMEGA	21/10/2005	12:13:00	310.19
ORB7705_2	OMEGA	05/01/2010	12:54:10	33.69
ORBL424_0	OMEGA	13/01/2020	10:45:53	330.67
ORBL068_0	OMEGA	31/08/2020	15:04:03	269.08
ORBL135_0	OMEGA	20/09/2020	14:29:01	281.28
ORBL142_0	OMEGA	22/09/2020	14:05:48	282.54
ORBL498_0	OMEGA	03/01/2022	10:08:10	342.28

Table 4 OMEGA images with cloud observations and demarcated AMEC seasons

CRISM images with VNIR +IR wavelength ranges were utilized for conducting spectral analysis for identification of H₂O ice, CO₂ ice and dust in cloud observations. Table 5 lists the MSP and HSP images which contain both VNIR and IR channels. One image which could not be used for spectral analysis due to full cloud coverage because of and the inability to mark non-cloud regions : MSP0000C6F9_01

Observation	Sensor	Date	LTST	Ls
MSP0000332F_05	CRISM	29/11/2006	15:30:03	142.62
MSP00003905_01	CRISM	26/12/2006	15:36:49	156.28
MSP00003C15_07	CRISM	05/01/2007	15:51:52	161.70
MSP00008D20_07	CRISM	18/12/2007	14:47:12	4.45
MSP0000C6F9_01	CRISM	11/09/2008	15:40:07	125.81
MSP0000C88C_01	CRISM	16/09/2008	15:49:04	128.26
MSP0000D404_01	CRISM	06/11/2008	15:44:51	153.29
MSP0000D67F_01	CRISM	16/11/2008	16:01:26	158.66
MSP000101F5_01	CRISM	25/12/2008	15:59:34	179.94
MSP00010649_05	CRISM	05/01/2009	15:52:52	186.37
MSP00014570_01	CRISM	13/08/2009	17:06:20	320.83
MSP000147B9_01	CRISM	18/08/2009	14:45:54	323.67
MSP0001481C_01	CRISM	19/08/2009	14:25:19	324.24
MSP00015155_01	CRISM	30/12/2009	14:44:50	30.94
HSP00015A7D_01	CRISM	15/01/2010	14:51:29	38.40
MSP0001AB4F_01	CRISM	05/09/2010	15:28:44	143.56
HSP0001BB17_01	CRISM	04/11/2010	15:35:07	175.57
MSP0001C5E7_01	CRISM	11/12/2010	16:09:19	196.79
MSP0001C61D_01	CRISM	12/12/2010	15:48:57	197.39
MSP00021FDD_01	CRISM	22/12/2011	15:04:37	46.87
MSP0002AF02_01	CRISM	21/08/2013	14:24:38	10.09
MSP0002B0A8_01	CRISM	26/08/2013	14:34:22	12.57
MSP0002B0A9_01	CRISM	26/08/2013	14:37:27	12.57
MSP0002B66D_01	CRISM	16/09/2013	14:54:08	22.79
HSP0002B874_05	CRISM	22/09/2013	14:43:14	25.65
MSP0002B99B_03	CRISM	28/09/2013	14:52:22	28.03
MSP0002BA41_01	CRISM	04/10/2013	14:45:17	30.86
HSP0002BC73_01	CRISM	15/10/2013	14:40:15	36.00
MSP0002CA4B_01	CRISM	09/12/2013	15:14:14	60.20
MSP00037EA1_01	CRISM	27/08/2015	14:50:10	33.41
MSP00038012_01	CRISM	02/09/2015	14:40:59	36.20
HSP0003976A_01	CRISM	15/12/2015	15:18:58	81.93
HSP0003E425_03	CRISM	30/08/2016	15:28:13	213.60

Table 5 CRISM images with cloud observations in VNIR + IR wavelengths

CRISM images with only VNIR wavelength ranges were utilized for conducting spectral analysis for identification of dust in cloud observations. Table 5 lists the MSV and HSV images which contain VNIR channels. The rows highlighted in blue depict AMEC occurring seasons.

Observation	Sensor	Date	LTST	Ls
HSV0001AF9E_01	CRISM	21/09/2010	15:31:40	151.92
HSV0001BCED_01	CRISM	09/11/2010	15:43:47	178.44
HSV0001C006_01	CRISM	21/11/2010	15:39:05	184.84
HSV0001CE9E_03	CRISM	13/01/2011	16:06:04	216.64
HSV000200BC_01	CRISM	03/09/2011	14:21:09	355.13
HSV00020EF4_01	CRISM	28/10/2011	14:52:25	21.63
HSV00021888_03	CRISM	26/11/2011	14:39:01	34.88
HSV00021A3A_05	CRISM	01/12/2011	14:48:45	37.21
HSV00022158_01	CRISM	28/12/2011	15:15:24	49.16
MSV00027D5D_01	CRISM	14/12/2012	15:41:22	225.19
MSV0002C556_03	CRISM	22/11/2013	15:03:37	52.97
HSV000325ED_01	CRISM	05/09/2014	15:53:40	190.66
HSV00032CC8_01	CRISM	25/09/2014	16:16:26	202.80
HSV00032EAC_01	CRISM	30/09/2014	16:19:41	205.81
MSV0003356F_01	CRISM	23/10/2014	15:46:52	219.70
MSV000352F8_01	CRISM	30/01/2015	14:36:01	281.80
HSV000379E5_05	CRISM	06/08/2015	14:33:10	23.47
MSV000383FB_01	CRISM	19/09/2015	14:48:40	43.59
MSV00038530_01	CRISM	24/09/2015	14:55:38	45.88
MSV00038F9B_01	CRISM	12/11/2015	15:12:19	67.57
MSV0003DBAB_01	CRISM	02/08/2016	15:30:46	196.90
MSV0003DD56_01	CRISM	08/08/2016	15:39:46	199.95
MSV0003DDA7_01	CRISM	09/08/2016	15:20:29	200.55
MSV0003DEDD_01	CRISM	13/08/2016	15:46:44	203.02
MSV0003E5BE_01	CRISM	03/09/2016	15:54:52	216.13
HSV0003E689_01	CRISM	05/09/2016	15:13:42	217.38
MSV0003E867_01	CRISM	10/09/2016	15:21:06	220.56
MSV0003ED27_03	CRISM	26/09/2016	15:42:40	230.19
MSV0003ED27_01	CRISM	27/09/2016	15:17:48	230.83
MSV0003F37C_01	CRISM	25/10/2016	15:07:43	248.37
HSV0003F88E_01	CRISM	05/11/2016	14:54:53	255.54
HSV00040A1D_05	CRISM	25/12/2016	14:20:28	287.11
MSV00041109_01	CRISM	15/01/2017	14:40:06	299.59
MSV00041173_01	CRISM	16/01/2017	14:21:14	300.20
MSV00041343_01	CRISM	21/01/2017	14:26:35	303.30
HSV000414DA_07	CRISM	26/01/2017	14:30:20	303.26
MSV0004447F_01	CRISM	20/08/2017	14:45:25	49.72
MSV0004493B_03	CRISM	09/09/2017	15:19:41	58.78
MSV00045CB2_01	CRISM	26/11/2017	15:27:38	92.98

MSV0004AA3E_01	CRISM	08/09/2018	15:09:30	246.03
MSV0004B163_01	CRISM	30/09/2018	14:59:04	259.72
HSV0004BC66_05	CRISM	13/12/2018	14:45:27	305.33
MSV0004C076_03	CRISM	24/12/2018	14:39:52	311.95
MSV0004C0D6_01	CRISM	25/12/2018	14:18:31	312.54
MSV0004C130_01	CRISM	26/12/2018	14:01:58	313.12
MSV0004C300_01	CRISM	31/12/2018	14:06:27	316.09
MSV0004FC08_01	CRISM	08/08/2019	15:18:02	63.46
MSV00050A60_01	CRISM	08/11/2019	15:51:38	104.19
MSV00050DAF_01	CRISM	26/11/2019	15:40:01	112.13
MSV000513EB_01	CRISM	24/12/2019	15:47:29	125.06
MSV000548B8_01	CRISM	22/08/2020	15:13:40	263.25
MSV0005503D_01	CRISM	17/09/2020	15:26:12	279.39
MSV00055341_01	CRISM	28/09/2020	15:08:30	286.38
MSV0005539D_05	CRISM	29/09/2020	14:47:00	287.00
MSV0005570A_01	CRISM	09/10/2020	14:51:21	293.28
MSV00055E44_01	CRISM	31/10/2020	14:38:16	306.19
MSV00056143_03	CRISM	09/11/2020	15:06:13	311.61
MSV00056807_01	CRISM	02/12/2020	14:37:58	324.49
MSV000569B5_01	CRISM	07/12/2020	14:39:39	327.36
MSV0005724B_01	CRISM	03/01/2021	14:36:22	341.84
MSV00057792_05	CRISM	19/01/2021	14:29:17	350.42

Table 6 CRISM observations with cloud observations in VNIR wavelengths

Figure 10 and Figure 11 show examples of cloud observations from CRISM and OMEGA respectively. All images listed in the inventory have been added to the Annex for reference.

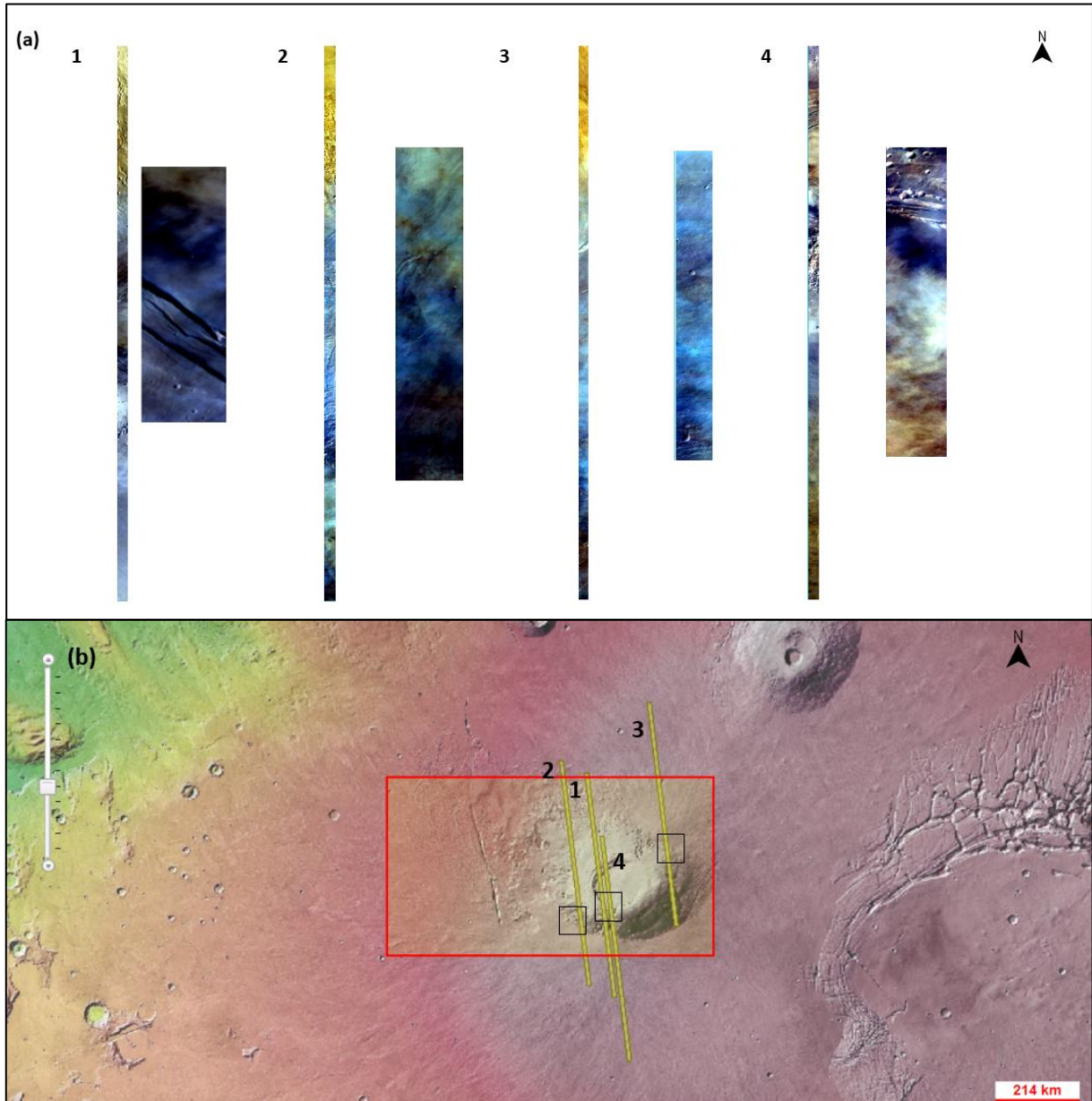


Figure 10 Examples of cloud images obtained from CRISM sensor with entire data strip on the left and zoomed cloud image on the right. Images appear bluish white in the specified band combinations

(a) image 1: HSP0003E425_03; 30th August 2016, Ls: 213.60° with RGB combination (52,35,25)

image 2: MSP0002CA4B_01; 9th December 2013, Ls: 60.20° with RGB combination (5,2,1)

image 3: MSP00038012_01; 2nd September 2015, Ls: 36.20° with RGB combination (5,2,1)

image 4: MSV00038530_01; 24th September 2015, Ls: 45.88° with RGB combination (42,31,21)

(b) Footprints of images shown in Figure 10 (a). The red box shows the spatial extent considered for the study and the scale corresponds to the entire image. Black boxes show the locations of the clouds observed

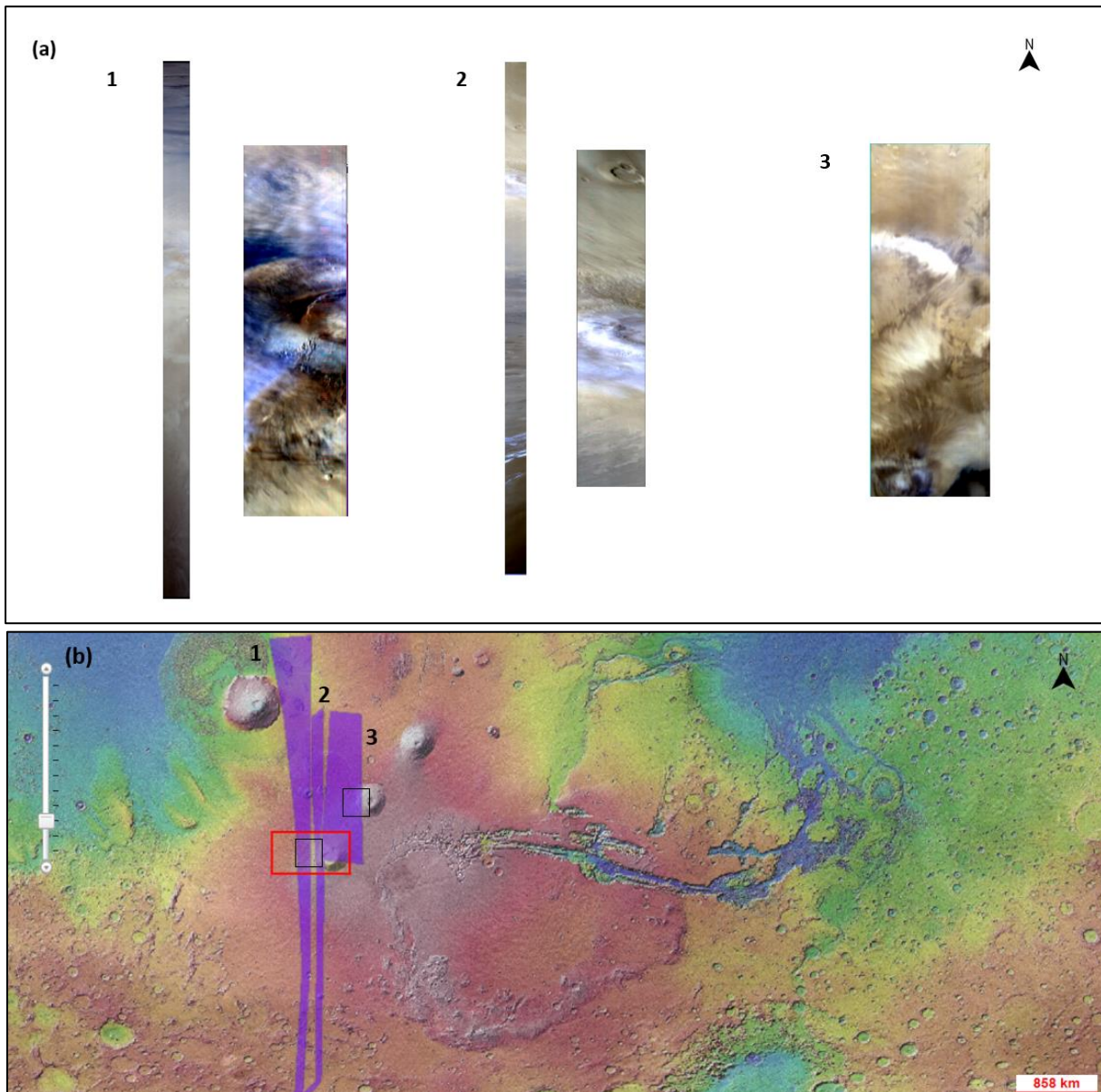


Figure 11 Examples of cloud images obtained from OMEGA sensor with entire data strip on the left and zoomed cloud image on the right. RGB combination (47,33,24) for all images.

(a) image 1: ORBL135_0; 20th September 2020, Ls: 281.28°

image 2: ORBL142_0; 22nd September 2020, Ls: 282.54°

image 3: ORB7705_2; 5th January 2010, Ls: 33.69°

(b) Footprints of images shown in Figure 11 (a). The red box shows the spatial extent considered for the study and scale corresponds to the entire image. Black boxes show the locations of the clouds observed

4.2. Cloud Morphologies

Interpretation of cloud morphologies was concluded after visual inspection of all OMEGA and CRISM observations studied during this research. There were five major kinds of morphologies that have been observed. Among these morphologies, four (streaky, spiral, small cloudy regions and elongated orographic clouds) match with the types observed in previous studies, while one represents a previously unreported cloud morphology.

4.2.1. Cloud streaks or cirrus clouds

Cirrus or streaky cloud was the second most observed morphology in this study. Generally streaky clouds can be observed in both dust and condensate clouds (Kahn, 1984). In this study, visual inspection and spectral analysis (explained in section 4.3) of streaky clouds did not reveal any traces of dust in the clouds. Furthermore, there were also variations in the pattern of streaky clouds ranging from blurred to wavy filaments which will be further discussed in Chapter 5. Streaky clouds were observed only in CRISM images. Figure 12 (a.1) shows an example of streaky cloud.

4.2.2. 'Puffy' cloud

A different kind of cloud morphology was discovered in this study which resembles a 'puffy' shaped cloud. The patterns in the cloud resemble somewhat that in the plume type cloud (mentioned in Chapter 1.2). However, plume cloud morphology is studied to be present in the 90° – 180° Ls in Tharsis region (French et al., 1981), which does not match with the Ls of this cloud observation. The puffy cloud was observed in Ls 67.57° which also indicates that it occurs in the Southern autumn season. Cumulus clouds are observed to be fluffier in appearance, whereas this observation shows distinct bubble-like patterns in its structure. Figure 12 (a.2) shows an example of puffy cloud.

4.2.3. Spiral cloud

An interesting morphology observed in one of the CRISM multispectral images includes the spiral cloud. Occurrences of spiral clouds have been recorded previously with varying seasonal and extents on Mars. A specific kind of spiral cloud was previously discovered on Arsia Mons which was noted to occur only in a particular season (Rafkin et al., 2002). This phenomenon is caused when the sun warms up the air near the slopes of the volcanic mountain. Consequently, the fine sediments blow up and form a spiraling cloud. Previous observations show that the Arsia Mons spiral cloud is composed of dust, however dust was not identified in this observation after visual inspection and spectral analysis (discussed in section 4.3). The spiral cloud observed in this study occurs in Ls 43.59° and hence the same season (Southern Autumn) as the Arsia Mons dust spiral cloud. The disc of the spiral cloud can also be seen in the image obtained as showed in Figure 12 (a.3)

4.2.4. Small cloudy regions

Most of the observations obtained were classified as small cloudy areas. These include small rounded/clumpy clouds, cumulus shaped clouds and hazy areas. However, the possibility that these may be a part of a larger cloud remains, which will be further discussed in chapter 5. There is no particular seasonal occurrence that could be inferred for this morphology as they were observed in almost all seasons. Figure 12 (a.4) shows an example of small cloud regions.

4.2.5. Orographic clouds

A new observation of an elongated orographic cloud was discovered in this study at Pavonis Mons, the neighboring volcano to Arsia Mons as shown in Figure 12 (a.5). The cloud resembles AMEC in its appearance. The Pavonis Mons elongated cloud is observed to occur in Ls 33.69° in the Northern spring season. The cloud is observed to extend westwards which also corresponds to the lee side of the volcanic mountain. Other observations of orographic clouds were also obtained over Arsia Mons; however, they cannot be classified as elongated given the limited spatial coverage of the associated image strips. Observations of orographic clouds were only obtained from OMEGA.

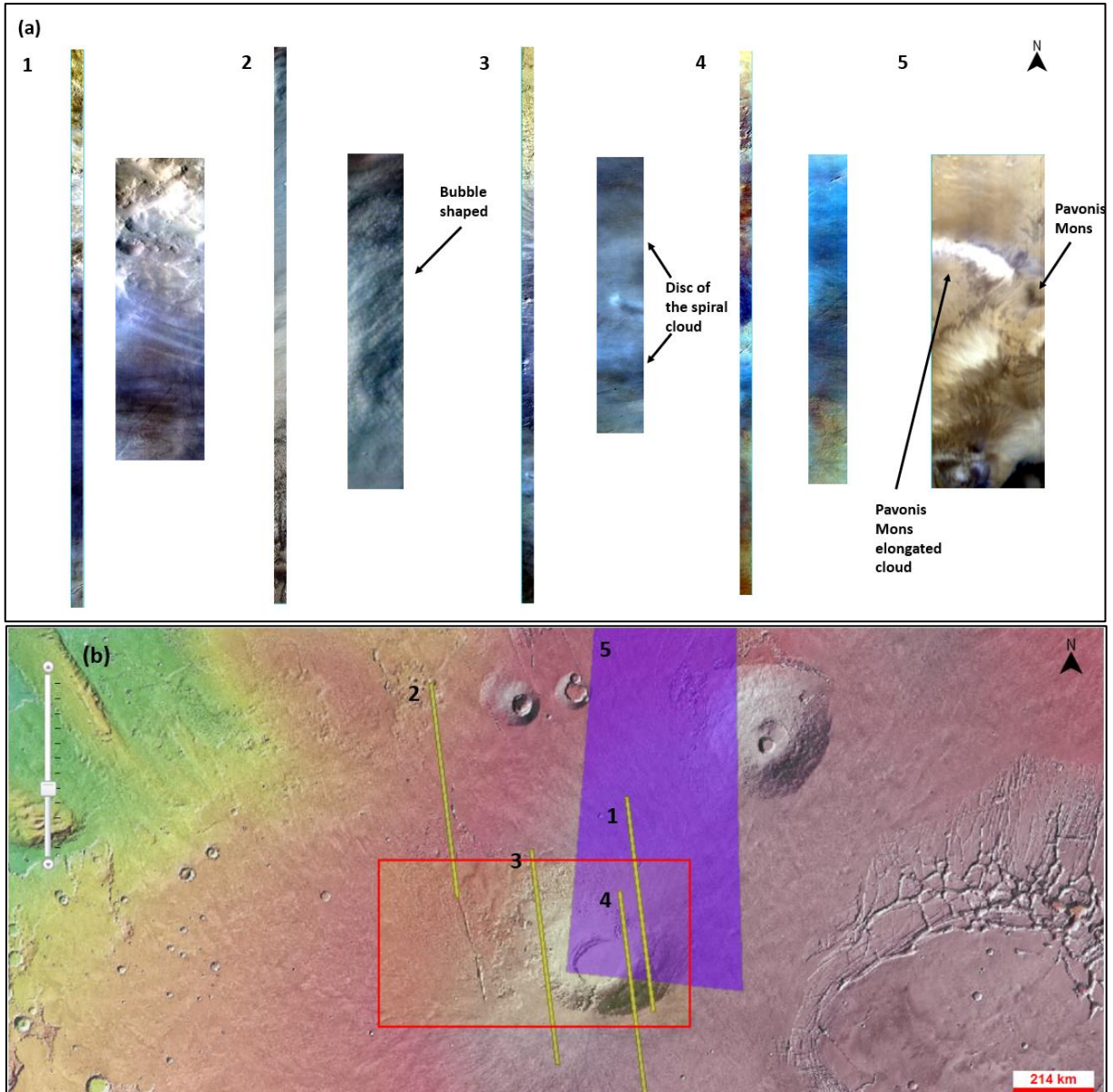


Figure 12 Examples of cloud morphologies obtained from CRISM and OMEGA with entire.

(a) entire data strip on the left and zoomed cloud image on the right.

image 1: MSV0003DDA7_01; 9th August 2016, Ls: 200.55° with RGB combination is (42,31,21)

image 2: MSV0003ED27_03; 26th September 2016, Ls: 230.19° with RGB combination is (42,31,21)

image 3: MSV00038F9B_01; 12th November 2015, Ls: 67.57° with RGB combination is (42,31,21)

image 4: MSP0000332F_05; 29th November 2006, Ls: 142.62° with RGB combination is (5,2,1)

image 5: ORB7705_2; 5th January 2010, Ls: 33.69° with RGB combination is (47,33,24)

(b) Footprints of images from CRISM (yellow strips) and OMEGA (purple strip) shown in Figure 12 (a). The red box shows the spatial extent considered for the study and scale corresponds to the entire image

4.3. Spectral Analysis

The primary aim of the spectral analysis was to confirm the presence or absence of three main constituents in the obtained cloud images, namely, dust, H₂O ice, and CO₂ ice. Based on the current understanding of atmospheric dynamics and chemical processes on Mars, it is assumed that these are the three main components that can compose Martian clouds. This section explains the results obtained after estimating the reflectance ratio (C_R/S_R) and difference ($C_R - S_R$) from the cloud vs non-cloud regions.

4.3.1. Identifying dust aerosols in clouds

To examine the potential presence of dust in clouds, reflectance ratio and difference obtained from the average VNIR wavelength range (0.4 μm to 1 μm) of the cloud and non-cloud regions were investigated. All cloud images listed in the inventory were analysed and studied for this purpose except for images with full cloud coverage as stated in section 4.1. The analysed cloud observations based on the reflectance plots for both ratio and difference did not show any significant evidence for the presence of dust. Figure 13 and 14 show examples of plots obtained after performing ratio and difference to the reflectance values. Figure 13(a) and (b) correspond to CRISM observations HSV00021A3A_05 and MSV0004C0D6_01 respectively. The spectral graphs on the left present the resultant spectra after performing reflectance ratio. It can be observed that the slope approaches to 1 confirming lack of dust contribution in the cloud examined. Spectral graphs on the right present the resultant spectra after calculating reflectance difference where, the slope of the difference spectra approaches 0, indicating the absence of dust influence in the cloud. Spectra for reflectance ratio and difference corresponding to all the studied cloud images have been listed in the Annex.

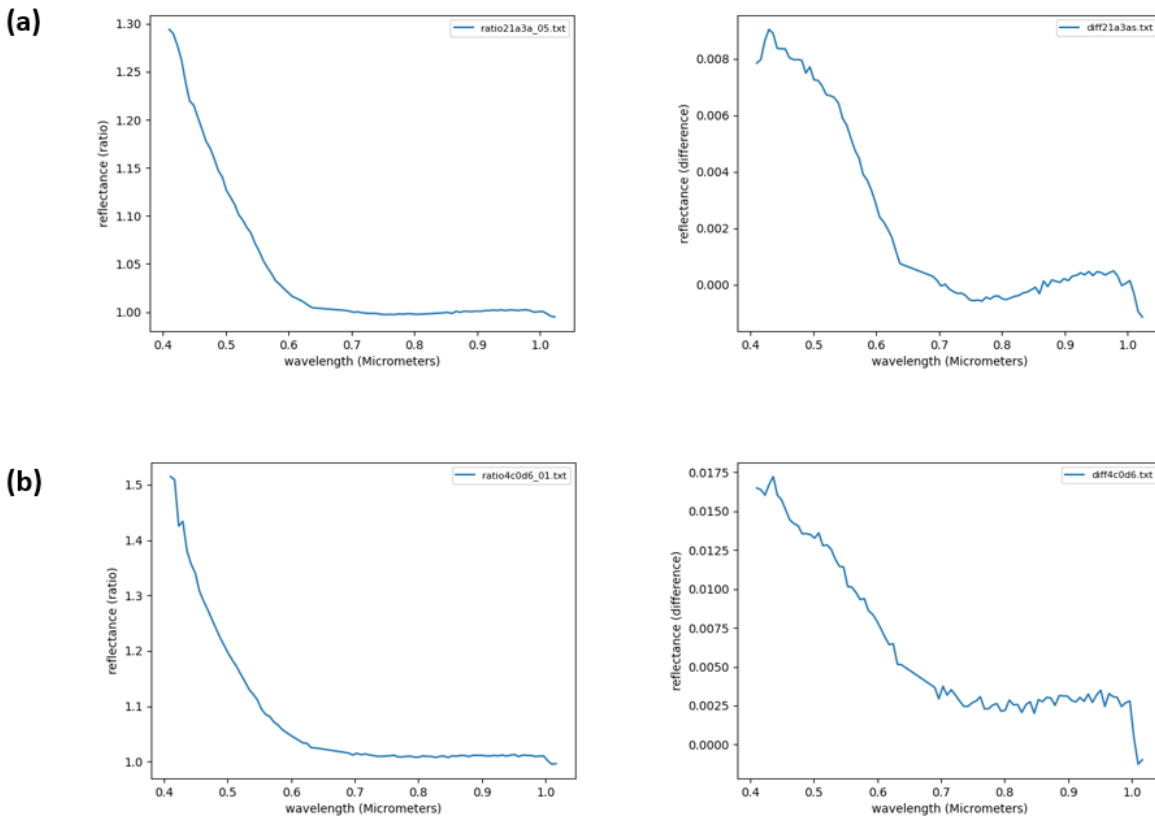


Figure 13(a) reflectance ratio (left) and difference (right) for HSV00021A3A_05; (b) reflectance ratio (left) and difference (right) for MSV0004C0D6_01 in the wavelength range 0.4 μm -1 μm

Figure 14(a) and (b) correspond to OMEGA observations ORBL142_0 and ORBL424_0 respectively. Results from OMEGA cloud images show similar spectra to CRISM results with the reflectance ratio approaching 1 and difference approaching 0 indicating no dust contribution.

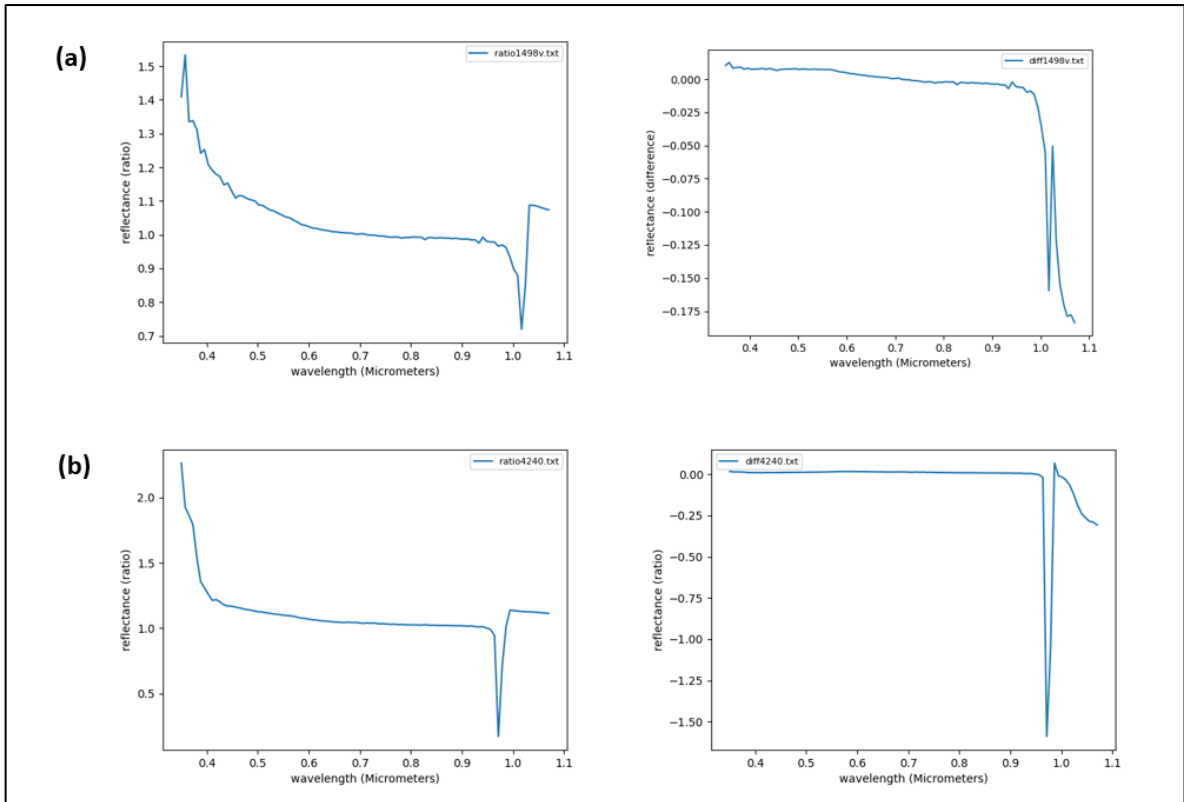


Figure 14 (a) reflectance ratio (left) and difference (right) for ORBL142_0; (b) reflectance ratio (left) and difference (right) for ORBL424_0 in the wavelength range 0.4 μm - 1 μm

Reflectance spectra derived from this study were further compared with the dust spectrum obtained from the CRISM spectral library (*CRISM Spectral Library*, 2001). Figure 15 (a) and (b) shows the reflectance spectra obtained for cloud observations in HSV00021A3A_05 and ORBL142_0 respectively plotted with the CRISM spectral library dust spectra. It can be noted that dust clearly shows an increasing slope from 0.4 to 1 (orange) while the results obtained in this study (blue) show no such indication, thus concluding that these clouds do not show indications of dust composition.

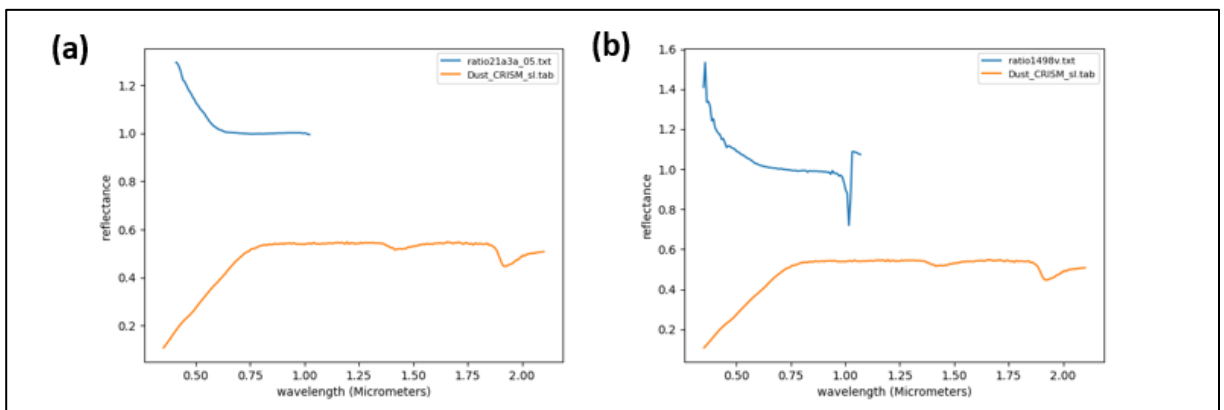


Figure 15 Comparison of resultant spectra with dust spectrum from CRISM spectral library (a) CRISM observation: HSV00021A3A_05 (b) OMEGA observation: ORBL142_0 in the wavelength range 0.2 μm - 2 μm

4.3.2. Identifying H₂O ice and CO₂ ice clouds

Following the spectral analysis of visible wavelengths to confirm the presence or absence of dust, wavelength ranges containing the NIR (Near-Infrared) channels were examined to detect evidence for the presence of H₂O ice or CO₂ ice in clouds. OMEGA datasets have been extensively used in the past to identify the CO₂ ice absorption feature at 4.26 μm (Mid infrared range). This study will focus on identifying the presence of H₂O ice or CO₂ ice based on their absorption features in the near infrared wavelength ranges. After spectral analysis, a prominent absorption feature at around 3.2 μm was noted in both reflectance ratio and difference spectra obtained for clouds in this study, indicating the presence of H₂O ice. All images listed in Table 4 and 5 were analyzed except those with full cloud coverage as stated in section 4.1. Figure 16 shows an example of reflectance spectra obtained after performing ratio and difference to the reflectance values for an image in CRISM observation (MSP00021FDD_01). Results after performing reflectance ratio and difference have been depicted in the left and right image respectively, showing the prominent water-ice feature at around 3.2 μm . The spectral results for all images can be referred to in the Annex.

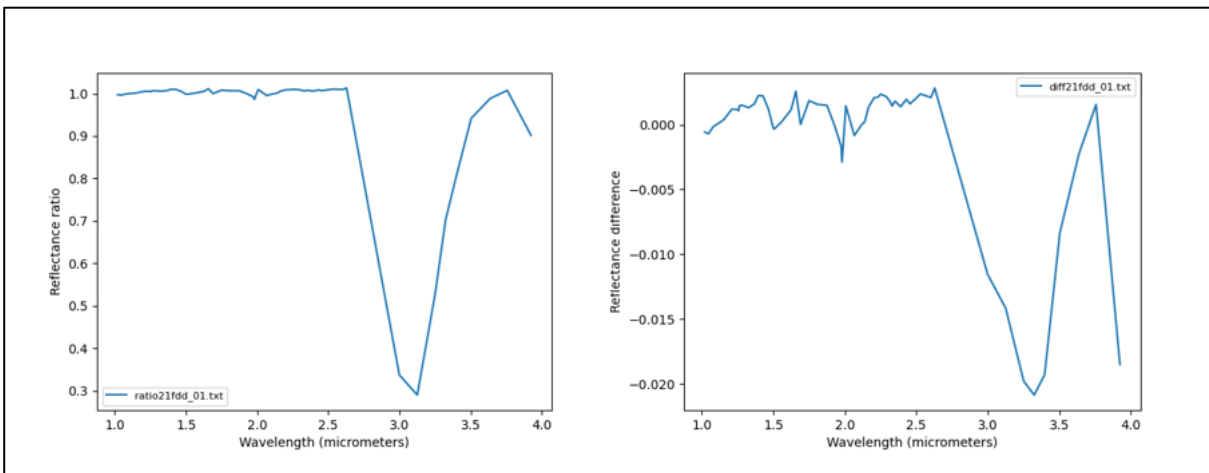


Figure 16 reflectance ratio (left) and difference (right) for MSP00021FDD_01 in the wavelength range 1 μm -4 μm

Only two OMEGA images could be spectrally analyzed for identifying H₂O ice and CO₂ ice due to data availability and sensor malfunctioning, which will be further discussed in Chapter 5. Figure 17 (a) and (b) show the spectral analysis results obtained for OMEGA observations ORB1316_2 and ORB2274_3.

- Figure 17(a): A prominent H₂O ice absorption feature is observed around 3.2 μm in the reflectance ratio spectrum (left image). Reflectance difference shows a less pronounced absorption depth of the feature, although it is noticeable that the absorption around 3.2 μm is stronger than in other wavelengths. This indicates the potential presence of water ice in the cloud associated with observation ORB1316_2.
- Figure 17 (b): Resultant spectra obtained from the reflectance ratio (left image) and difference (right image) shows absorption increasing towards 3 μm and then decreasing abruptly stopping around 3 μm . Since no strong absorption feature can be observed

around 3.2 μm , it is inferred that there is no indication that the cloud associated with observation ORB2274_3 contains water-ice from the interpretation of the near infrared part of the spectrum. Since the spectra also do not match with the CO₂ ice spectrum (as shown in Figure 9, there is no indication showing the presence of CO₂ ice either.

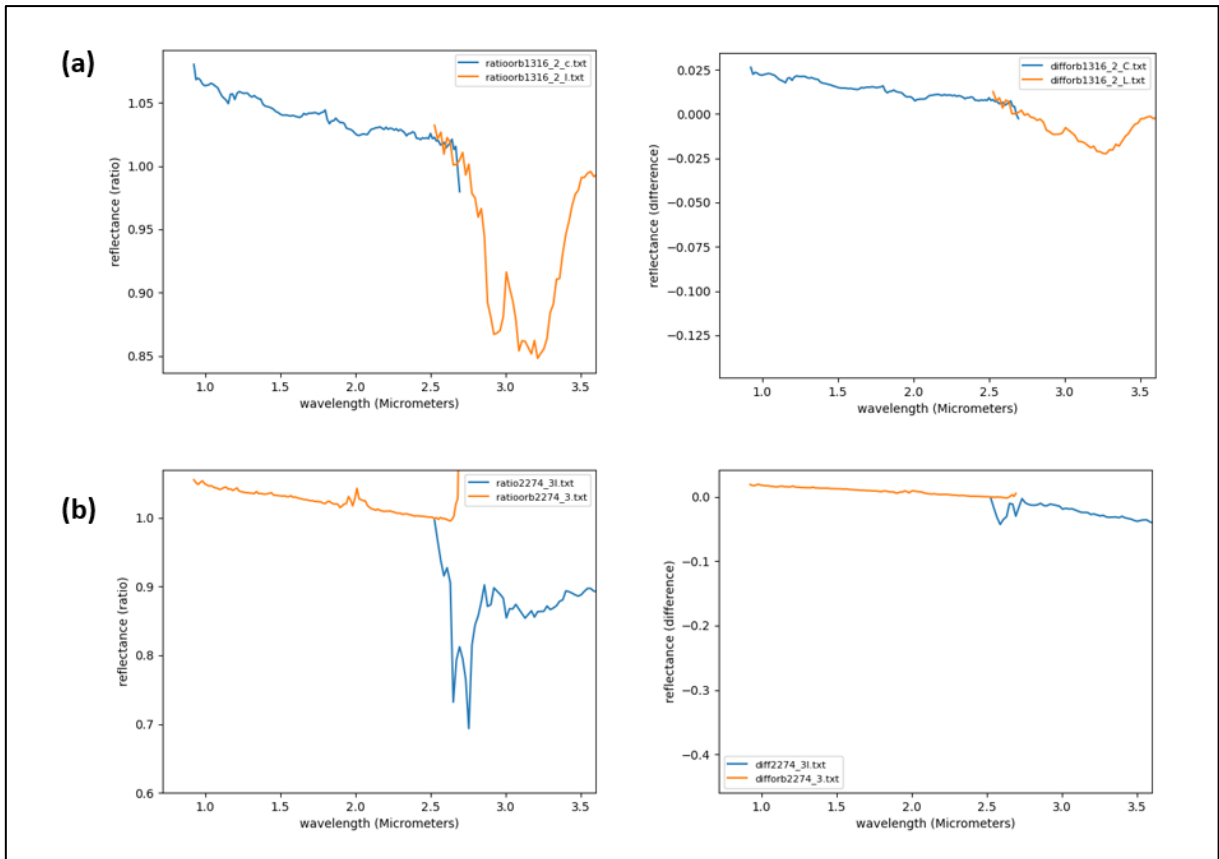


Figure 17 (a) reflectance ratio (left) and difference (right) for ORB1316_2 in the wavelength range 0.8 μm – 3.6 μm
 (b) reflectance ratio (left) and difference (right) for ORB2274_3 in the wavelength range 0.8 μm – 3.6 μm

5. DISCUSSION

This chapter discusses the research techniques utilized, the results obtained thereafter and the various aspects that were considered during the course of this study. It will progress with the details of data collection, visual inspection and identifying cloud morphologies, spectral processing to estimate cloud composition and limitations of the proposed methods.

5.1. Data collection

The study area for this research was chosen as Arsia Mons because of its history of exhibiting unique and varied kinds of cloud structures as opposed to other regions on Mars. Recently, a mysterious cloud phenomenon called the Arsia Mons Elongated Cloud (AMEC) was discovered accidentally by the VMC (Visual Monitoring Camera) onboard the Mars Express mission. Later, it was found that the cloud had been occurring since the Viking era but had never caught scientists' attention. In addition, other distinct cloud occurrences such as Spiral and Aster clouds are also observed in the Arsia Mons region, making it an interesting region for studying Martian clouds. As discussed in Chapter 2, OMEGA and CRISM are two imaging spectrometers onboard Mars missions which have been used for spectral investigation of surface and atmospheric elements. This study utilized spectral datasets from both sensors to characterize and analyze cloud occurrences in the Arsia Mons region. Figure 18 is a map of Arsia Mons region showing the distribution of clouds (considered as centrepoin of the cloudy region) as collected from both sensors. There were few OMEGA observations acquired as compared to CRISM observations in this study. Figure 19 shows a graph of the Arsia Mons region and distribution of the collected cloud observations in the four main Ls ranges or Martian seasons.

During data collection, it was found that OMEGA SWIR channels (C and L) were broken after the year 2009. This meant that spectral data after 2009 was not useful for the study of cloud constituents such as H₂O ice and CO₂ ice. This restricted the available data for studying the spectral absorption features of clouds that were present in the OMEGA datasets. CRISM datasets were obtained for studying the afternoon clouds in the AMEC months. The multispectral and hyperspectral survey modes of CRISM were collected for 18 years, ensuring sufficient data to carry out the research objectives. None of the OMEGA and CRISM images obtained could have captured the AMEC, given that the AMEC occurs between 5 to 8 LTST and the data acquired at the earliest local time was around 10 AM LTST from both sensors. Thus, this research focusses on the clouds that form after the AMEC from the acquired data. CRISM datasets were obtained for studying the afternoon clouds in the AMEC months. The multispectral and hyperspectral survey modes of CRISM were collected for 18 years, ensuring sufficient data to carry out the research objectives.

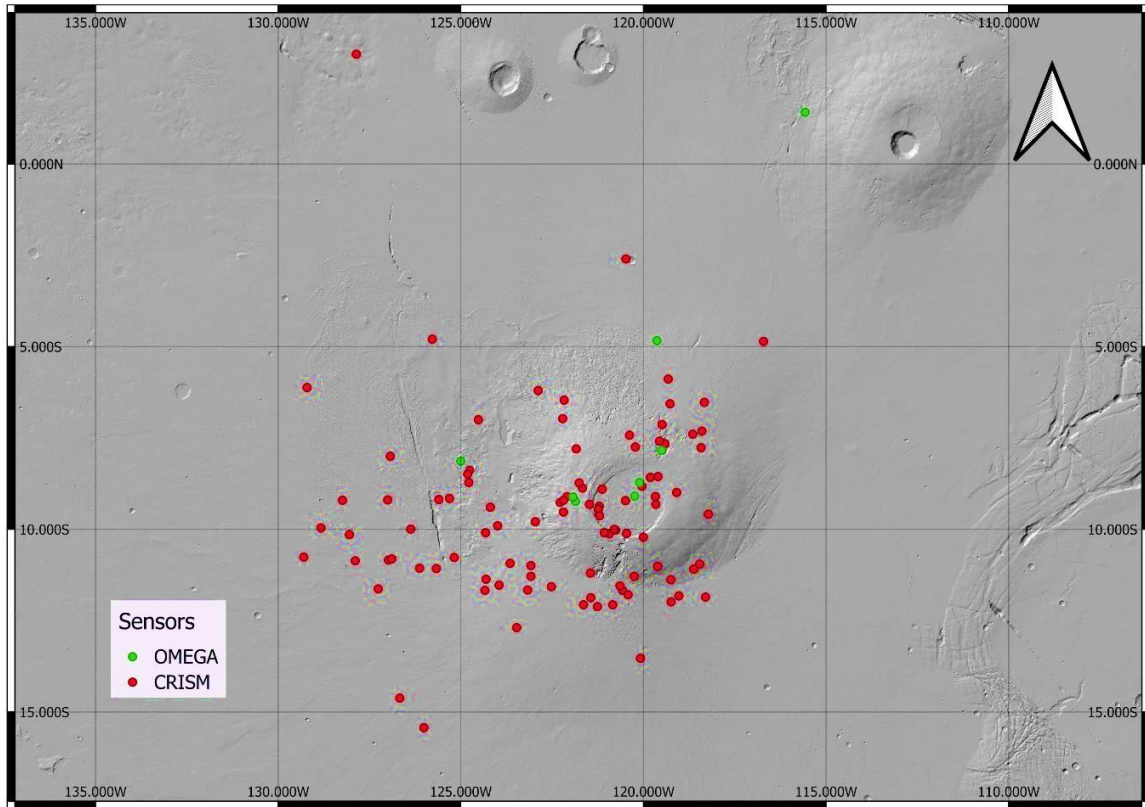


Figure 18 Distribution of cloud observations obtained from OMEGA and CRISM sensors.

Furthermore, distribution of cloud observations in the various seasons showed the highest occurrence in the Ls range 270° - 360° (Southern Summer) and the least in the Ls range 90° - 180° (Southern Winter). Figure 19 shows the frequency of cloud observations acquired in the four seasons (Ls ranges). The higher occurrence of clouds in Southern summer maybe attributed to a number of atmospheric conditions such as temperature and humidity gradients as well as atmospheric circulation.

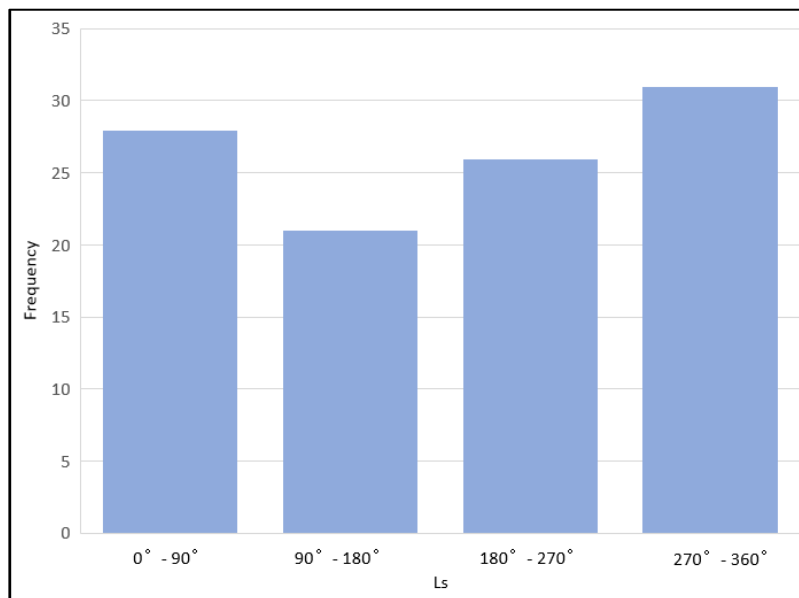


Figure 19 Cloud observation distribution in the Ls ranges

5.2. Visual inspection and identifying morphologies

Before processing the images to inspect their spectral properties, I performed a visual inspection to filter out the images that contained clear indications of the presence of a cloud. A total of 102 cloud observations were collected and utilized for identification of cloud morphologies and further spectral analysis. Four main kinds of cloud morphologies were found in this study. It was realized that the identification of morphologies is greatly influenced by the resolution of the sensor and footprint of the image. OMEGA images had varying resolution (ranging from mid to high resolution). The morphology of clouds observed by OMEGA was mostly observed to be orographic clouds forming on the lee side of the mountain. CRISM's higher resolution has aided in revealing many different cloud morphologies. This included observations of streaky clouds, spiral cloud, 'puffy' cloud, and smaller cloud regions.

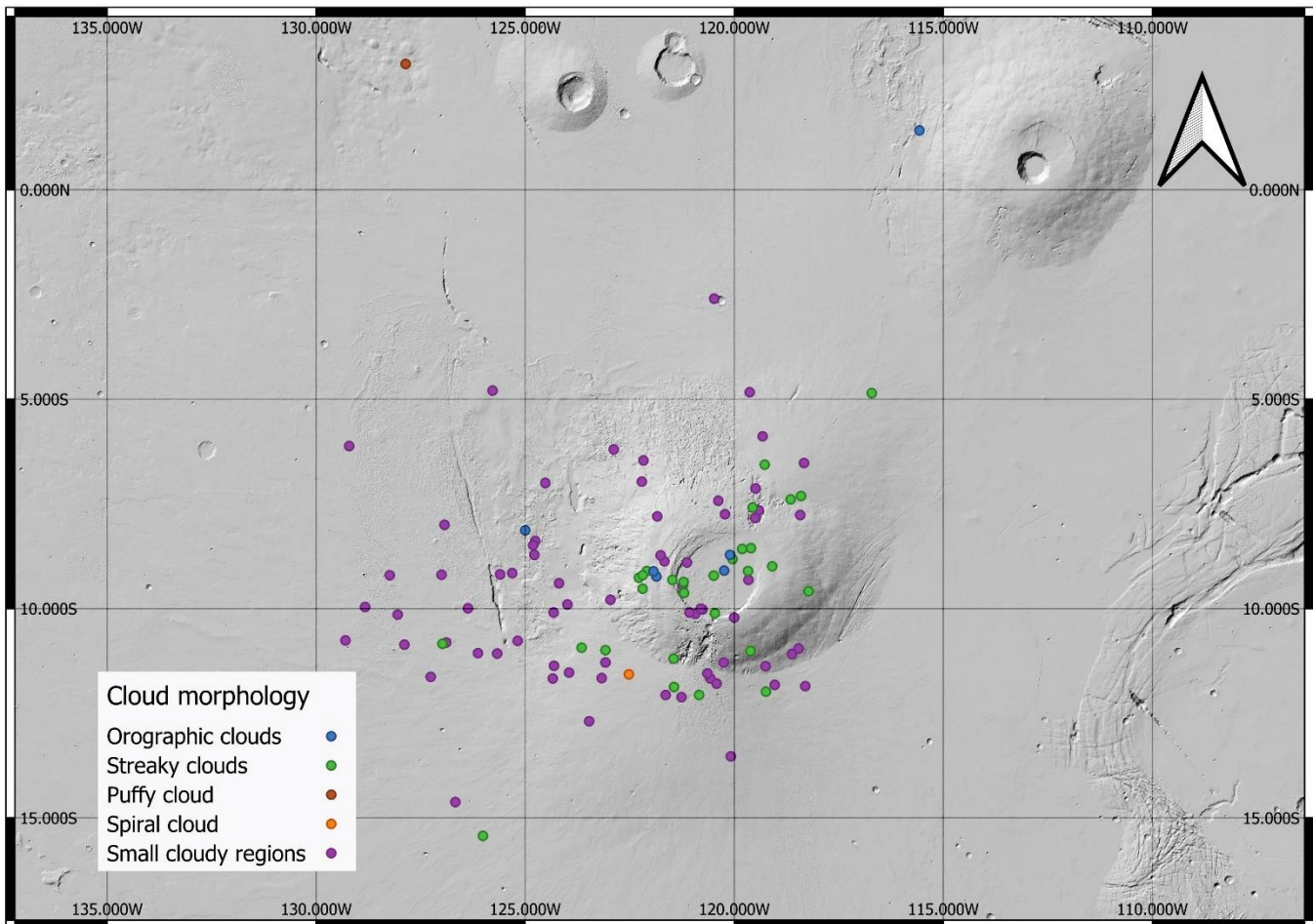


Figure 20 Morphologies observed in the collected cloud observations

Figure 20 shows the distribution of cloud observations and their morphologies. Orographic clouds were observed to occur on the lee side of the volcanic mountains, Arsia Mons and Pavonis Mons. This also includes the elongated cloud observed at Pavonis Mons extending to the west or the leeward side. Streaky clouds were noted to be more concentrated nearer to the caldera of the Arsia Mons volcano with few observations towards the base of the volcano and farther away. There was only one observation of puffy cloud morphology which is observed to occur far west of the Pavonis Mons volcano at 127.86°W and 2.97°N . The location of the cloud suggests that it might be related to the cloud occurrences observed in the Pavonis Mons region. Spiral cloud observation was spotted towards the base of the volcano at 122.52°W and 11.44°S . Spiral clouds in Arsia Mons are a rare and seasonal phenomenon which occur only in the southern autumn (Rafkin et al., 2002). The occurrence of the spiral cloud in this study was noted to be in the same season as previous observations (Ls 43.59°). However, the Arsia Mons spiral clouds observed in the past were studied to be dust clouds whereas the observation obtained in this research was inferred to be composed of water ice after spectral analysis. Small cloudy regions were the most observed cloud morphology type which were observed to be concentrated in a more linear pattern west of the Arsia Mons volcano. Figure 21 shows the number of cloud morphologies observed for the entire study with most clouds being observed as small cloudy regions.

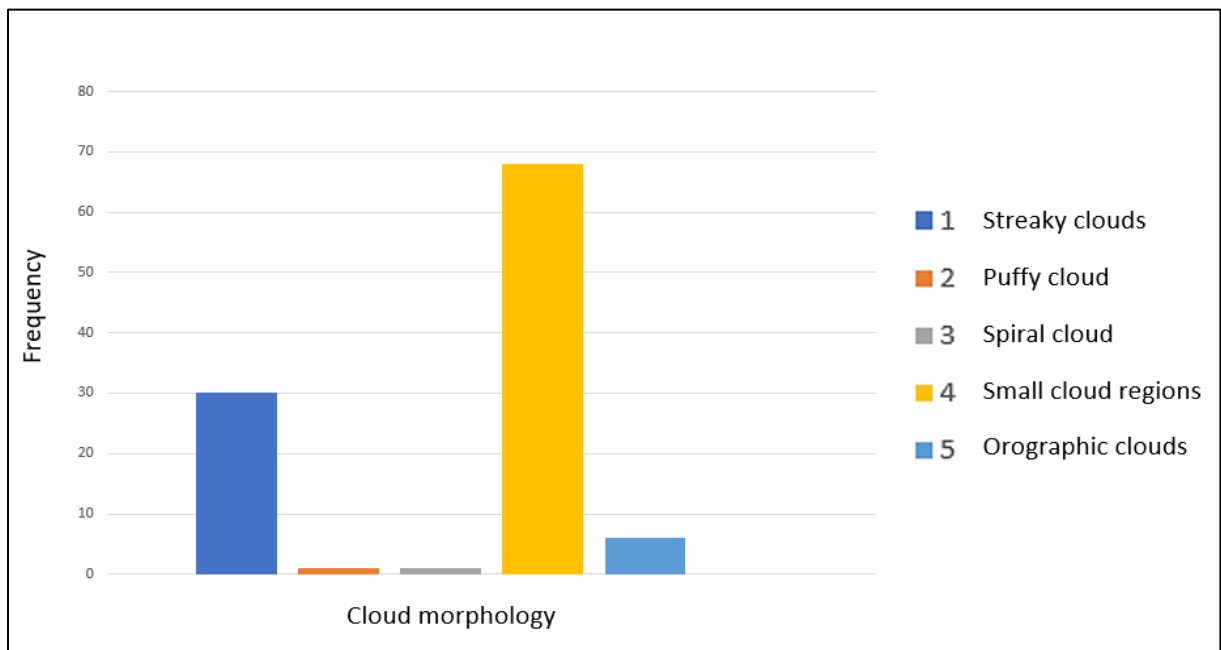


Figure 21 Total number of cloud observations for each morphology

Figure 22 represents the distribution of cloud observations in the AMEC occurring seasons (220° to 320° Ls) as opposed to other seasons. Clouds in the AMEC seasons were observed to be a bit more widespread across the N-S extent of the volcano's caldera, while in other months they are mostly concentrated nearer to the volcano. However, these interpretations are subject to observational bias based on the time period and datasets selected.

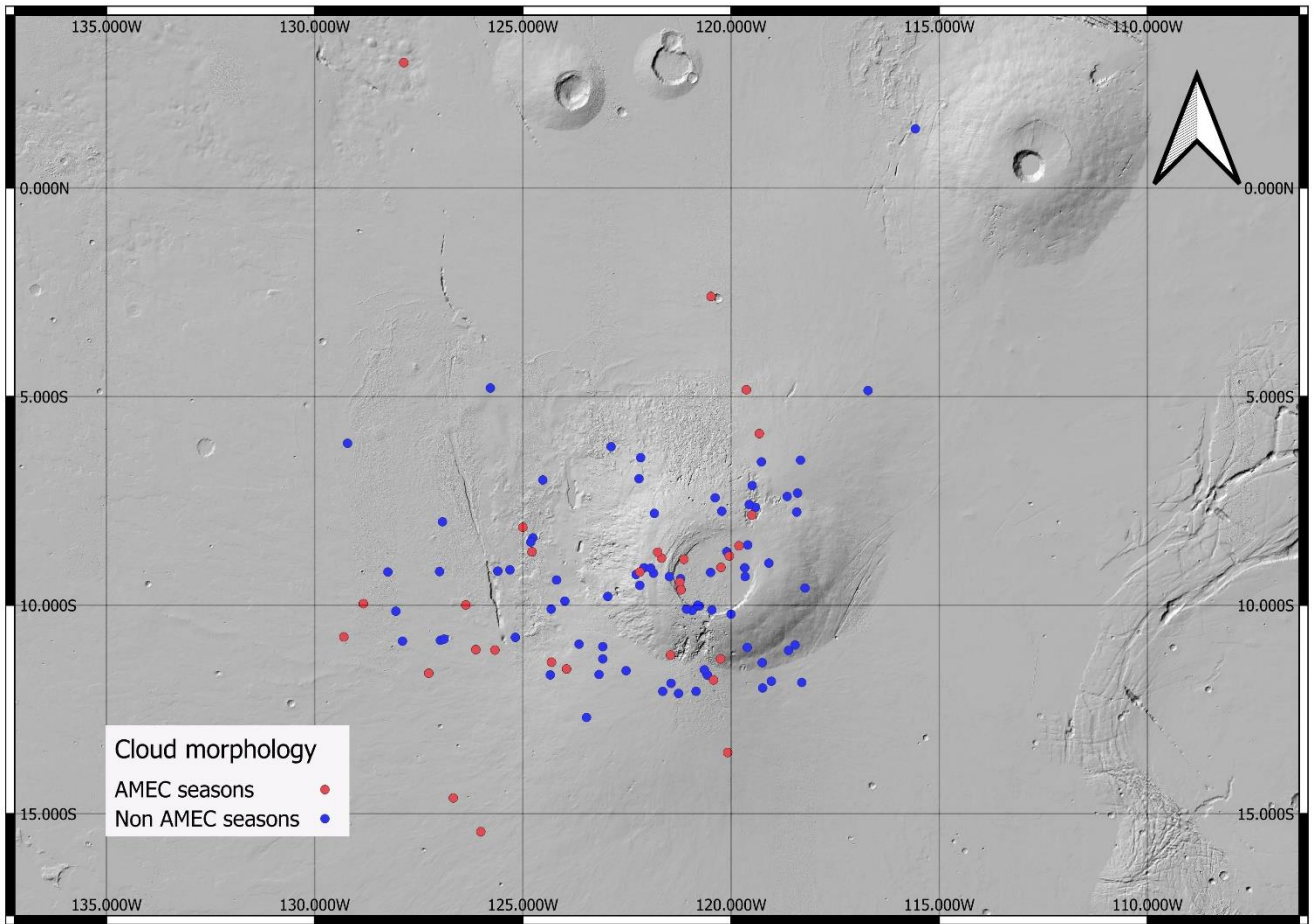


Figure 22 Cloud occurrences in the AMEC vs non-AMEC seasons

5.3. Spectral Analysis

The following section discusses the details of the techniques used to investigate the spectral characteristics of clouds and assumptions considered, selection of ROIs, interpretation of the reflectance curves obtained.

5.3.1. Technique used for spectral investigation

This study sought to investigate the cloud composition using a simple spectral method proposed previously (Vincendon et al., 2011). The employed methodology is considered to be an effective technique to investigate clouds, providing a preliminary assessment of their constituents. However, the technique also includes certain assumptions related to the energy interaction process such as scattering and transmission which can impact the accuracy of the results. Equation 1 stated in section 3.3 attempts to estimate the values for transmission factor (C_T) and cloud reflectance from scattering (C_S), based on the measurements derived from C_R (Reflectance over the cloud area) and S_R (reflectance obtained over the surface area without clouds). Since the formula contains two knowns (C_R and S_R) and two unknowns (C_T and C_S), certain assumptions need to be considered to calculate the unknown variables. The assumptions considered in the original method include the following:

- **Reflectance ratio:** The effect of the light scattered downwards by the cloud and upwards from the surface to the cloud is neglected considering the smaller extent and altitude of the clouds. This means it can be effective to analyze streaky and small clouds but may not be as effective for hazy cloud regions or puffy clouds which are noted to occur in a larger spatial extent.
- **Reflectance difference:** The transmission factor accounts for multiple scattering within the cloud and is assumed to be close to 1. Two things can be understood from this. Firstly, the clouds are assumed to be smaller in extent and occurring at higher altitudes. Clouds at higher altitudes are typically thinner as compared to low altitude clouds, due to which the transmission through these clouds is considerably higher with minimal scattering and absorption effects. Secondly, the transmission of the atmosphere has not been considered in this equation, which is also related to the assumption that the clouds considered are at higher altitudes. Since high altitude clouds are located above a significant portion of the atmosphere, there is minimal attenuation and scattering encountered by the light passing through these clouds. Consequently, atmospheric transmission becomes less significant and can be neglected for high altitude clouds.

Thus, the equation seems to be more effective for high altitude clouds as compared to clouds that are present at lower altitudes. Since the Arsia Mons volcano is an extremely elevated region on Mars, the technique provides reasonable results for the clouds in this study. Furthermore, since the equation assumes higher altitude clouds, it does not take into account the changes in surface variations, as there is very less influence of the

reflectance of the surface due to the large difference in the distance of the cloud from the surface. This might not be true for the volcanic mountain since it is already positioned at a higher altitude. To ensure robust conclusions additional modelling techniques should be employed which can give an insight into the cloud spectral properties such as optical depth, particle size as well as accurate discrimination of the surface and cloud spectra, which were out of the scope of this research due to time constraints. Nevertheless, the method proves to be an effective means to obtain reliable results with a primary estimation of cloud constituents.

5.3.2. Selection of ROIs

In order to estimate the values of C_R and S_R , ROIs were created in the images corresponding to 'cloud' and 'non-cloud' regions. The extent of cloud coverage within each strip varied from minimal to extensive, making the selection of ROIs a challenging task. For example, images with significantly higher cloud coverage require careful selection of ROIs to ensure that the non-cloud region does not have any influence of clouds and can be discriminated efficiently. Ensuring the selected ROIs have enough representation from each region can be tricky in this instance. This can lead to misclassification and consequently wrong spectral interpretations. Additionally, images with full cloud coverage were not considered for spectral analysis as they did not allow for the specification of the non-cloud region. Considering these factors, it was estimated that a maximum of five ROIs were suitable with enough pixel coverage of more than 100 pixels in each region. The next factor which affected the selection of ROIs was the influence of surface elevation. Classes selected from different surface elevations can influence the total atmospheric column making it difficult to compare the results from both regions. Image strips obtained at the base of the mountain did not show much difference in their surface elevations ensuring little to no changes in the total atmospheric column. Figure 23 shows an example of CRISM observation (MSP0002B66D_01) and its resultant spectra. The strip covers a footprint with relatively same average elevation. Hence, when the reflectance from the two ROI regions is divided, the CO_2 column at $2 \mu\text{m}$ does not influence the final spectra as shown in Figure 23(a). However, it is noted that reflectance difference still shows the absorption features at $2 \mu\text{m}$ in Figure 23(b). This is because spectral subtraction does not explicitly eliminate the prominent CO_2 absorption feature which is a characteristic feature of the Martian atmosphere. On the other hand, reflectance ratio normalizes the spectral response for the entire spectrum causing the CO_2 absorption feature to become less prominent. Images which extend across the caldera of the Arsia Mons mountain in N-S extent experience drastic difference in their surface elevation. Since the strip covers an area along the slope of the mountain, the elevation keeps changing every few pixels further. In this case, the ROIs are specified either if the two regions are closer in the image strip (which would still account for slight changes in the air column), or they were present at the same elevation on either side of the mountain. Figure 24(a) and (b) shows an example of spectra

when the surface elevations are extremely different. Figure 24(c) shows the footprint for the corresponding CRISM image strip



Figure 23 CRISM observation MSP0002B66D_01 (a) reflectance ratio (b) reflectance difference (c) footprint of image strip

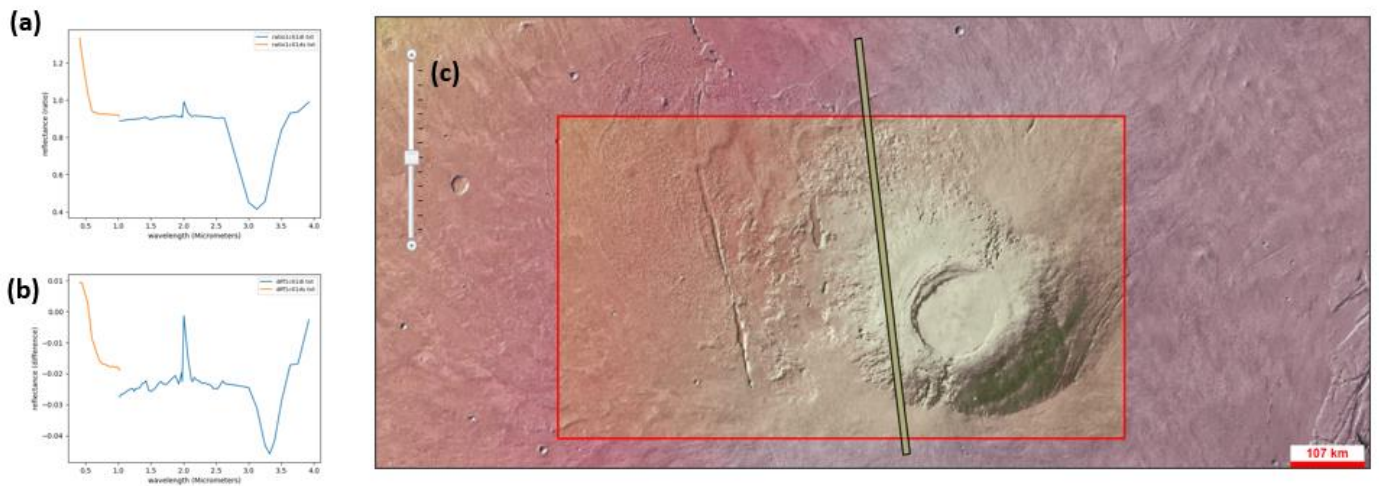


Figure 24 CRISM observation MSP0001C61D_01 (a) reflectance ratio (b) reflectance difference (c) footprint of image strip

5.3.3. Interpretation of spectral results

The final processing of the ROIs for the cloud and non-cloud regions is compared followed by applying Equation 1 as discussed before to find the reflectance ratio and difference. OMEGA and CRISM datasets showed consistent results showing no detections of dust. The spectral plots obtained for the two regions show no major differences in the absorption features except that the cloud regions show a higher absorption at 3.2 μm . Since 3.2 μm is a characteristic feature of water ice, it is inferred that the cloud has a strong absorption for water ice particles. Small absorption features in addition to discrepancies in the spectral results are attributed to spectral noise in the utilized data. Furthermore, spectral library containing different components analyzed and compared during this research have been represented in Figure 25. CRISM and OMEGA refer to the water ice spectra obtained in this study, along with frost, water ice, carbon dioxide ice and methane spectra from the ENVI spectral library. Water ice spectra obtained from the ENVI spectral library is observed to show sharp absorption at 1.5 and 2 μm as well whereas this feature is not prominent in the water-ice present in clouds studied in this research.

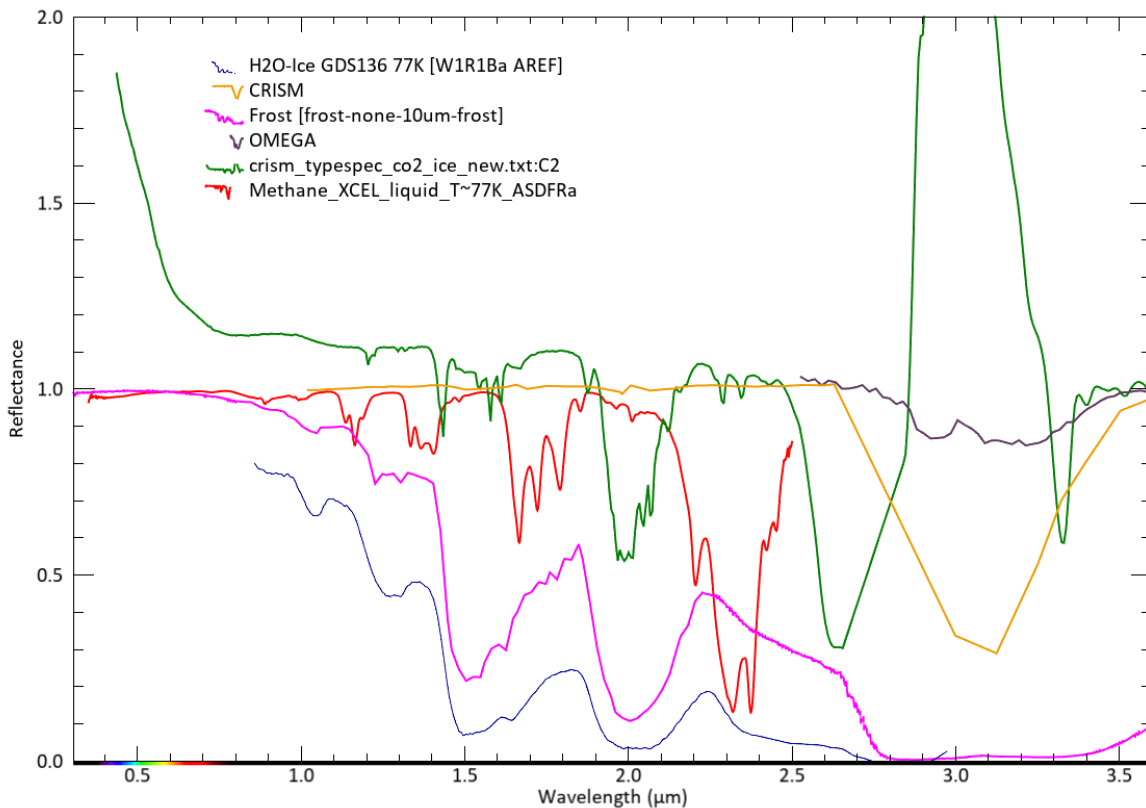


Figure 25 Spectral library of observed and compared cloud constituents

6. CONCLUSIONS AND RECOMMENDATIONS

The objective of this study was to study the cloud features over the Martian volcano, Arsia Mons using spectral datasets. The recent mysterious cloud formation, AMEC along with other distinct types of cloud occurrences seen particularly in the Arsia Mons region was the motivation to select this study area. OMEGA and CRISM datasets were used to detect clouds, identify their morphologies, and investigate the constituents of clouds.

More than 100 observations of clouds could be collected during the study from the two sensors which were further used for analysis. CRISM images provided high resolution images which made it possible to clearly inspect the clouds and their features. OMEGA images ranged from middle to high resolution, providing images with wider footprint that aided in better interpretation of the cloud extent. Five kinds of cloud morphologies were identified in total. This included the elongated cloud orographic cloud observed at Pavonis Mons in the course of this research along with a new and relatively recent observation of spiral cloud which was seen previously in the same season (Southern autumn). A distinct cloud morphology observed includes the puffy cloud which occurs in the Pavonis Mons region and does not match the cloud morphologies studied previously.

The methodology of this research is continued with the spectral investigation of cloud data. Reflectance ratios and differences were calculated utilizing the cloudy regions and the non-cloudy regions to identify the absorption features of cloud constituents. The visible wavelength range was used for identifying absorption slope resembling spectra of dust features, which did not show up in any of the analyzed spectra. Furthermore, the presence of water-ice and carbon-dioxide ice were investigated using the near infrared wavelength range. It was found that all clouds indicated the presence of water-ice, with one OMEGA observation as an exception which showed no indication for the presence of water ice or carbon dioxide ice composition.

Clouds that could be a part of the AMEC could not be identified due to the data unavailability in the exact local time. However, a comparison of the clouds in the AMEC occurring season and other seasons does not point out any major differences observed in its morphology with no differences in the constituents of the clouds. The only observational difference noted in the AMEC seasons was that the clouds were spread over a larger extent in N-S spatial extent as compared to other seasons. Furthermore, these conclusions have been drawn based on the data availability which are subject to observational bias.

The multispectral and hyperspectral datasets from both OMEGA and CRISM are effective in identifying clouds and their constituents. Though the identification of morphologies would require comparatively larger footprints in case of CRISM and higher resolution OMEGA images are more effective to be able to identify the cloud patterns. The spectral method chosen for this study is reliable to spectrally characterize clouds, primary assessment of cloud constituents and identify the presence or absence of basic cloud components such as dust, water ice and carbon dioxide ice. Results obtained from this study will be useful to understand the cloud occurrences in the Arsia Mons region in terms of its spatial and temporal variability as well as spectral characteristics. New clouds were also observed in the adjacent volcanic mountain, which encourages further studies on the clouds in the nearby regions for future research.

6.1. Recommendations

- This research mainly focused on the Arsia Mons region. Analysis of cloud images at a local level in other parts of Mars which show distinct atmospheric phenomena can help in understanding the properties of clouds in that region and might explain more about the regional cloud occurrences. The elongated cloud and the ‘puffy’ cloud observed at the Pavonis Mons volcanic mountain in this study indicate there are interesting cloud occurrences that can be studied in this volcanic region too.
- The elongated cloud at Pavonis Mons resembles the AMEC in its shape and further investigation of the microphysics or structure of the cloud can aid in better comparison with the AMEC. It is also useful to see if observations of this cloud have been made in the same seasonal range or by other sensors.
- The spectral method applied in this study can be further backed up with modelling techniques to estimate cloud optical depth and particle sizes as a part of future work.

LIST OF REFERENCES

- Allison, M. (1997a). Accurate analytic representations of solar time and seasons on Mars with applications to the Pathfinder/Surveyor missions. *Geophysical Research Letters*, 24(16), 1967–1970. <https://doi.org/10.1029/97GL01950>
- Allison, M. (1997b). Accurate analytic representations of solar time and seasons on Mars with applications to the Pathfinder/Surveyor missions. *Geophysical Research Letters*, 24(16), 1967–1970. <https://doi.org/10.1029/97GL01950>
- Benson, J. L., Bonev, B. P., James, P. B., Shan, K. J., Cantor, B. A., & Caplinger, M. A. (2003). The seasonal behavior of water ice clouds in the Tharsis and Valles Marineris regions of Mars: Mars Orbiter Camera Observations. *Icarus*, 165(1), 34–52. [https://doi.org/10.1016/S0019-1035\(03\)00175-1](https://doi.org/10.1016/S0019-1035(03)00175-1)
- Benson, J. L., James, P. B., Cantor, B. A., & Remigio, R. (2006). Interannual variability of water ice clouds over major martian volcanoes observed by MOC. *Icarus*, 184(2), 365–371. <https://doi.org/10.1016/J.ICARUS.2006.03.014>
- Bhattacharyya, D., Clarke, J. T., Bertaux, J. L., Chaufray, J. Y., & Mayyasi, M. (2015). A strong seasonal dependence in the Martian hydrogen exosphere. *Geophysical Research Letters*, 42(20), 8678–8685. <https://doi.org/10.1002/2015GL065804>
- Bibring, J.-P., Soufflot, A., Berthé, M., Langevin, Y., Gondet, B., Drossart, P., Bouyé, M., Combes, M., Puget, P., Semery, A., Bellucci, G., Formisano, V., Moroz, V., Kottsov, V., Bonello, G., Erard, S., Forni, O., Gendrin, A., Manaud, N., ... Forget, & F. (2004). *OMEGA: Observatoire pour la Minéralogie, l'Eau, les Glaces et l'Activité*.
- Clancy, R. T., Grossman, A. W., Wolff, M. J., James, P. B., Rudy, D. J., Billawala, Y. N., Sandor, B. J., Lee, S. W., & Muhleman, D. O. (1996). Water vapor saturation at low altitudes around Mars aphelion: A key to Mars climate? *Icarus*, 122(1), 36–62. <https://doi.org/10.1006/ICAR.1996.0108>
- Clancy, R. T., Montmessin, F., Benson, J., Daerden, F., Colaprete, A., & Wolff, M. J. (2017a). Mars clouds. *The Atmosphere and Climate of Mars*, 76–105. <https://doi.org/10.1017/9781139060172.005>
- Clancy, R. T., Montmessin, F., Benson, J., Daerden, F., Colaprete, A., & Wolff, M. J. (2017b). Mars clouds. *The Atmosphere and Climate of Mars*, 76–105. <https://doi.org/10.1017/9781139060172.005>
- Clancy, R. T., Montmessin, F., Benson, J., Daerden, F., Colaprete, A., & Wolff, M. J. (2017c). *Mars Clouds*. 76–105. <https://doi.org/10.1017/9781139060172.005>
- Clancy, R. T., Smith, M. D., Wolff, M. J., Murchie, S. L., Nair, H., & Seelos, K. D. (2014). *CRISM LIMB OBSERVATIONS OF MARS MESOSPHERIC ICE CLOUDS: TWO NEW RESULTS*.
- Clancy, R. T., Wolff, M. J., Smith, M. D., Kleinböhl, A., Cantor, B. A., Murchie, S. L., Toigo, A. D., Seelos, K., Lefèvre, F., Montmessin, F., Daerden, F., & Sandor, B. J. (2019). The distribution, composition, and particle properties of Mars mesospheric aerosols: An analysis

- of CRISM visible/near-IR limb spectra with context from near-coincident MCS and MARCI observations. *Icarus*, 328, 246–273. <https://doi.org/10.1016/J.ICARUS.2019.03.025>
- CRISM Spectral Library. (2001). https://speclib.rsl.wustl.edu/detail.aspx?specimename=PN-09_CP_LT1000M_0020-0045M_DCB
- Curran, R. J., Conrath, B. J., Hanel, R. A., Kunde, V. G., & Pearl, J. C. (1973). Mars: Mariner 9 Spectroscopic Evidence for H₂O Ice Clouds. *Science*, 182(4110), 381–383. <https://doi.org/10.1126/SCIENCE.182.4110.381>
- Daerden, F., Whiteway, J. A., Davy, R., Verhoeven, C., Komguem, L., Dickinson, C., Taylor, P. A., & Larsen, N. (2010). Simulating observed boundary layer clouds on Mars. *Geophysical Research Letters*, 37(4). <https://doi.org/10.1029/2009GL041523>
- Dollfus Audouin. (1957). Étude des planètes par la polarisation de leur lumière. *Supplements Aux Annales d'Astrophysique*, 4, 3–114. <https://articles.adsabs.harvard.edu/pdf/1957SAnAp...4....3D>
- French, R. G., Gierasch, P. J., Popp, B. D., & Yerdon, R. J. (1981). Global patterns in cloud forms on Mars. *Icarus*, 45(2), 468–493. [https://doi.org/10.1016/0019-1035\(81\)90047-6](https://doi.org/10.1016/0019-1035(81)90047-6)
- Hanel, R. A., Conrath, B. J., Kunde, V. G., Prabhakara, C., Revah, I., Salomonson, V. V., & Wolford, G. (1972). The Nimbus 4 infrared spectroscopy experiment: 1. Calibrated thermal emission spectra. *Journal of Geophysical Research*, 77(15), 2629–2641. <https://doi.org/10.1029/JC077I015P02629>
- Hernández Bernal, J., Sánchez-Lavega, A., Río-Gaztelurrutia, T., Hueso, R., Cardesin-Moinelo, A., Ravanis, E., Titov, D., Wood, S., Connour, K., Schneider, N., Gondet, B., Tirsch, D., Jaumann, R., & Hauber, E. (2019, November). *Dynamics of the extremely elongated cloud on Mars Arsia Mons volcano*.
- Hernández-Bernal, J., Sánchez-Lavega, A., del Río-Gaztelurrutia, T., Ravanis, E., Cardesín-Moinelo, A., Connour, K., Tirsch, D., Ordóñez-Etxeberria, I., Gondet, B., Wood, S., Titov, D., Schneider, N. M., Hueso, R., Jaumann, R., & Hauber, E. (2021). An Extremely Elongated Cloud Over Arsia Mons Volcano on Mars: I. Life Cycle. *Journal of Geophysical Research: Planets*, 126(3), e2020JE006517. <https://doi.org/10.1029/2020JE006517>
- Hinson, D. P., & Wilson, R. J. (2004). Temperature inversions, thermal tides, and water ice clouds in the Martian tropics. *Journal of Geophysical Research: Planets*, 109(E1), 1002. <https://doi.org/10.1029/2003JE002129>
- Hunt, G. E., Pickersgill, A. O., James, P. B., & Johnson, G. (1980). Some diurnal properties of clouds over the martian volcanoes. *Nature* 1980 286:5771, 286(5771), 362–364. <https://doi.org/10.1038/286362a0>
- Hyperspectral Python*. (2017). <http://hyppy.is-great.org/>
- Inada, A., Garcia-Comas, M., Altieri, F., Gwinner, K., Poulet, F., Bellucci, G., Keller, H. U., Markiewicz, W. J., Richardson, M. I., Hoekzema, N., Neukum, G., & Bibring, J.-P. (2008). Dust haze in Valles Marineris observed by HRSC and OMEGA on board Mars Express. *Journal of Geophysical Research*, 113(E2). https://www.academia.edu/19471938/Dust_haze_in_Valles_Marineris_observed_by_HRS_C_and_OMEGA_on_board_Mars_Express

- Jakosky, B. M., Lin, R. P., Grebowsky, J. M., Luhmann, J. G., Mitchell, D. F., Beutelschies, G., Priser, T., Acuna, M., Andersson, L., Baird, D., Baker, D., Bartlett, R., Benna, M., Bougher, S., Brain, D., Carson, D., Cauffman, S., Chamberlin, P., Chaufray, J. Y., ... Zurek, R. (2015). The Mars atmosphere and volatile evolution (MAVEN) mission. *Space Science Reviews*, 195(1–4), 3–48. <https://doi.org/10.1007/S11214-015-0139-X>
- James, P. B. (1982). The clouds of Mars as seen by Viking. *Advances in Space Research*, 2(2), 67–74. [https://doi.org/10.1016/0273-1177\(82\)90106-5](https://doi.org/10.1016/0273-1177(82)90106-5)
- James, P. B., Bell III, J. F., Todd Clancy, R., Martin, L. J., Wolff, M. J., & Lee, S. W. (1996). Global imaging of Mars by Hubble space telescope during the 1995 opposition. *JOURNAL OF GEOPHYSICAL RESEARCH*, 101, 883–901. <https://doi.org/10.1029/96JE01605>
- Jaquin, F., Gierasch, P., & Kahnt, R. (1986). The Vertical Structure of Limb Hazes in the Martian Atmosphere. *ICARUS*, 68, 442–461.
- Kahn, R. (1984). The spatial and seasonal distribution of Martian clouds and some meteorological implications. *Journal of Geophysical Research*, 89(A8), 6671–6688. <https://doi.org/10.1029/JA089IA08P06671>
- Khayat, A., Smith, M., Wolff, M., Guzewich, S., Mason, E., & Atwood, S. (2022). Mars atmospheric water ice climatology as retrieved by MRO/CRISM: 5 years of observations. *EPSC2022*. <https://doi.org/10.5194/EPSC2022-617>
- Kieffer, H. H., Jakosky, B. M., & Snyder, C. W. (1992). The planet Mars: from antiquity to the present. In M. George (Ed.), *Mars* (pp. 1–33).
- Leovy CB, SMITH BA, YOUNG AT, & LEIGHTON RB. (1971). Mariner Mars 1969: Atmospheric results. *Journal of Geophysical Research*, 76(2), 297–312. <https://doi.org/10.1029/JB076I002P00297>
- Määttänen, A. (2010). *THREE MARTIAN YEARS OF OBSERVATIONS OF MESOSPHERIC CO₂ CLOUDS ON MARS WITH OMEGA/MEX AND HRSC/MEX*.
- Määttänen, A., Montmessin, F., Gondet, B., Hoffmann, H., Scholten, F., Hauber, E., Gonzalez-Galindo, F., Forget, F., Bibring, J.-P., Bertaux, J.-L., & Neukum, G. (2009). *HIGH-ALTITUDE CO₂ CLOUDS ON MARS: OMEGA AND HRSC OBSERVATIONS*.
- Madeleine, J. B., Forget, F., Spiga, A., Wolff, M. J., Montmessin, F., Vincendon, M., Jouget, D., Gondet, B., Bibring, J. P., Langevin, Y., & Schmitt, B. (2012). Aphelion water-ice cloud mapping and property retrieval using the OMEGA imaging spectrometer onboard Mars Express. *Journal of Geophysical Research: Planets*, 117(5). <https://doi.org/10.1029/2011JE003940>
- Maltagliati, L., Titov, D. V., Encrenaz, T., Melchiorri, R., Forget, F., Garcia-Comas, M., Keller, H. U., Langevin, Y., & Bibring, J. P. (2008). Observations of atmospheric water vapor above the Tharsis volcanoes on Mars with the OMEGA/MEx imaging spectrometer. *Icarus*, 194(1), 53–64. <https://doi.org/10.1016/J.ICARUS.2007.09.027>
- Mars Orbital Data Explorer*. (2019). <https://ode.rsl.wustl.edu/mars/index.aspx>
- Mckay, C. P. (2010). An Origin of Life on Mars. *Cold Spring Harbor Perspectives in Biology*, v.2(4). <https://doi.org/10.1101/cshperspect.a003509>

- Michaels, T. I., Colaprete, A., & Rafkin, S. C. R. (2006). Significant vertical water transport by mountain-induced circulations on Mars. *Geophysical Research Letters*, *33*(16).
<https://doi.org/10.1029/2006GL026562>
- Michelangeli, D. V., Toon, O. B., Haberle, R. M., & Pollack, J. B. (1993). Numerical Simulations of the Formation and Evolution of Water Ice Clouds in the Martian Atmosphere. *Icarus*, *102*(2), 261–285. <https://doi.org/10.1006/ICAR.1993.1048>
- Montmessin, F., Gondet, B., Bibring, J. P., Langevin, Y., Drossart, P., Forget, F., & Fouchet, T. (2007). Hyperspectral imaging of convective CO₂ ice clouds in the equatorial mesosphere of Mars. *Journal of Geophysical Research: Planets*, *112*(11). <https://doi.org/10.1029/2007JE002944>
- Murchie, S., Arvidson, R., Bedini, P., Beisser, K., Bibring, J. P., Bishop, J., Boldt, J., Cavender, P., Choo, T., Clancy, R. T., Darlington, E. H., Des Marais, D., Espiritu, R., Fort, D., Green, R., Guinness, E., Hayes, J., Hash, C., Heffernan, K., ... Wolff, M. (2007). Compact Connaissance Imaging Spectrometer for Mars (CRISM) on Mars Reconnaissance Orbiter (MRO). *Journal of Geophysical Research: Planets*, *112*(5). <https://doi.org/10.1029/2006JE002682>
- NASA GISS: Mars24 Sunclock*. (2022). <https://www.giss.nasa.gov/tools/mars24/>
- Neary, L., & Daerden, F. (2017). The GEM-Mars general circulation model for Mars: Description and evaluation. *Icarus*, *300*, 458–476. <https://doi.org/10.1016/j.icarus.2017.09.028>
- Noe Dobrea, E. Z., & Bell, I. F. (2005). TES spectroscopic identification of a region of persistent water ice clouds on the flanks of Arsia Mons Volcano, Mars. *Journal of Geophysical Research: Planets*, *110*(5), 1–9. <https://doi.org/10.1029/2003JE002221>
- PDS Geosciences Node*. (2019). https://pds-geosciences.wustl.edu/missions/mars_express/omega.htm
- Petty, G. W. (2006). *A First Course in Atmospheric Science. 2. Edition*.
https://books.google.com/books/about/A_First_Course_in_Atmospheric_Radiation.html?hl=nl&id=YpspAQAAMAAJ
- Rafkin, S., Sta. Maria, M. R., & Michaels, T. (2002). Simulation of the atmospheric thermal circulation of a Martian volcano using a mesoscale numerical model. *Nature*, *419*, 697–699. <https://doi.org/10.1038/nature01114>
- Raponi, A., Ciarniello, M., Capaccioni, F., Filacchione, G., Tosi, F., De Sanctis, M. C., Capria, M. T., Barucci, M. A., Longobardo, A., Palomba, E., Kappel, D., Arnold, G., Mottola, S., Rousseau, B., Quirico, E., Rinaldi, G., Erard, S., Bockelee-Morvan, D., & Leyrat, C. (2016). The temporal evolution of exposed water ice-rich areas on the surface of 67P/Churyumov-Gerasimenko: Spectral analysis. *Monthly Notices of the Royal Astronomical Society*, *462*, S476–S490. <https://doi.org/10.1093/mnras/stw3281>
- Slipher, & C., E. (1962). The photographic story of Mars. *Psm*.
<https://ui.adsabs.harvard.edu/abs/1962psm..book....S/abstract>
- Song, M., Li, W., Zhou, B., & Lei, T. (2015). *Spatiotemporal data representation and its effect on the performance of spatial analysis in a cyberinfrastructure environment-A case study with raster zonal analysis*. <https://doi.org/10.1016/j.cageo.2015.11.005>
- Spiga, A., Gonzalez-Galindo, F., López-Valverde, M. A., & Forget, F. (2012). Gravity waves, cold pockets and CO₂ clouds in the Martian mesosphere. *Geophysical Research Letters*, *39*(2).
<https://doi.org/10.1029/2011GL050343>

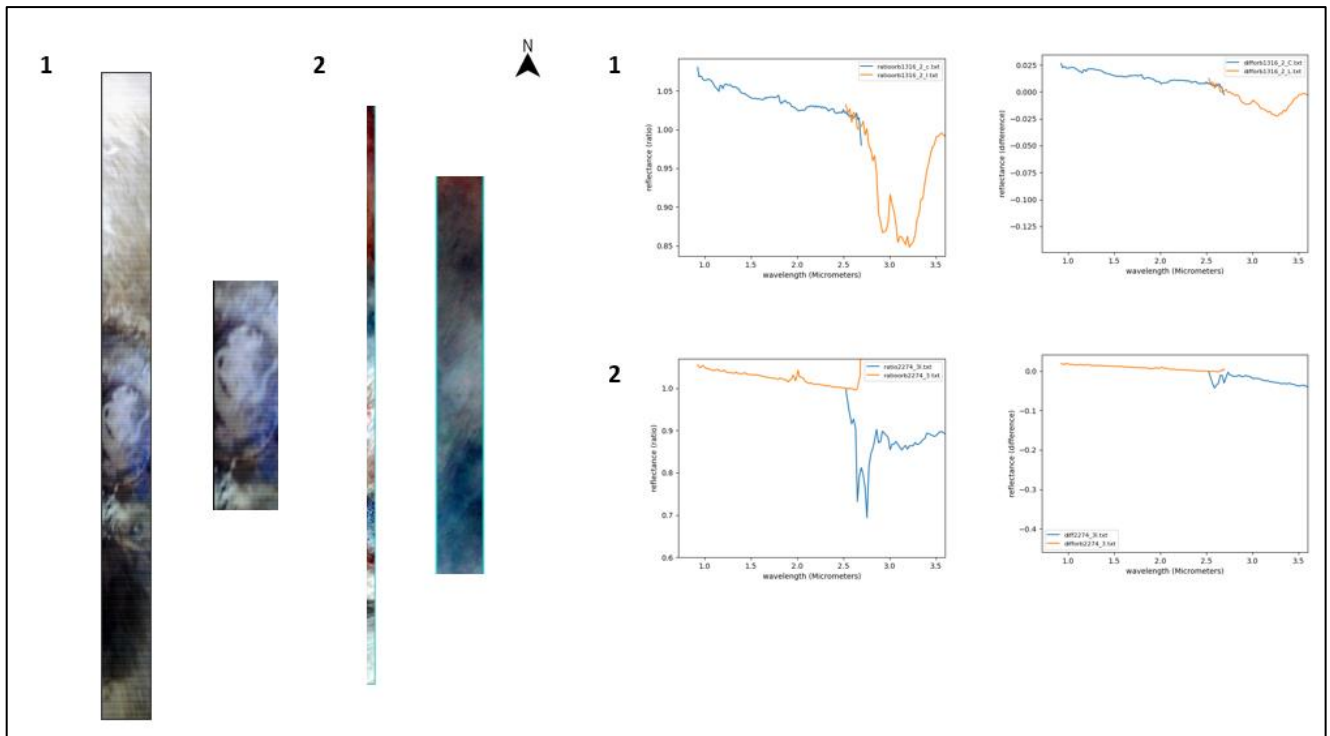
- Vincendon, M., Langevin, Y., Poulet, F., Pommerol, A., Wolff, M., Bibring, J.-P., Gondet, B., & Jouglet, D. (2009). Yearly and seasonal variations of low albedo surfaces on Mars in the OMEGA/MEx dataset: Constraints on aerosols properties and dust deposits. *Icarus*, *200*, 395–405. <https://doi.org/10.1016/j.icarus.2008.12.012>
- Vincendon, M., Pilorget, C., Gondet, B., Murchie, S., & Bibring, J.-P. (2011). New near-IR observations of mesospheric CO₂ and H₂O clouds on Mars. *Journal of Geophysical Research: Planets*, *116*(11), 0–02. <https://doi.org/10.1029/2011JE003827>
- Wang, H., & Ingersoll, A. P. (2002a). Martian clouds observed by Mars Global Surveyor Mars Orbiter Camera. *Journal of Geophysical Research: Planets*, *107*(E10), 8–1. <https://doi.org/10.1029/2001JE001815>
- Wang, H., & Ingersoll, A. P. (2002b). Martian clouds observed by Mars Global Surveyor Mars Orbiter Camera. *Journal of Geophysical Research: Planets*, *107*(10). <https://doi.org/10.1029/2001JE001815>
- Wang, H., & Ingersoll, A. P. (2002c). Martian clouds observed by Mars Global Surveyor Mars Orbiter Camera. *Journal of Geophysical Research: Planets*, *107*(E10), 8–1. <https://doi.org/10.1029/2001JE001815>
- Will Robertson. (2021). *Arsia Mons Elongated Cloud (AMEC) - Globe Activity (Robertson)*.
- Yiğit, E., England, S. L., Liu, G., Medvedev, A. S., Mahaffy, P. R., Kuroda, T., & Jakosky, B. M. (2015). High-altitude gravity waves in the Martian thermosphere observed by MAVEN/NGIMS and modeled by a gravity wave scheme. *Geophysical Research Letters*, *42*(21), 8993–9000. <https://doi.org/10.1002/2015GL065307>
- Yoder, C. F., & Standish, E. M. (1997). Martian precession and rotation from Viking lander range data. *Journal of Geophysical Research: Planets*, *102*(E2), 4065–4080. <https://doi.org/10.1029/96JE03642>

APPENDIX

This section compiles all the cloud images obtained and their corresponding spectral analysis results

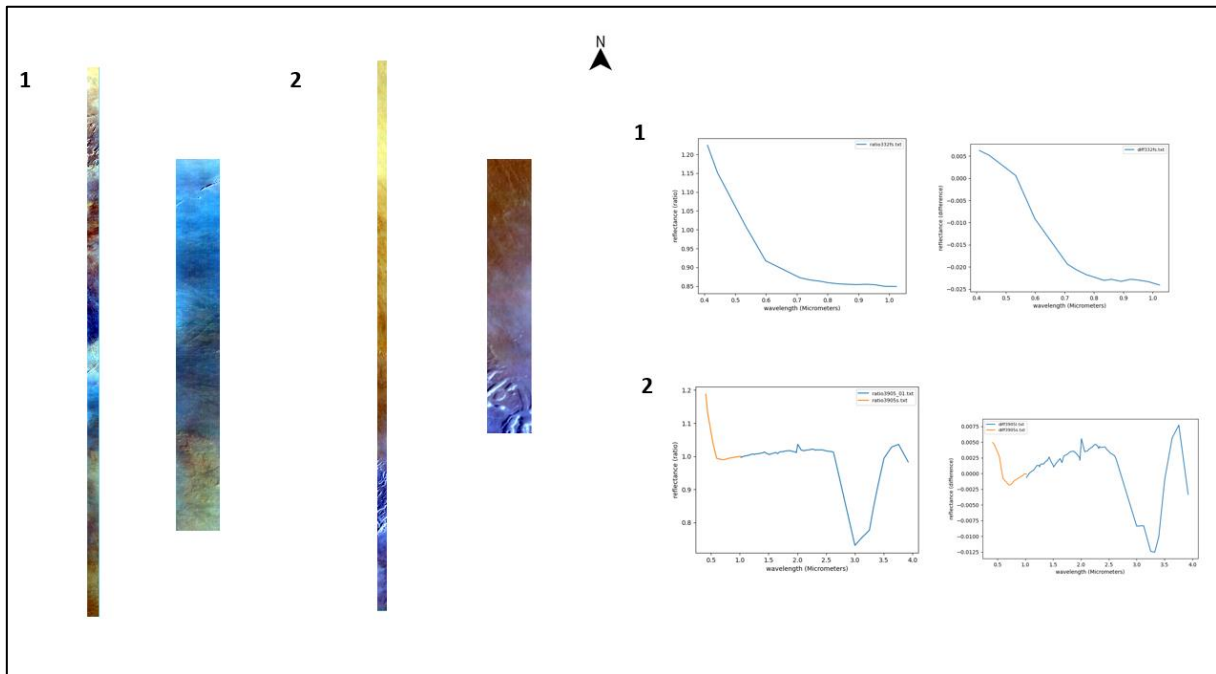
2005

1	ORB1316_2
2	ORB2274_3



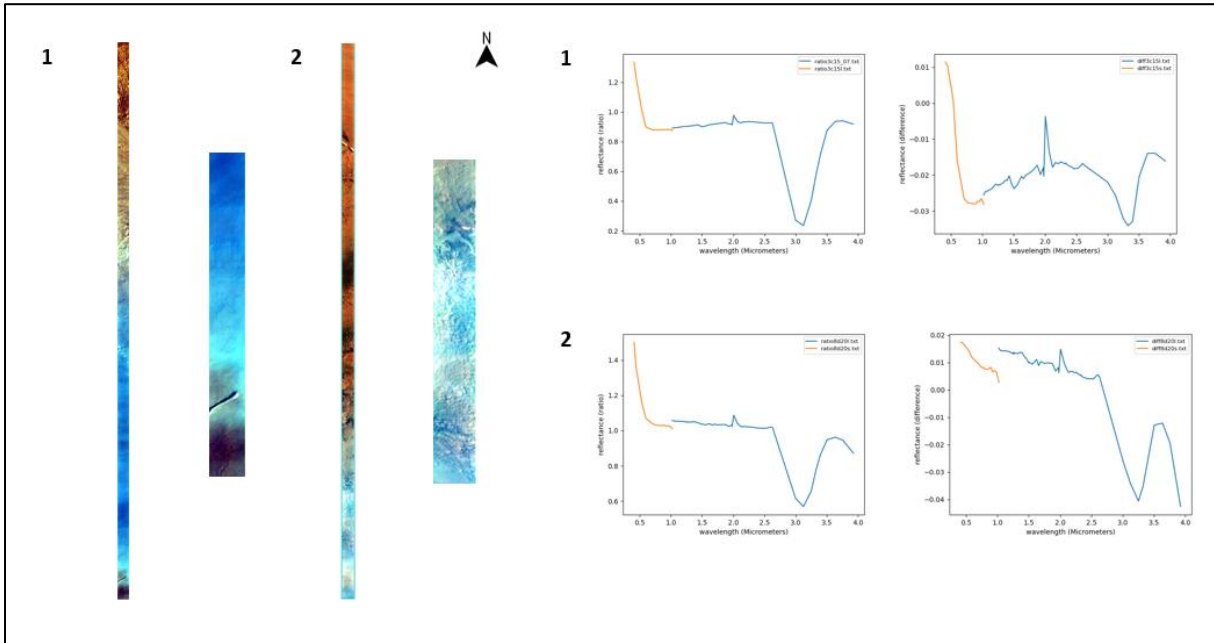
2006

1	MSP0000332F_05
2	MSP00003905_01



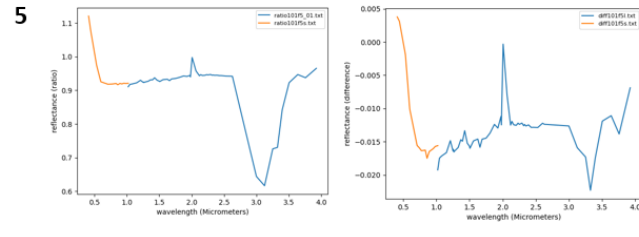
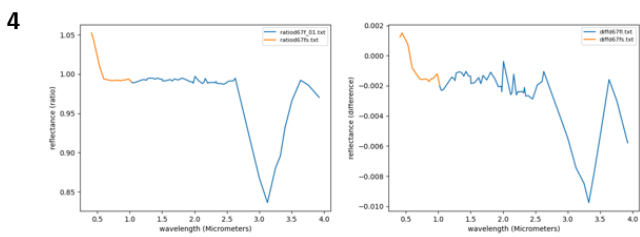
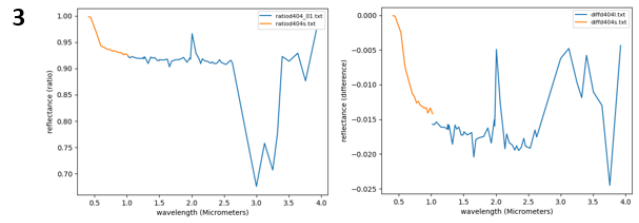
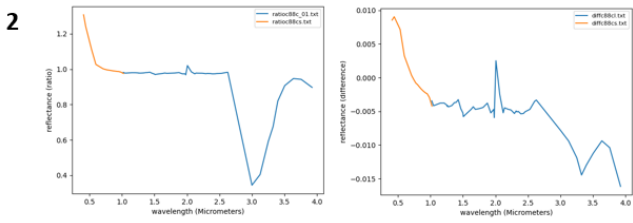
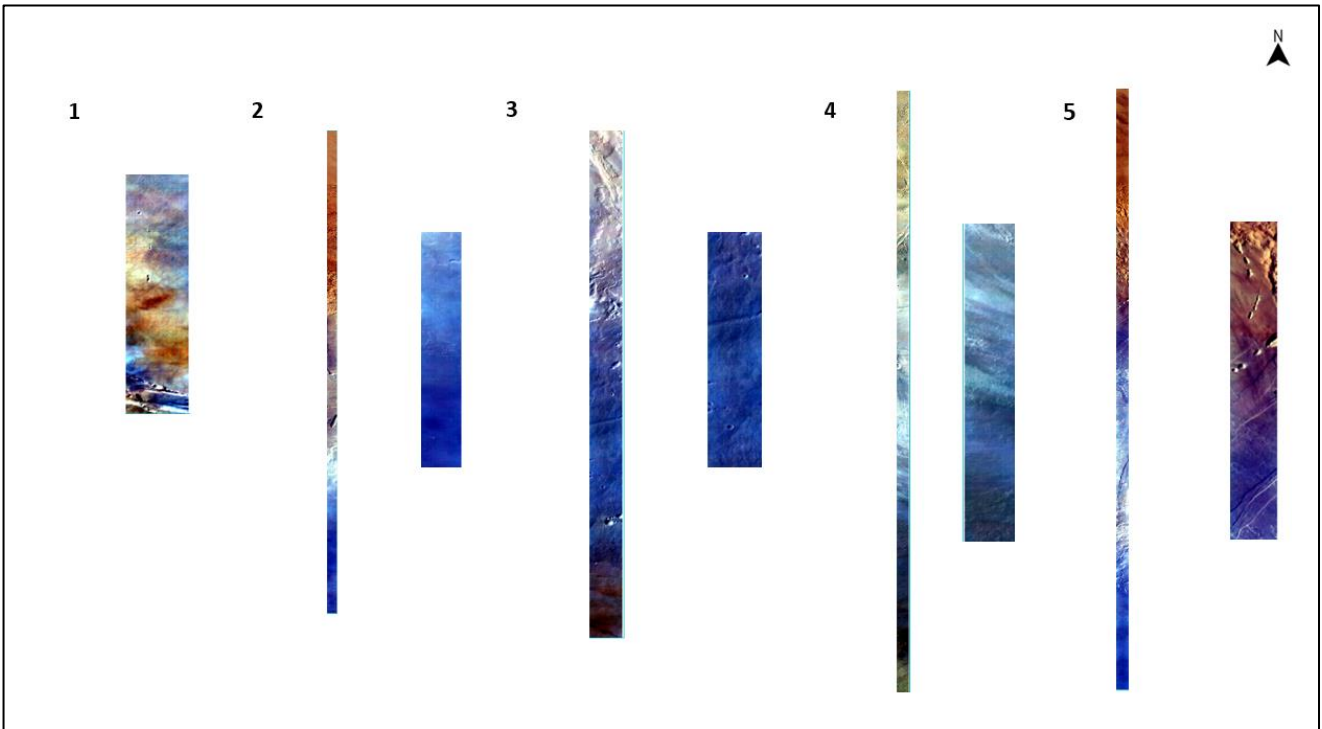
2007

1	MSP0000332F_05
2	MSP00003905_01



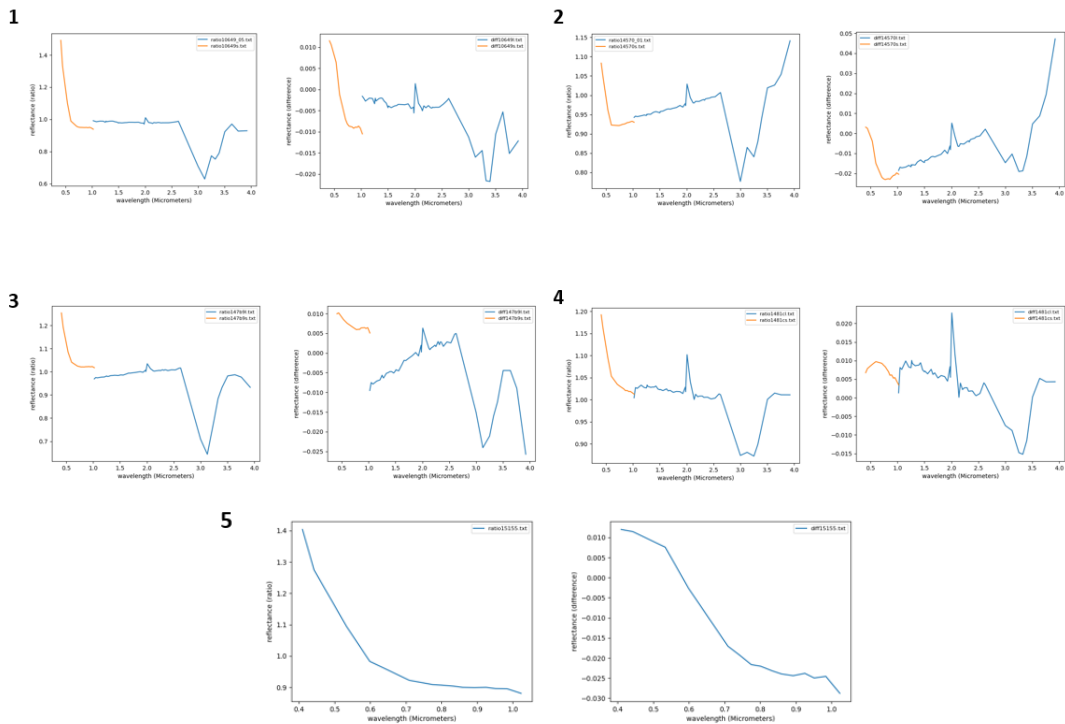
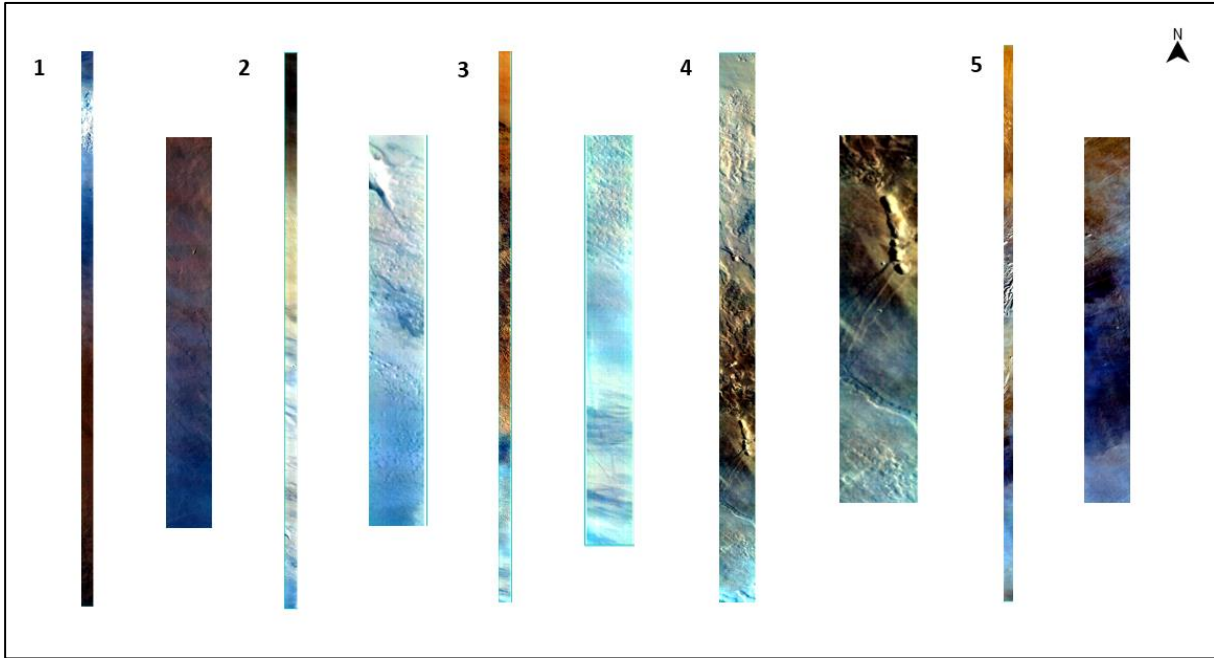
2008

1	MSP0000C6F9_01
2	MSP0000C88C_01
3	MSP0000D404_01
4	MSP0000D67F_01
5	MSP000101F5_01



2009

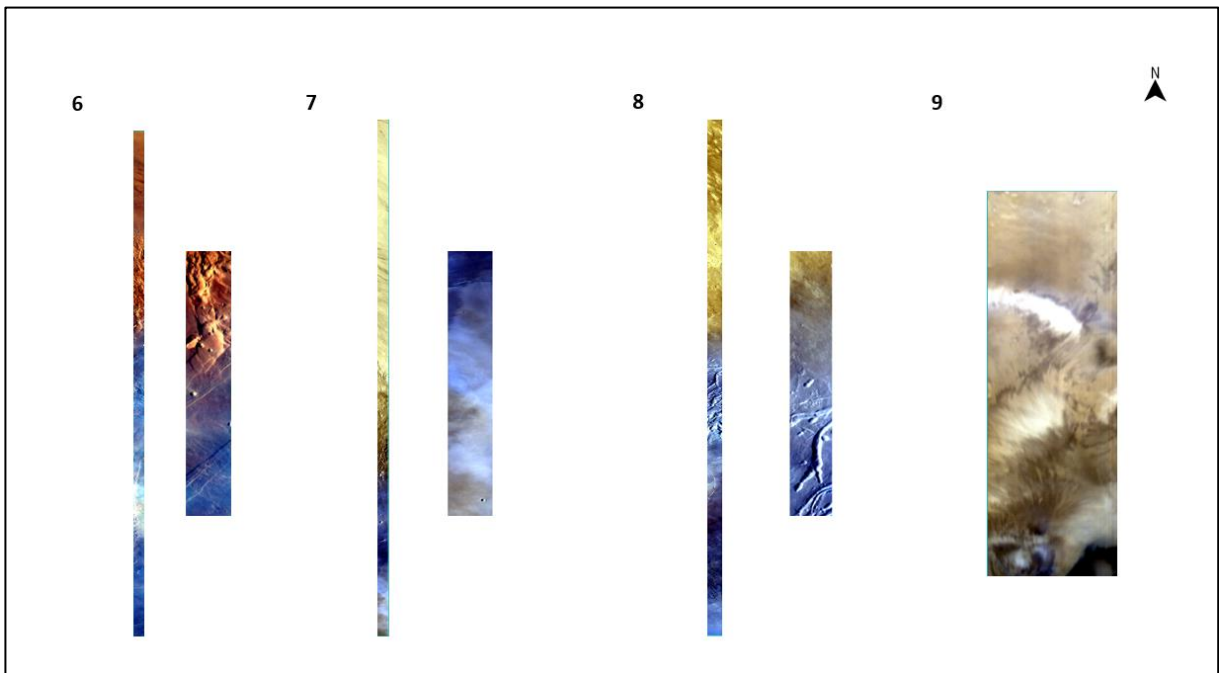
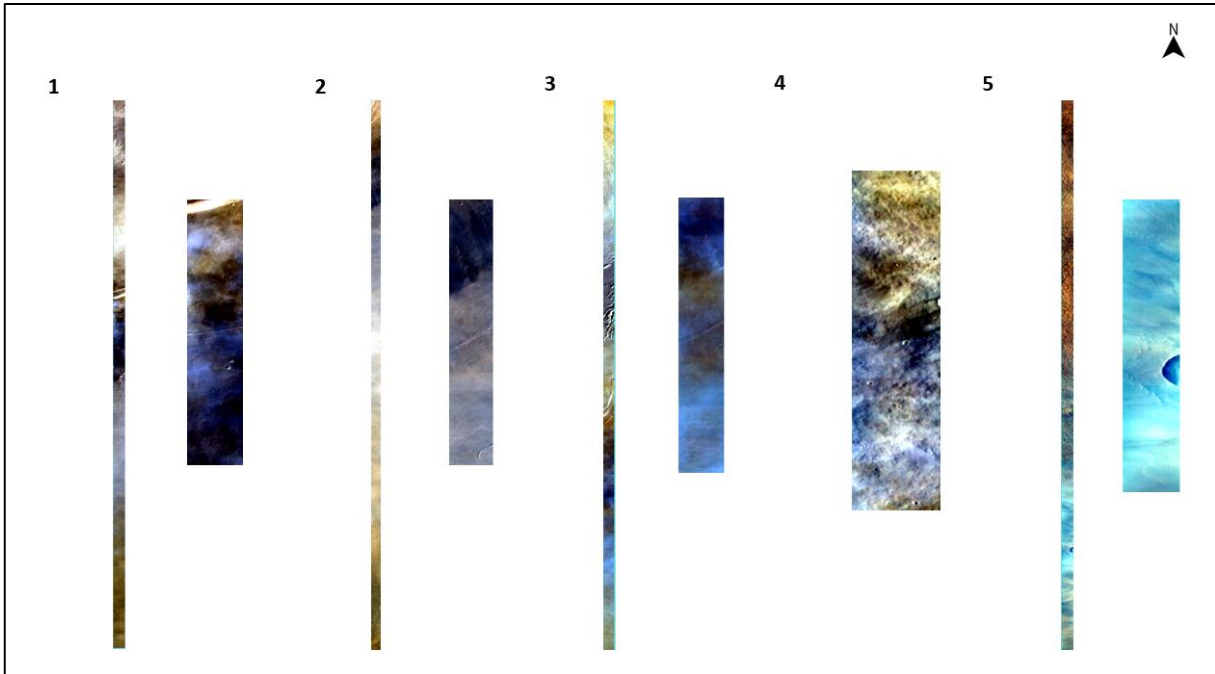
1	MSP00010649_05
2	MSP00014570_01
3	MSP000147B9_01
4	MSP0001481C_01
5	MSP00015155_01



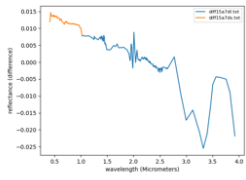
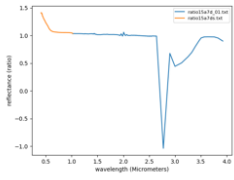
2010

1	HSP00015A7D_01
2	HSV0001AF9E_01
3	MSP0001AB4F_01
4	HSP0001BB17_01
5	MSP0001C5E7_01

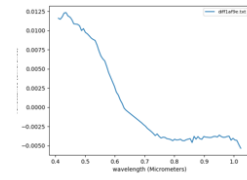
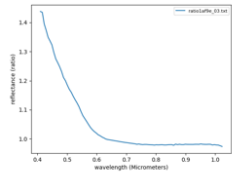
6	MSP0001C61D_01
7	HSV0001BCED_01
8	HSV0001C006_01
9	ORB7705_2



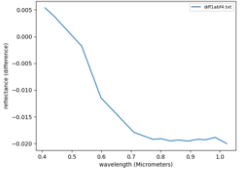
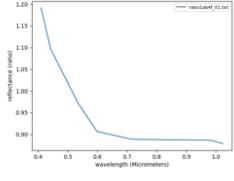
1



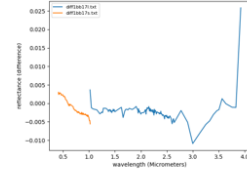
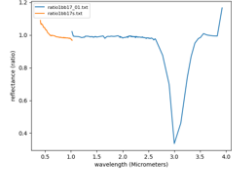
2



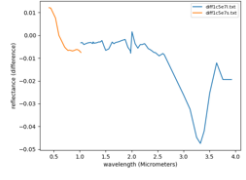
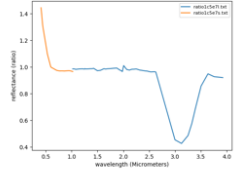
3



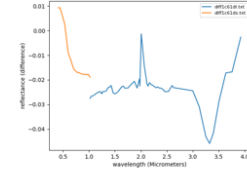
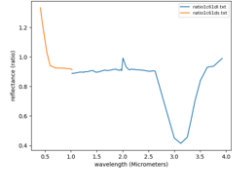
4



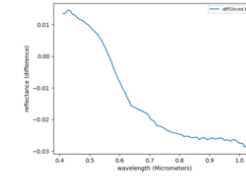
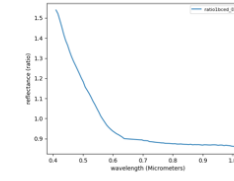
5



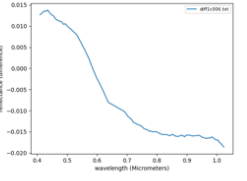
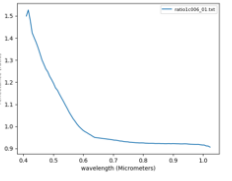
6



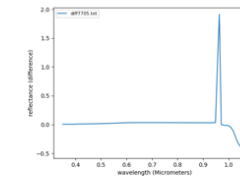
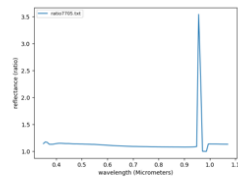
7



8



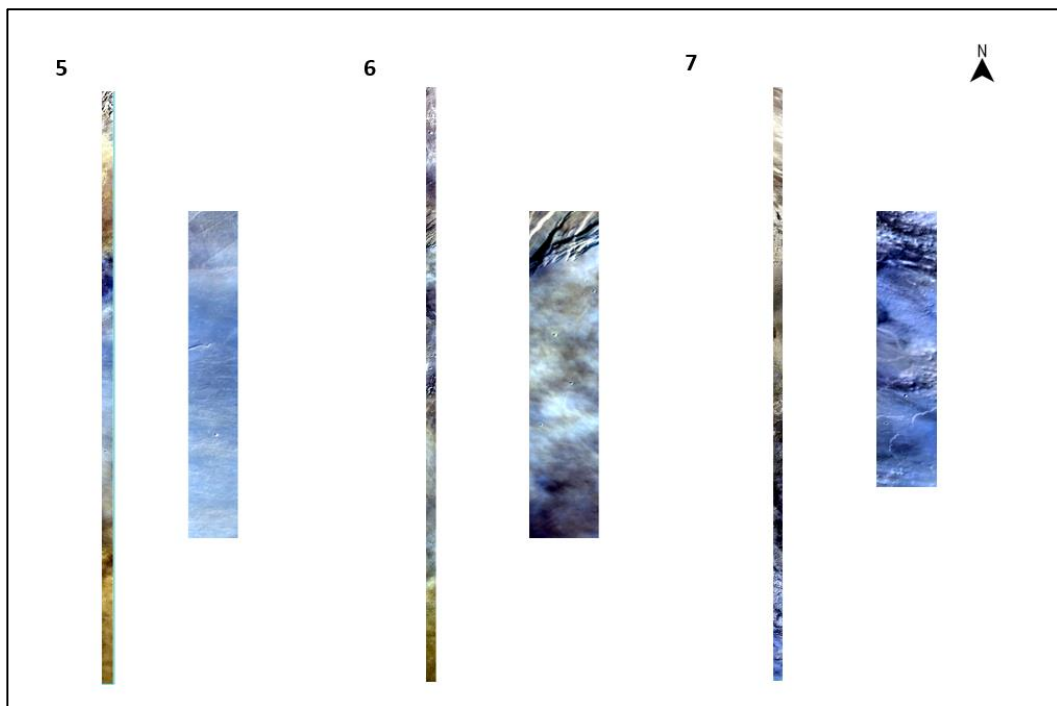
9



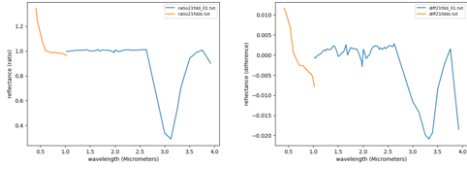
2011

1	MSP00021FDD_01
2	HSV0001CE9E_03
3	HSV000200BC_01
4	HSV00020EF4_01
5	HSV00021888_03

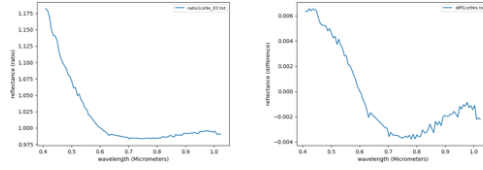
6	HSV00021A3A_05
7	HSV00022158_01



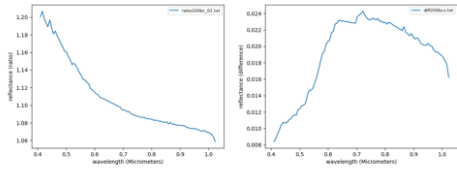
1



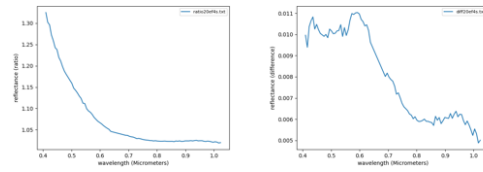
2



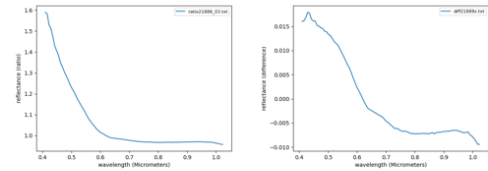
3



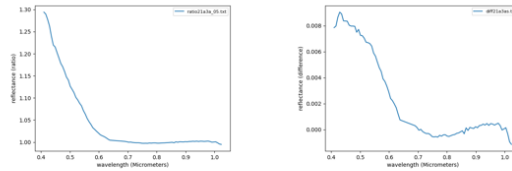
4



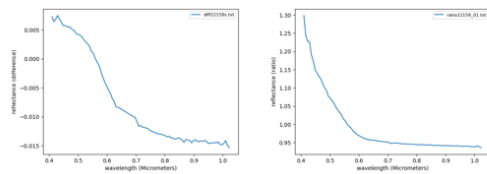
5



6



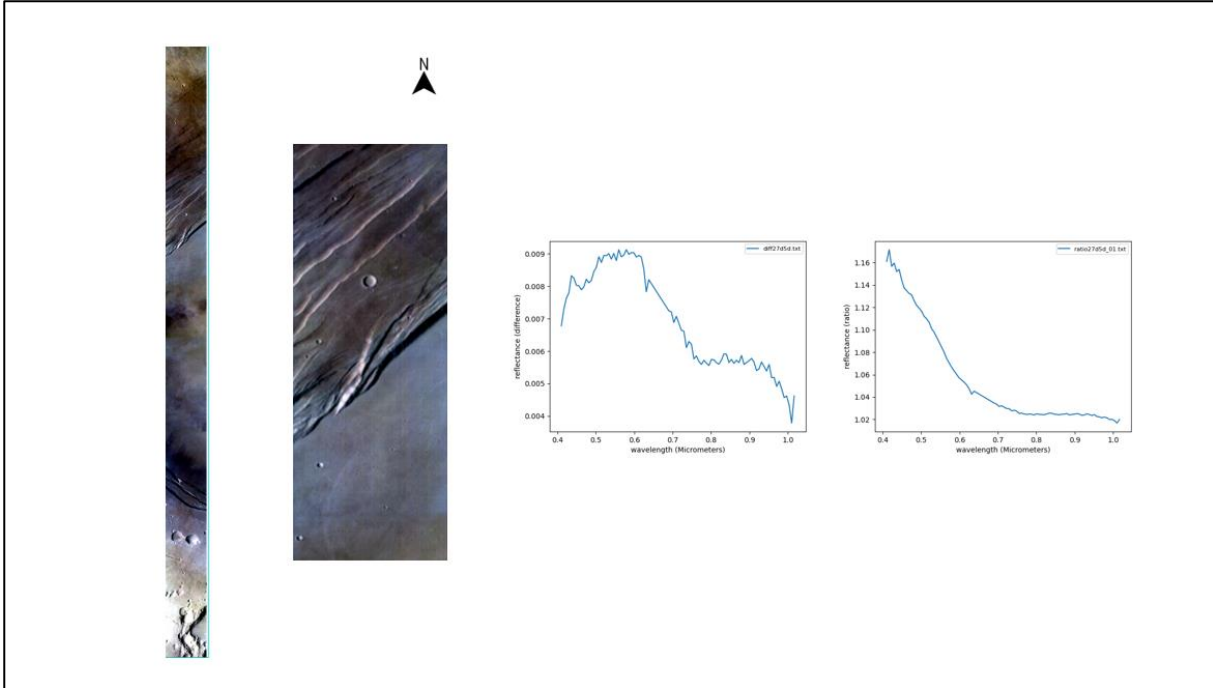
7



2012

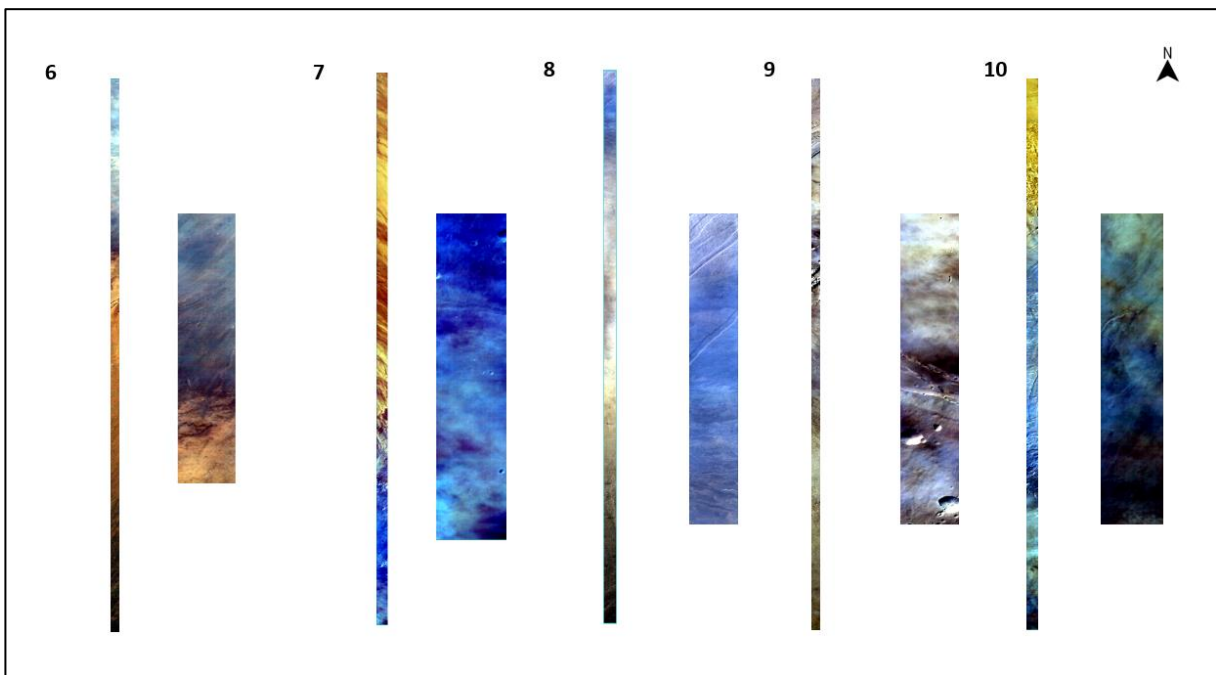
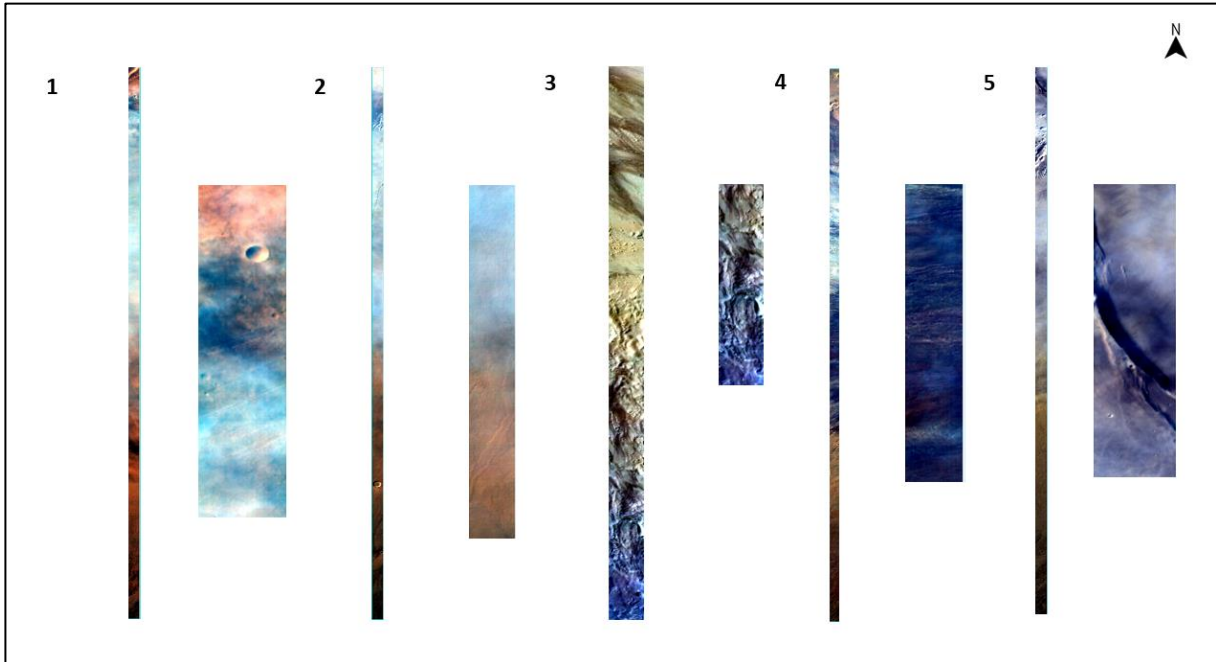
2

MSV00027D5D_01

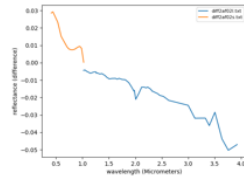
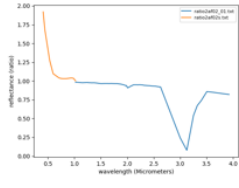


2013

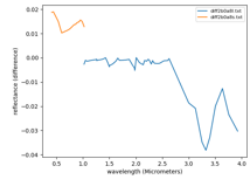
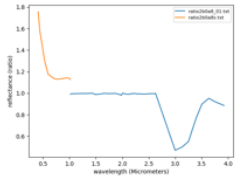
1	MSP0002AF02_01	6	MSP0002B99B_03
2	MSP0002B0A8_01	7	MSP0002BA41_01
3	MSP0002B0A9_01	8	HSP0002BC73_01
4	MSP0002B66D_01	9	MSP0002CA4B_01
5	HSP0002B874_05	10	MSV0002C556_03



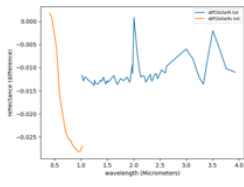
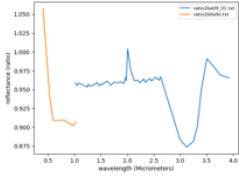
1



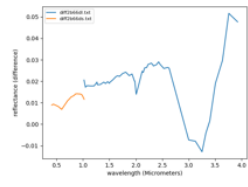
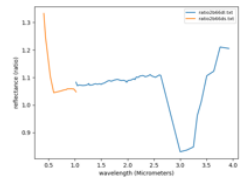
2



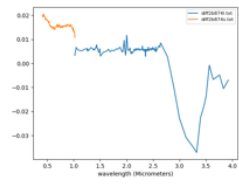
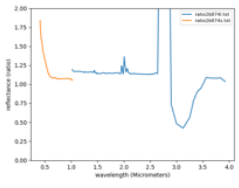
3



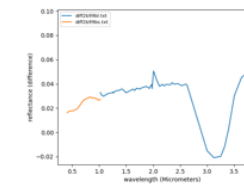
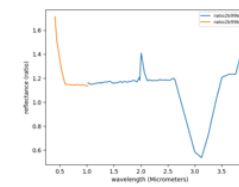
4



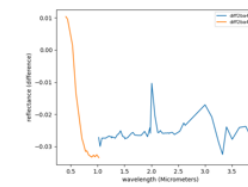
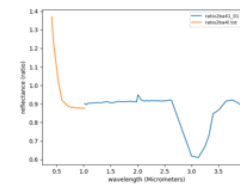
5



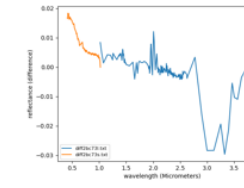
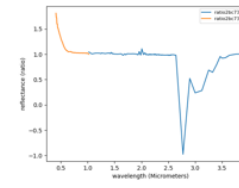
6



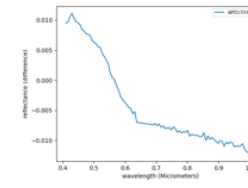
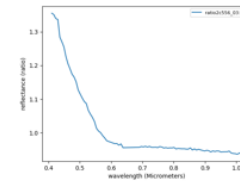
7



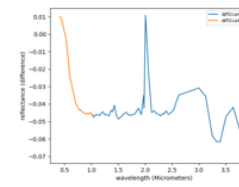
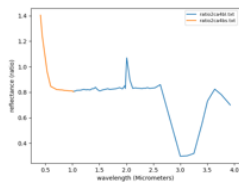
8



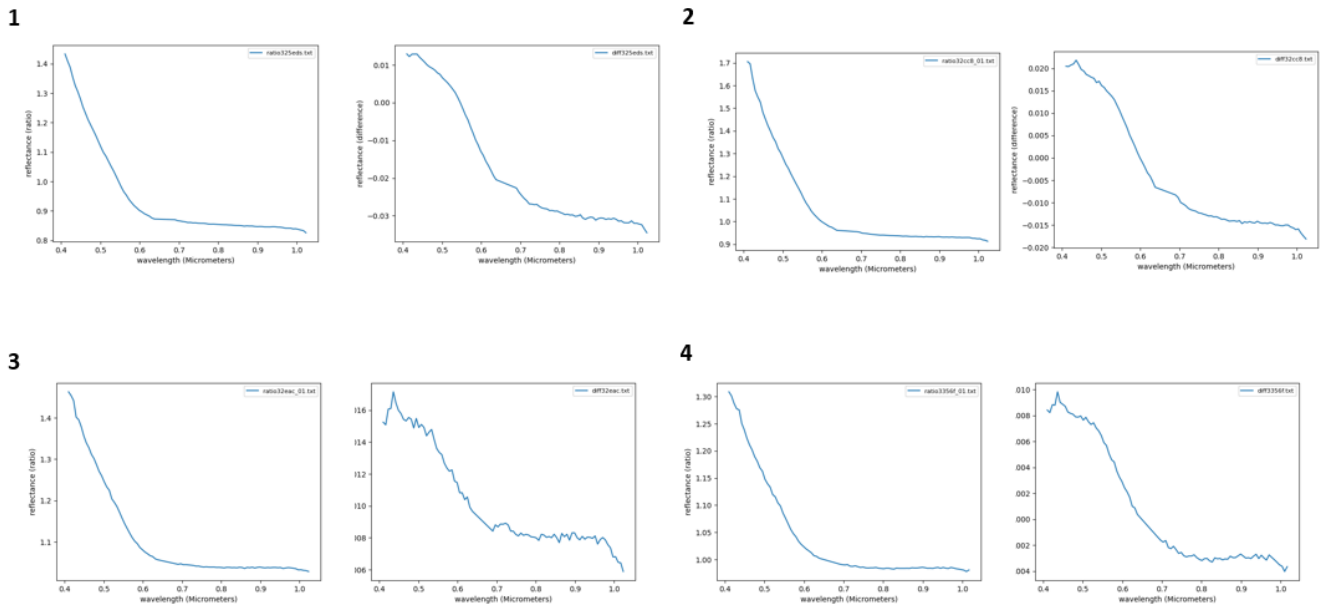
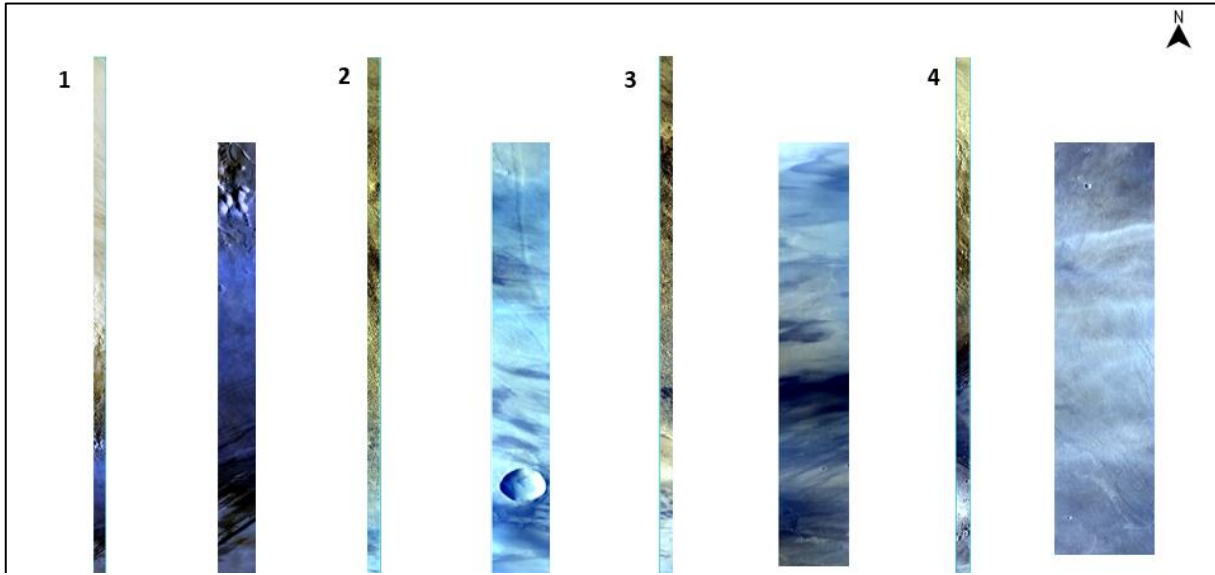
9



10



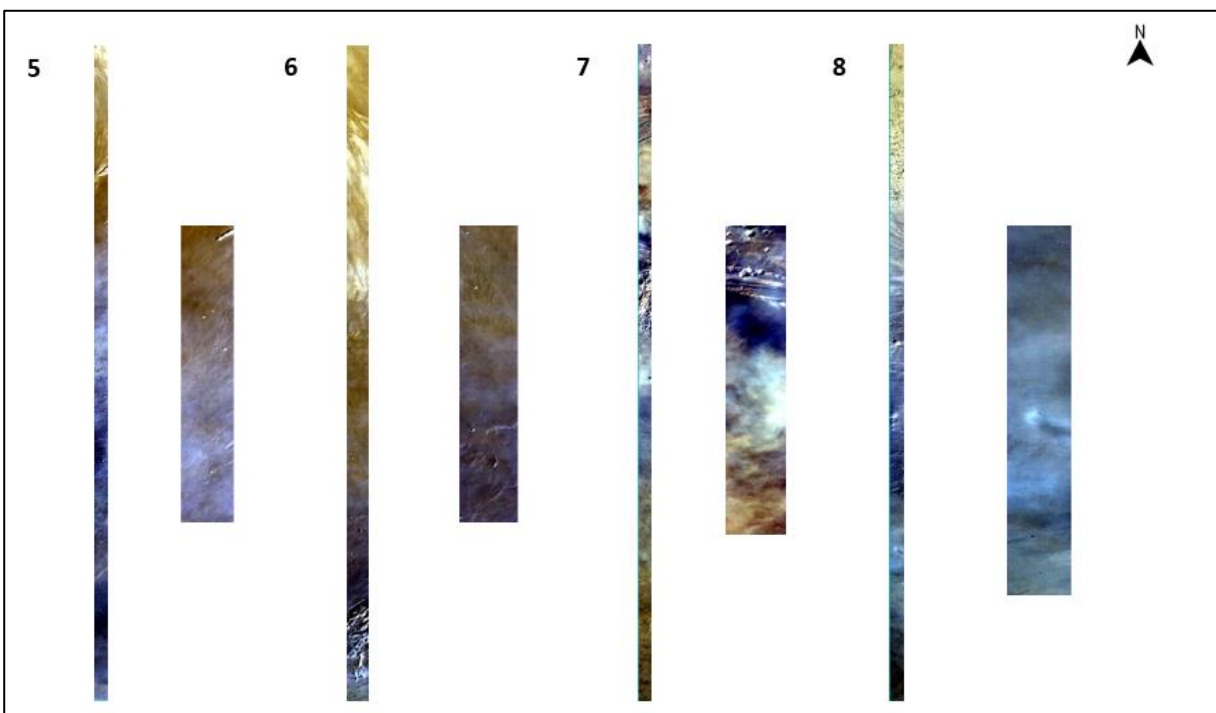
1	HSV000325ED_01
2	HSV00032CC8_01
3	HSV00032EAC_01
4	MSV0003356F_01

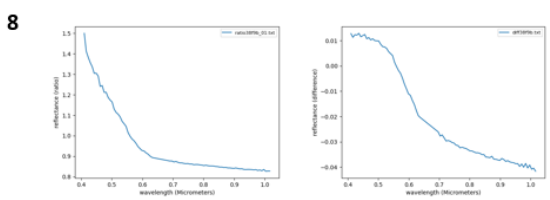
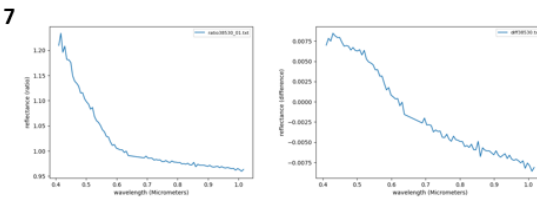
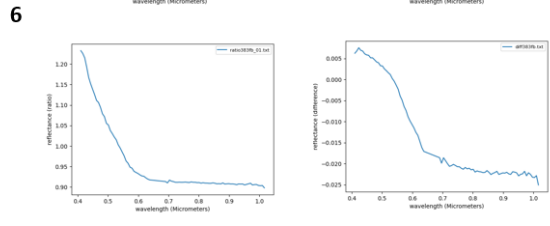
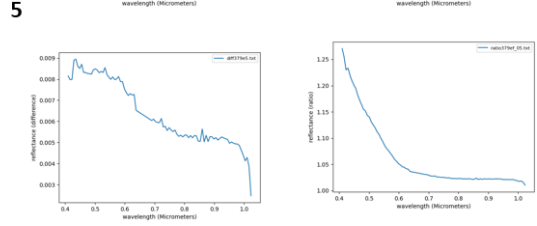
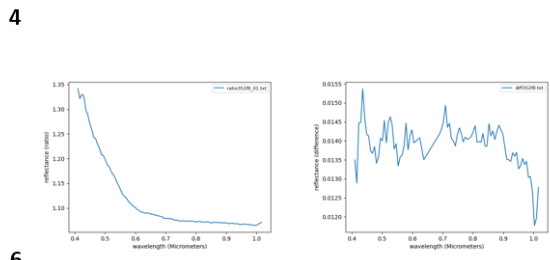
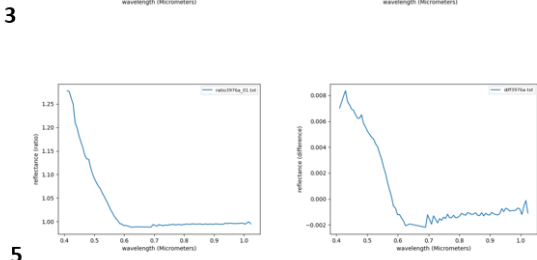
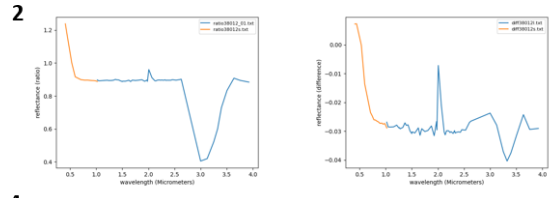
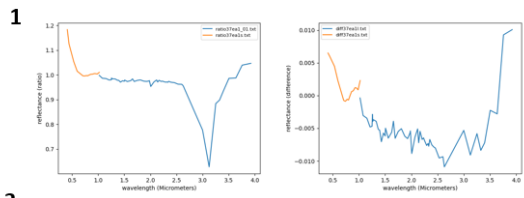


2015

1	MSP00037EA1_01
2	MSP00038012_01
3	HSP0003976A_01
4	MSV000352F8_01
5	HSV000379E5_05

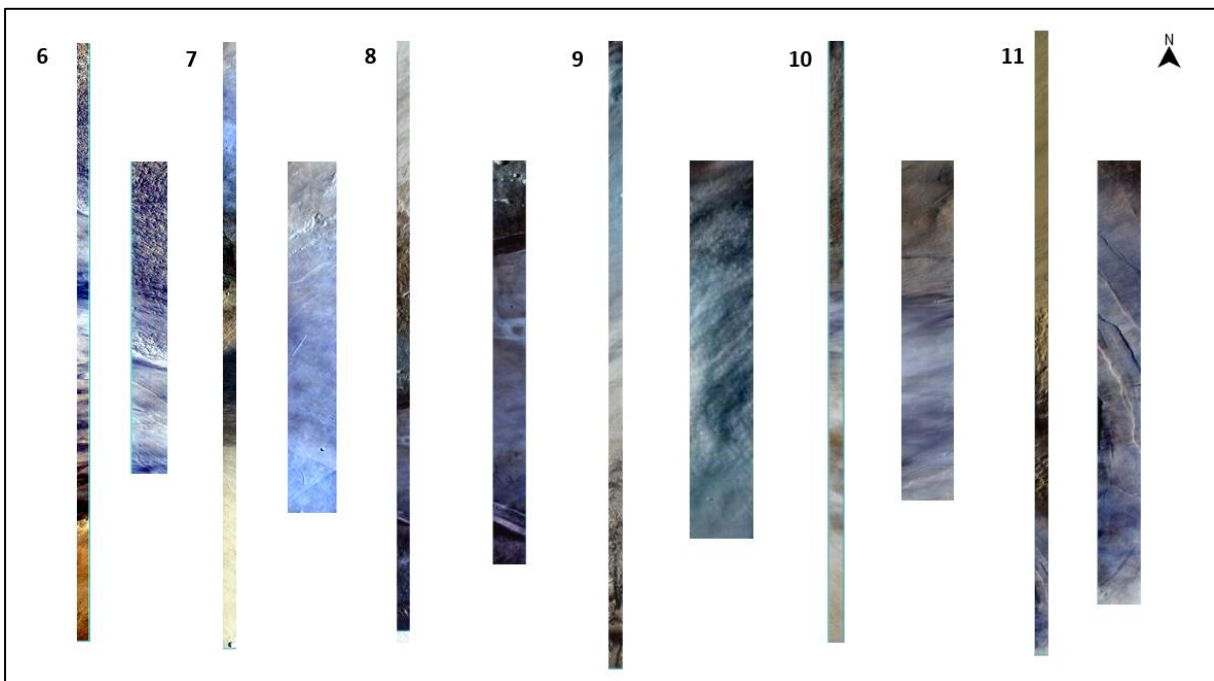
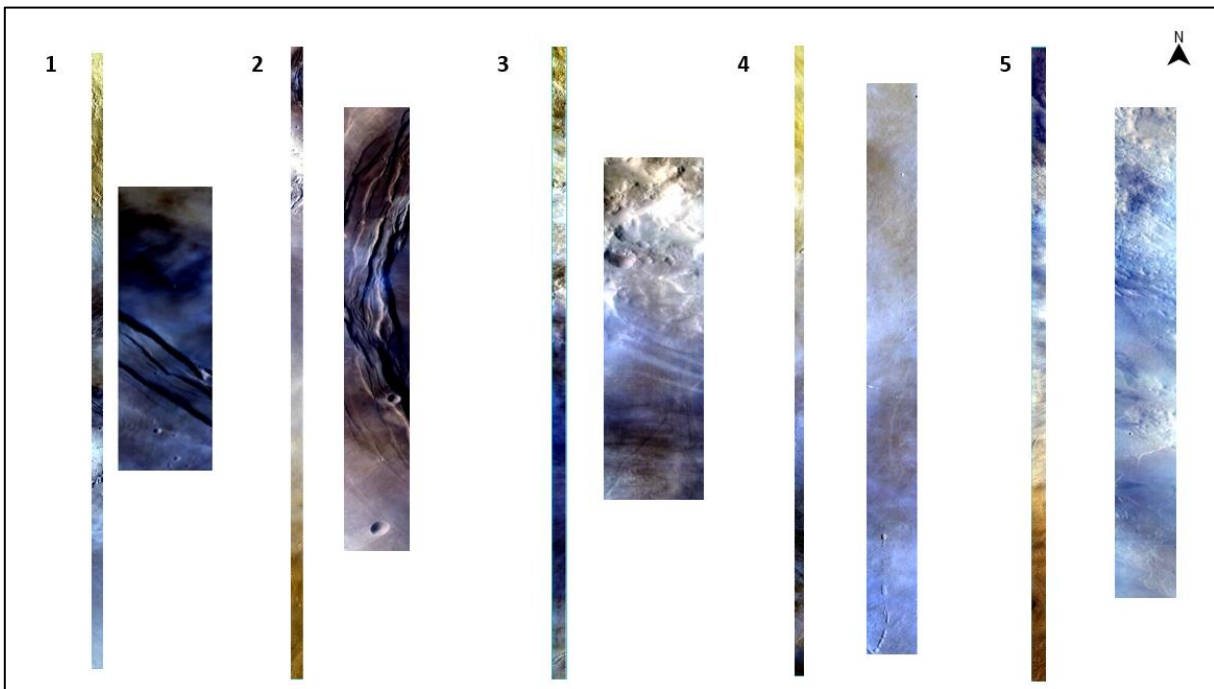
6	MSV000383FB_01
7	MSV00038530_01
8	MSV00038F9B_01

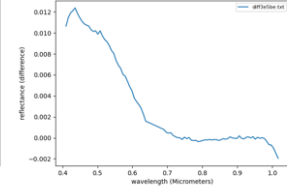
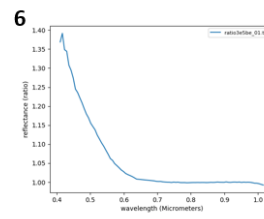
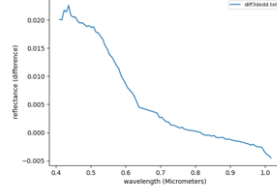
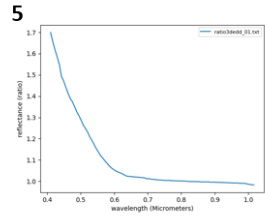
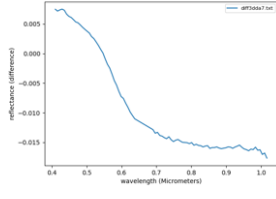
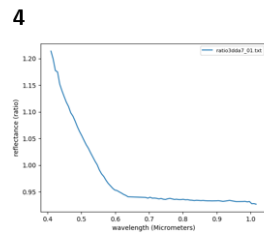
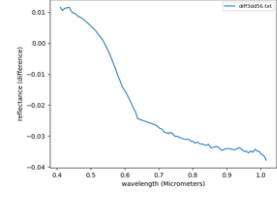
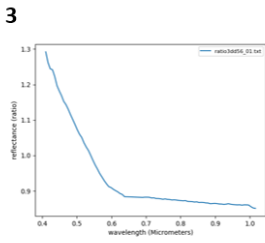
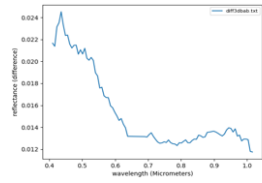
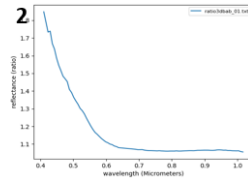
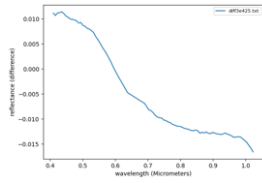
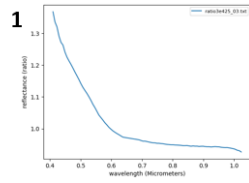


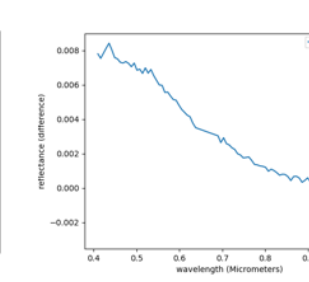
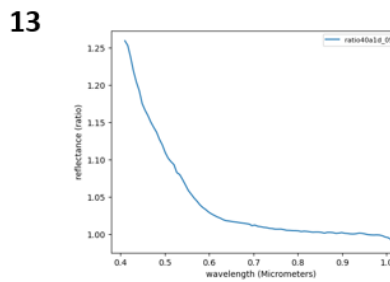
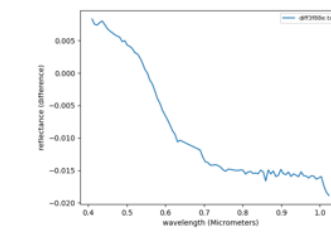
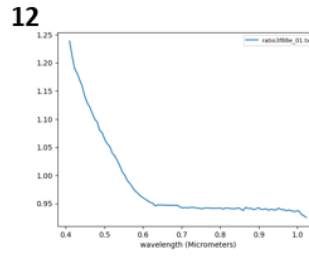
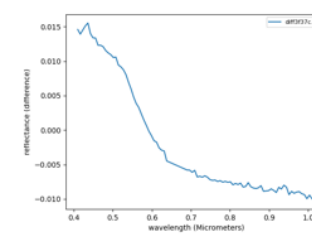
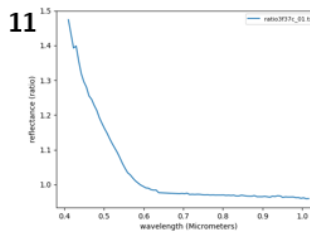
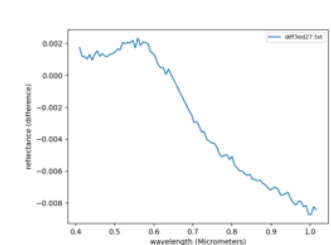
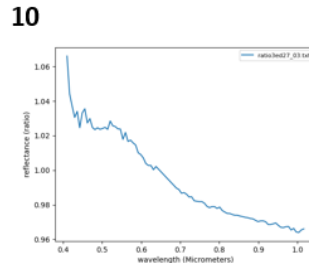
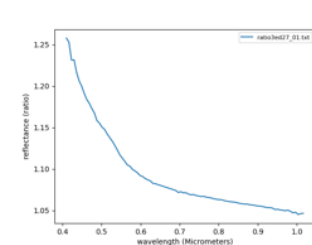
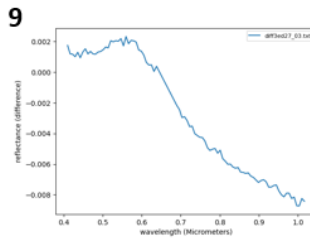
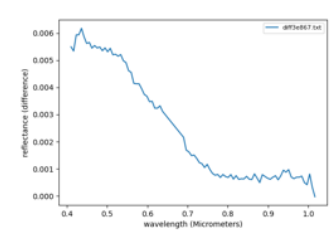
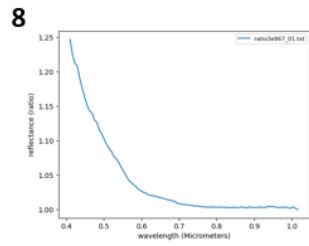
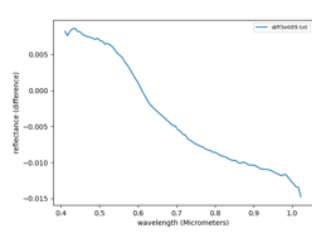
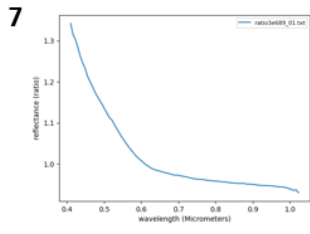


2016

1	MSV0003DBAB_01	6	HSV0003E689_01
2	MSV0003DD56_01	7	MSV0003E867_01
3	MSV0003DDA7_01	8	MSV0003ED27_03
4	MSV0003DEDD_01	9	MSV0003ED27_01
5	MSV0003E5BE_01	10	MSV0003F37C_01
		11	HSV0003F88E_01
		12	HSV00040A1D_05
		13	HSV0003E689_01



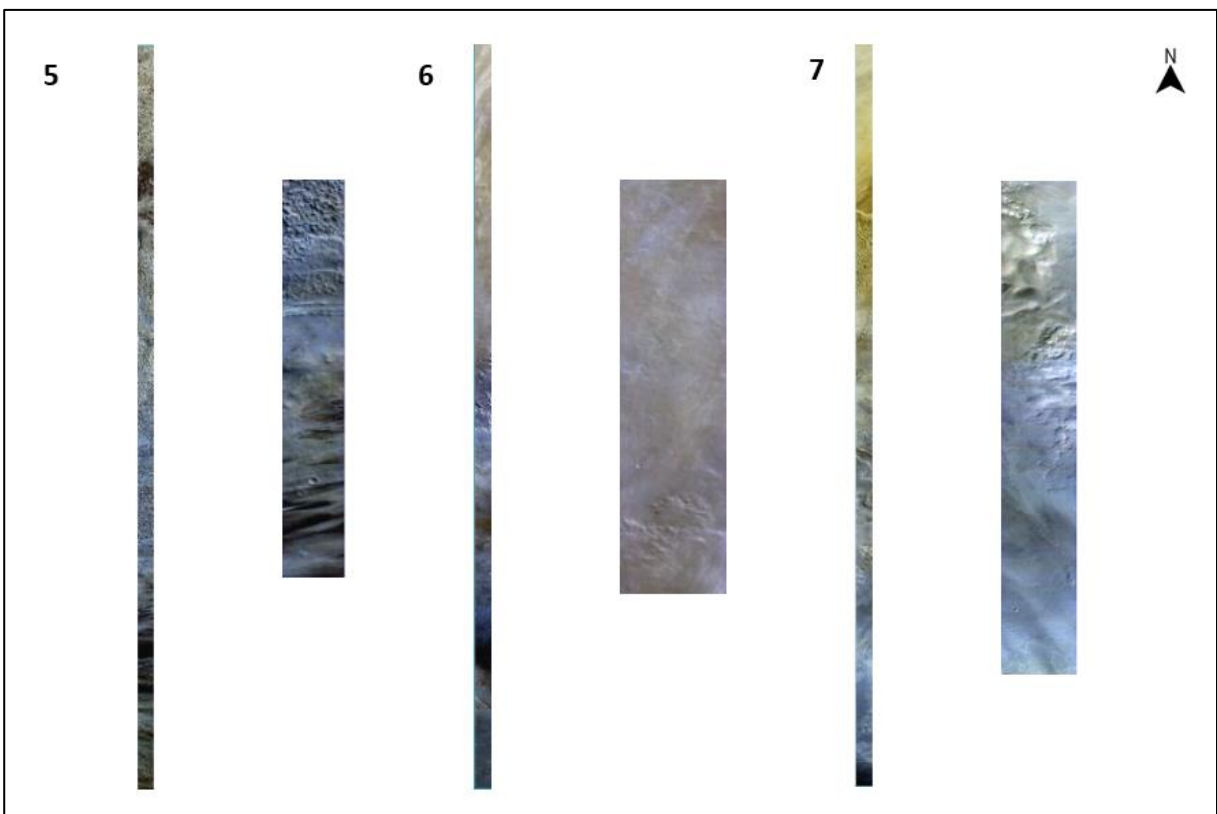
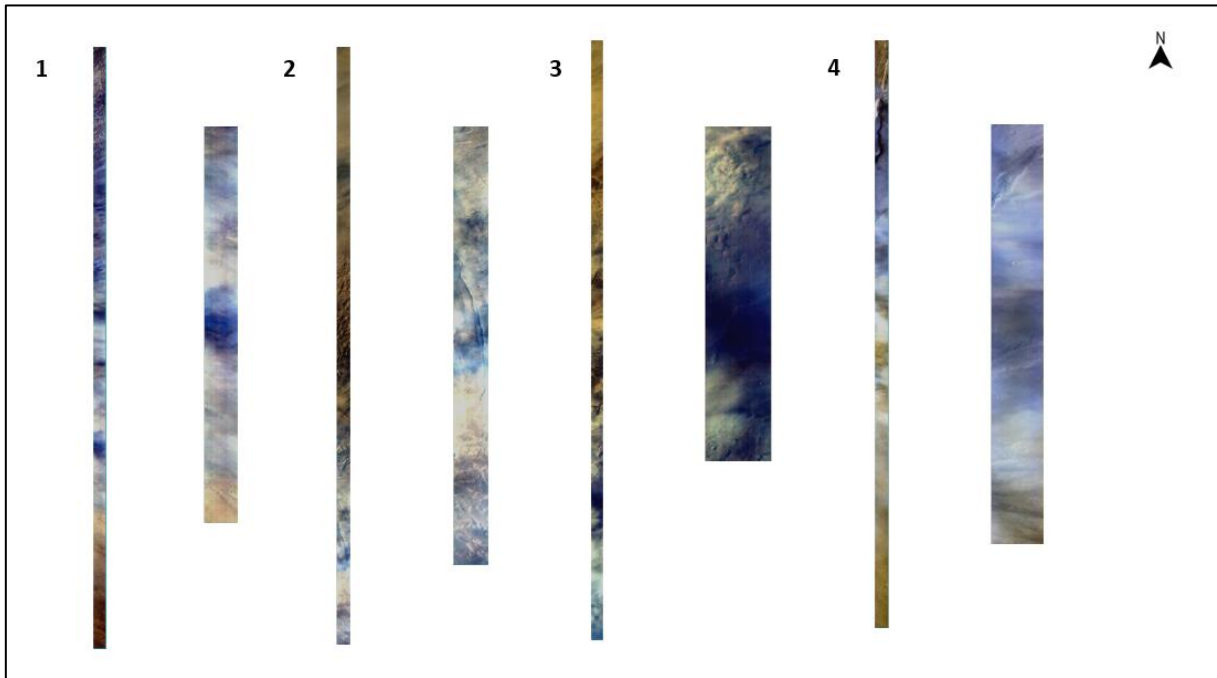




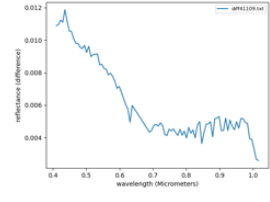
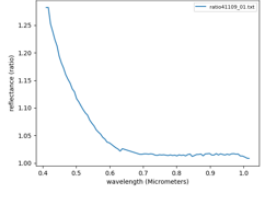
2017

1	MSV00041109_01
2	MSV00041173_01
3	MSV00041343_01
4	HSV000414DA_07
5	MSV0004447F_01

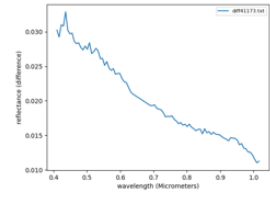
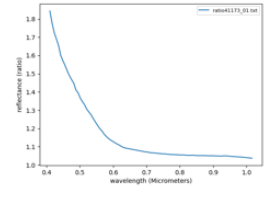
6	MSV0004493B_03
7	MSV00045CB2_01



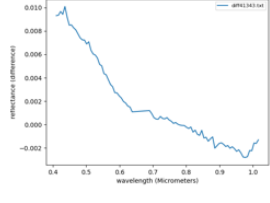
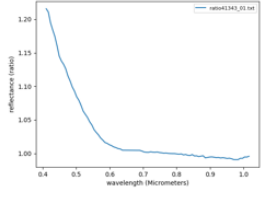
1



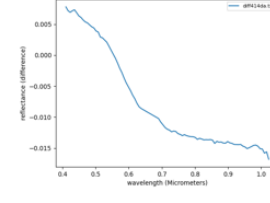
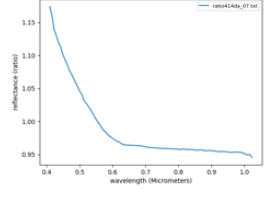
2



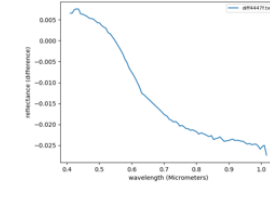
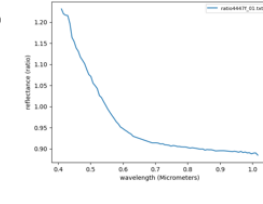
3



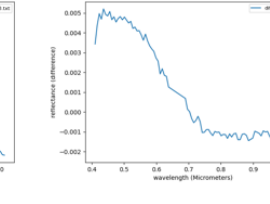
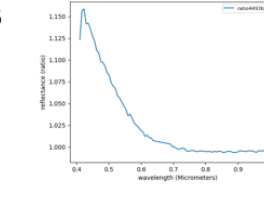
4



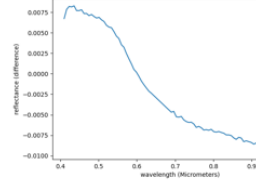
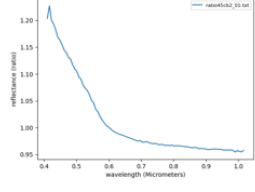
5



6



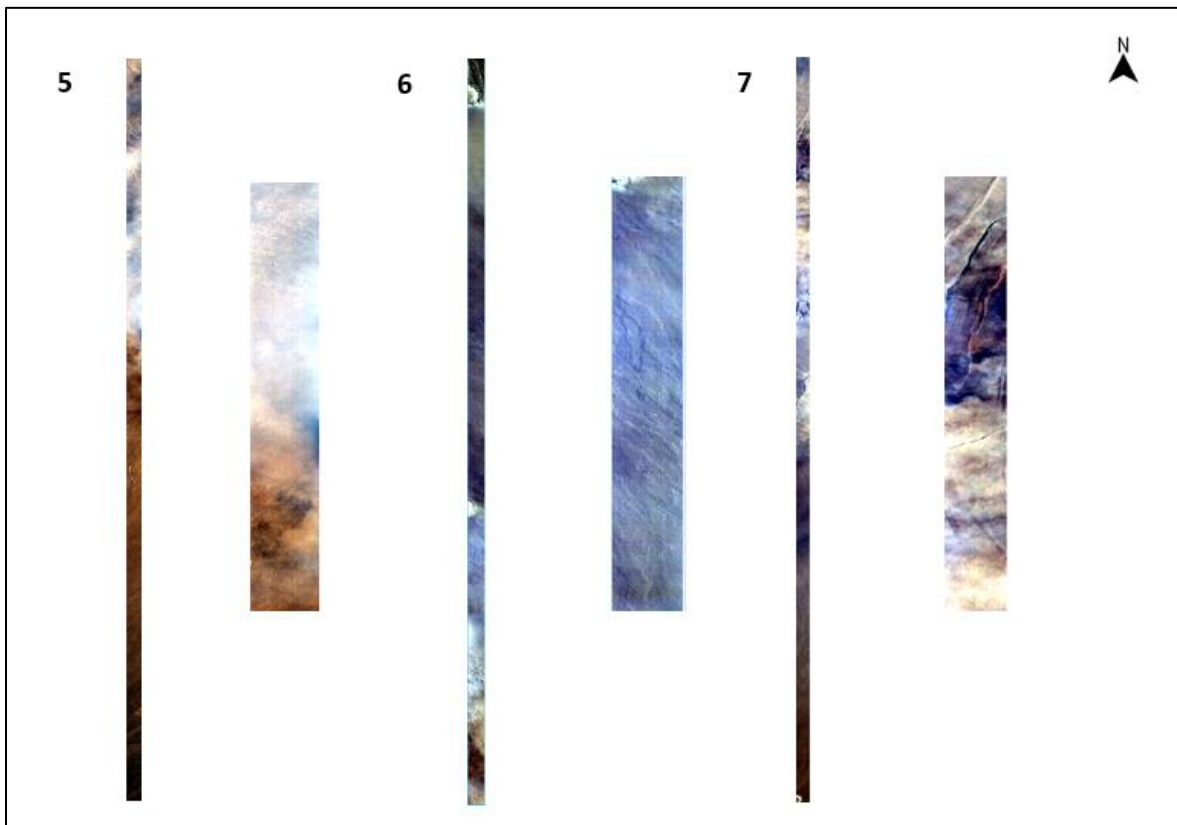
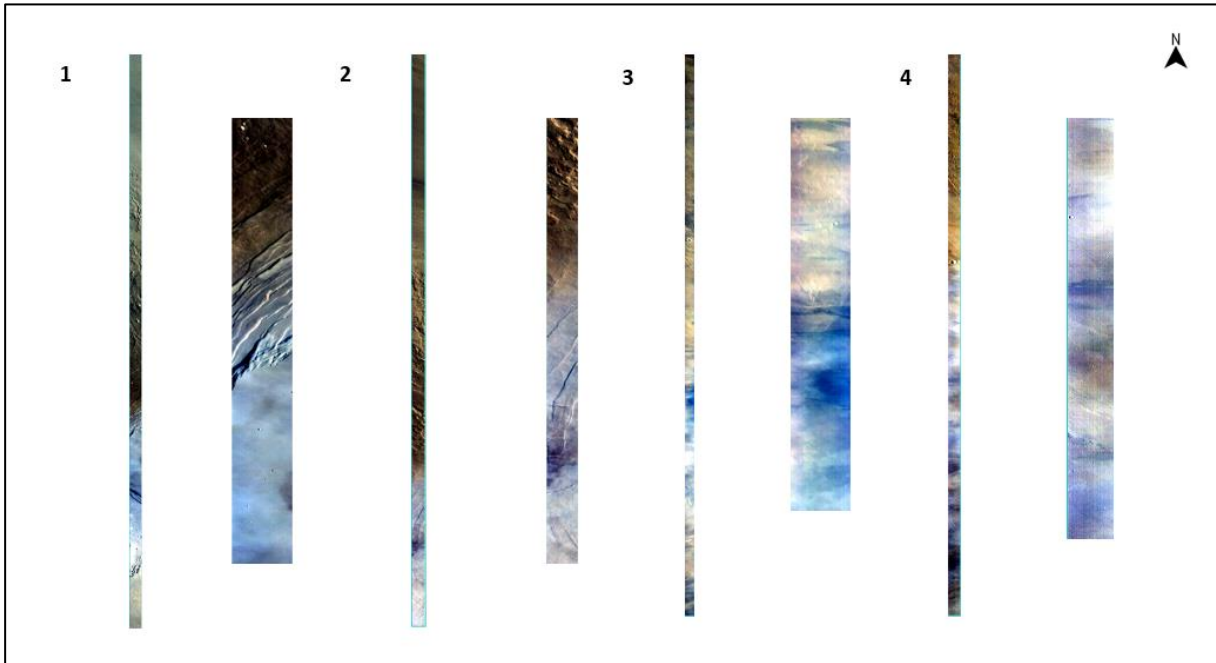
7



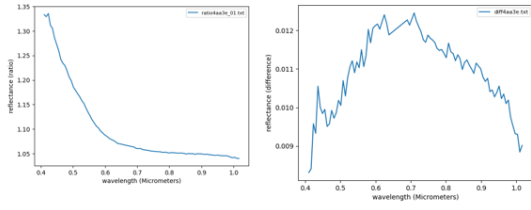
2018

1	MSV0004AA3E_01
2	MSV0004B163_01
3	HSV0004BC66_05
4	MSV0004C076_03
5	MSV0004C0D6_01

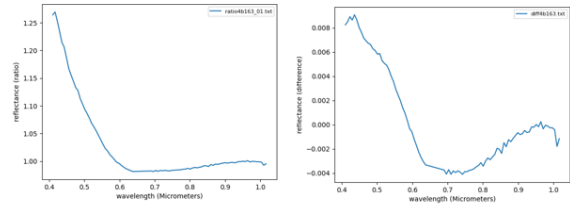
6	MSV0004C130_01
7	MSV0004C300_01



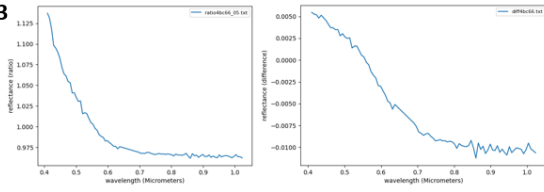
1



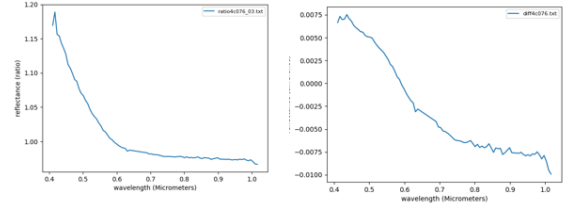
2



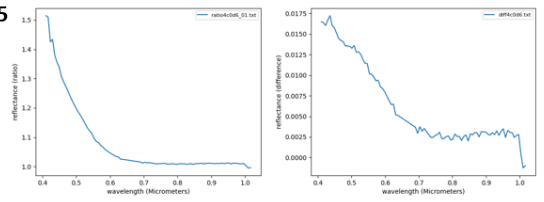
3



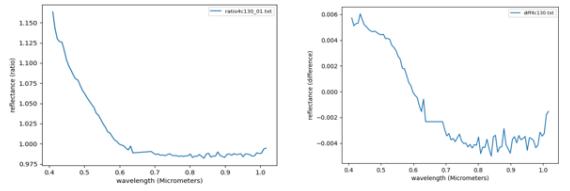
4



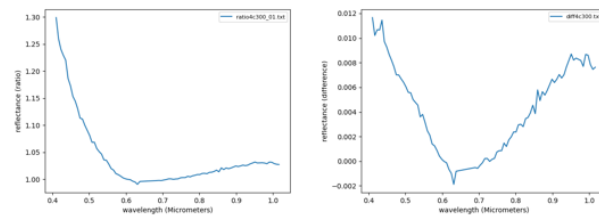
5



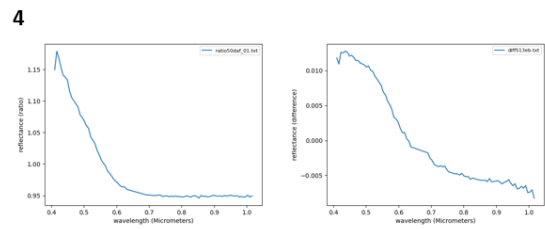
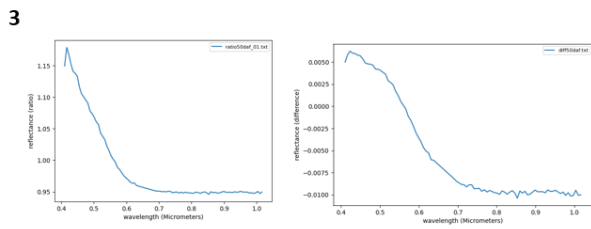
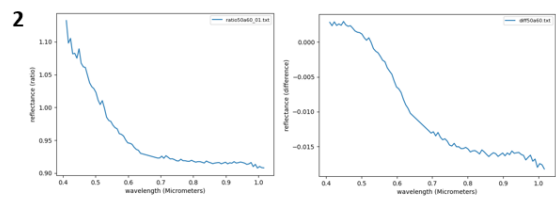
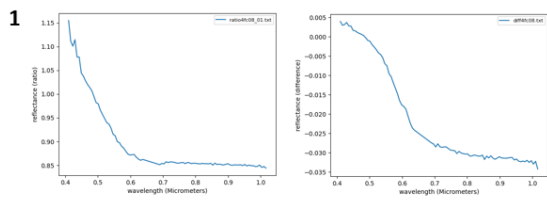
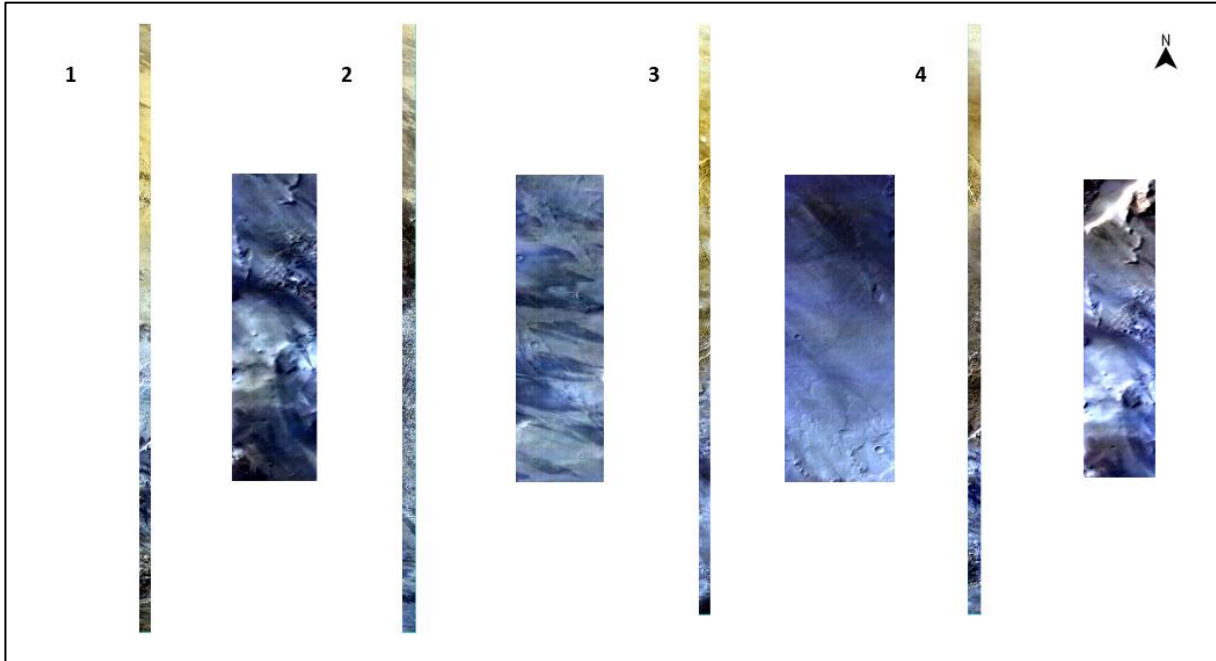
6



7



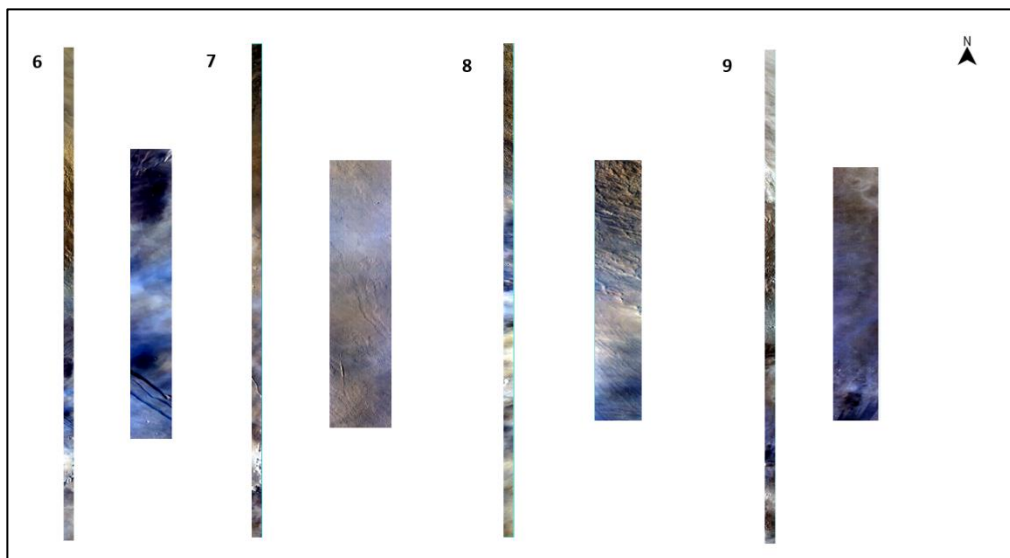
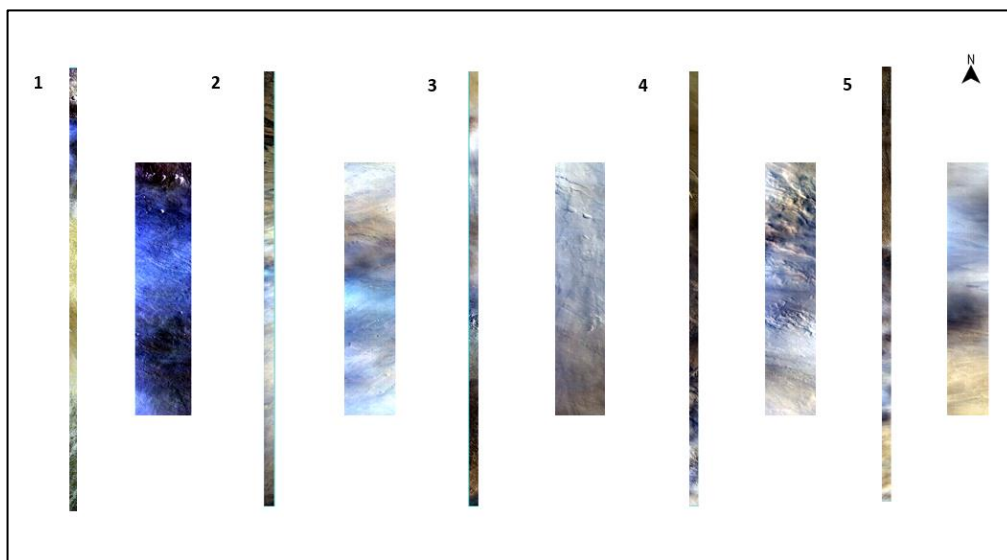
1	MSV0004FC08_01
2	MSV00050A60_01
3	MSV00050DAF_01
4	MSV000513EB_01

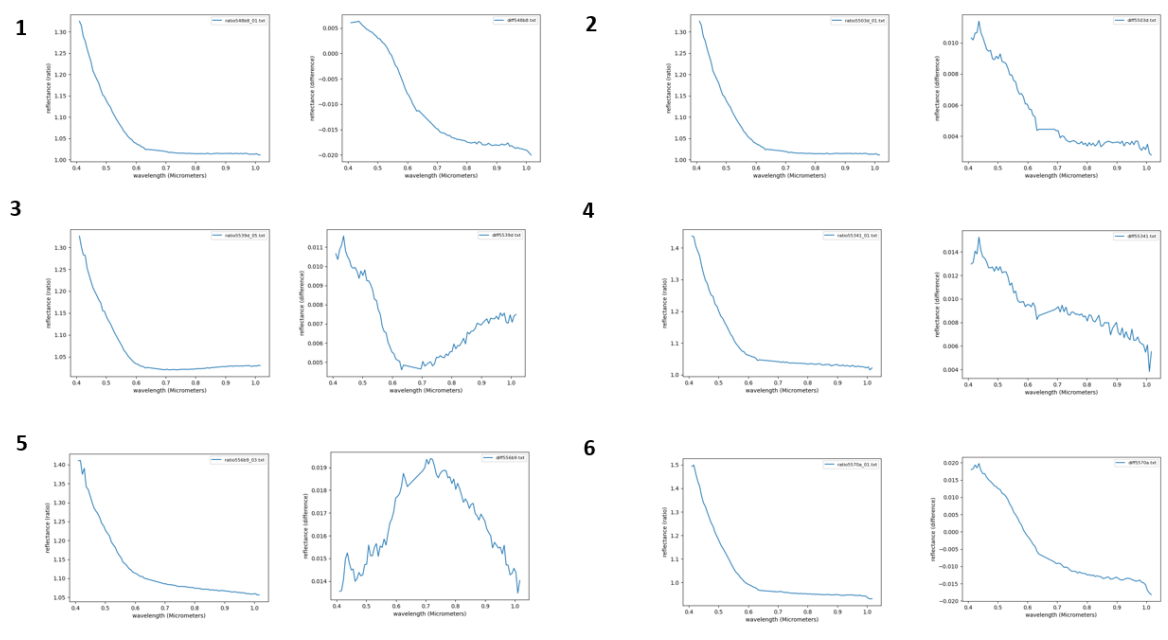
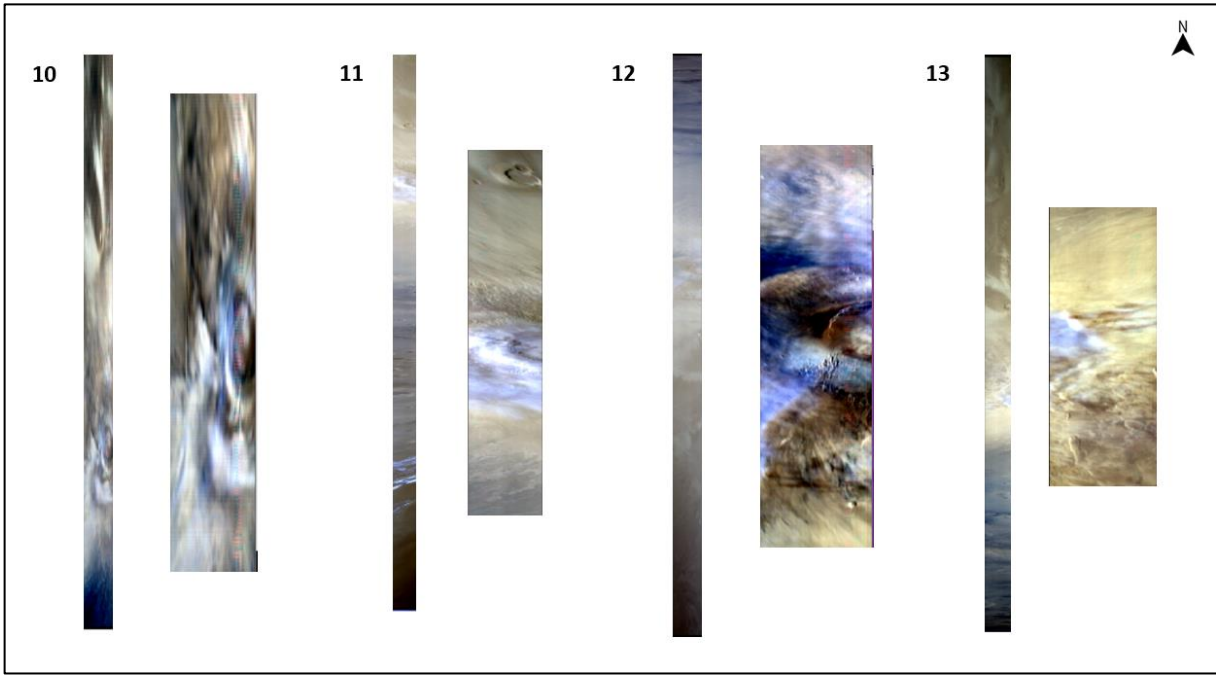


2020

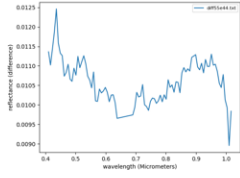
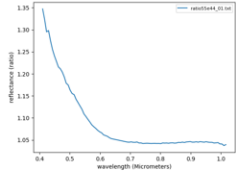
1	MSV000548B8_01
2	MSV0005503D_01
3	MSV0005539D_05
4	MSV00055341_01
5	MSV000556B9_03

6	MSV0005570A_01
7	MSV00055E44_01
8	MSV00056143_03
9	MSV00056807_01
10	ORBL424_0
11	ORBL068_0
12	ORBL135_0
13	ORBL142_0

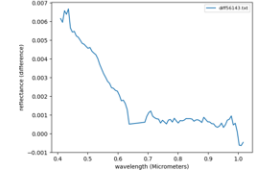
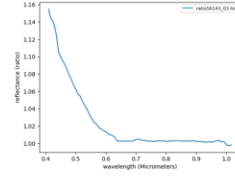




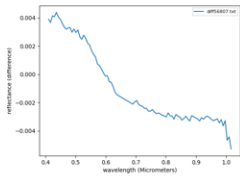
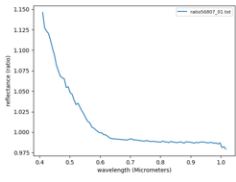
7



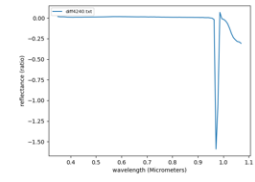
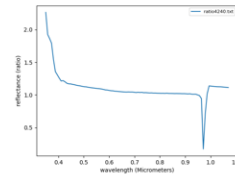
8



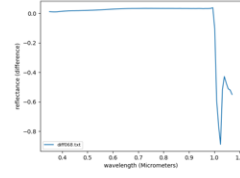
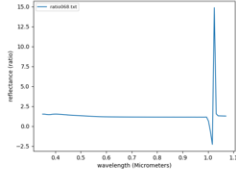
9



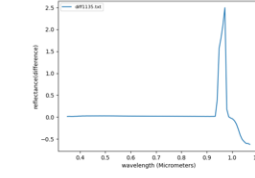
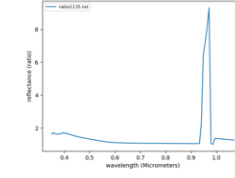
10



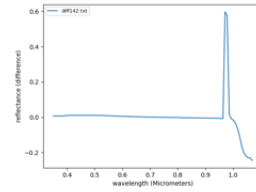
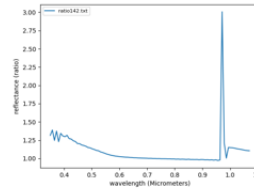
11



12

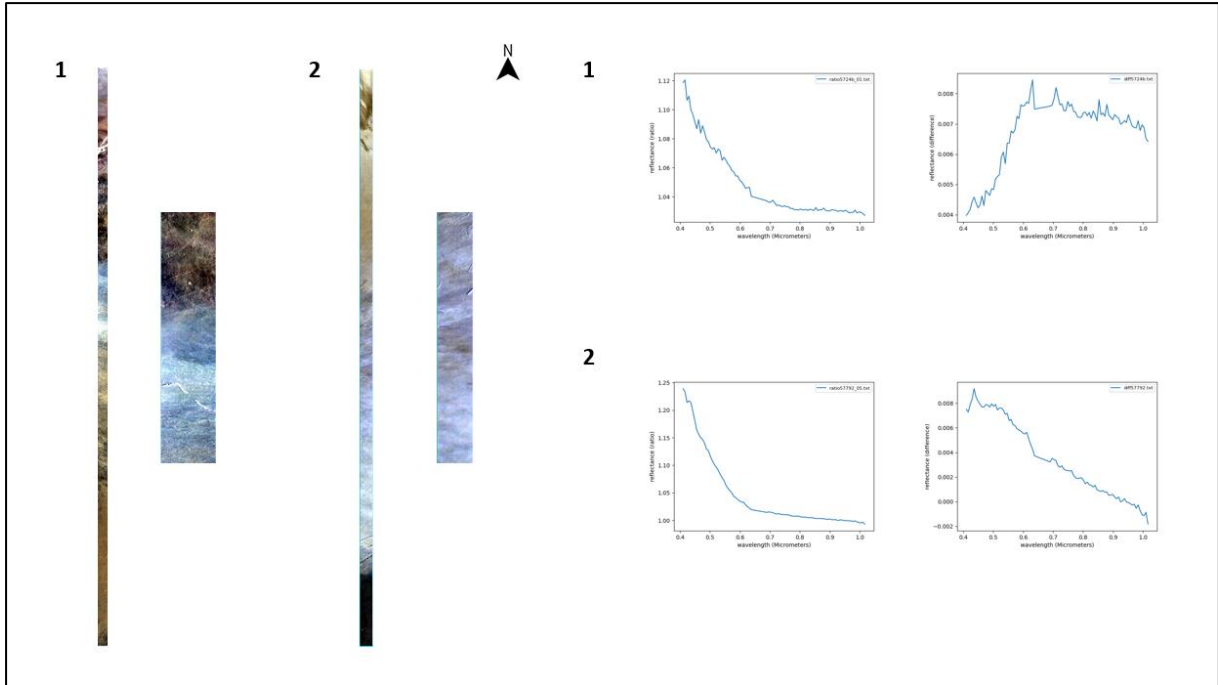


13



2021

1	MSV0005724B_01
2	MSV00057792_05



2022

1	ORBL498_0
---	-----------

